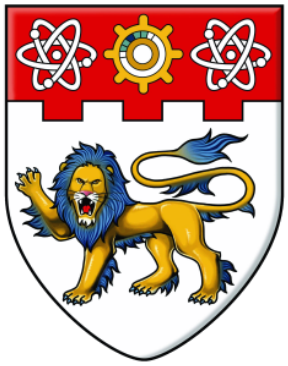

NANYANG TECHNOLOGICAL UNIVERSITY

# IMPROVING ADHESION OF COPPER THIN FILMS ON ALUMINA SUBSTRATE THROUGH INTERFACE ENGINEERING

**LIM JU DY**

**School of Materials Science and Engineering**

**2015**

# IMPROVING ADHESION OF COPPER THIN FILMS ON ALUMINA SUBSTRATE THROUGH INTERFACE ENGINEERING

**LIM JU DY**

**School of Materials Science and Engineering**

A thesis submitted to Nanyang Technological University in partial fulfilment of the requirement for the degree of

Doctor of Philosophy

**2015**

# ABSTRACT

Topic of adhesion has been well known in the scientific community due to its wide range of applications in microelectronics. Research on adhesion has been extensively carried out for improvement on the interfacial joining between materials. In microelectronic packaging, ceramic metallization has been the subject of interest due to its unique properties specifically under extreme environment. Although this topic has been extensively studied and reported using various bonding techniques, many open questions are still left to be addressed systematically to improve the device reliability.

In this thesis, a systematic study has been carried out for the methods to enhance the interfacial adhesion between Cu thin film and $Al_2O_3$ substrate. The Cu thin film was chosen for metallization onto the ceramic $Al_2O_3$ substrate by DC magnetron sputtering method as this method is simple, well-controlled, and compatible with industrial manufacturing process. Conventionally, an adhesion layer is required between Cu and $Al_2O_3$ due to poor wettability of Cu to the ceramic substrate. However such process inevitably requires a greater time and increases the production cost.

A direct bonding of Cu thin films to $Al_2O_3$ substrate without adhesion layer was implemented in this study. The key study was focused on the impact of bonding parameters to the mechanical integrity of the interfacial joining. In general, the metal film properties are strongly affected by the deposition parameters [1]. In addition, the residual film stress is the major challenge for good bonding. In this

study, the effects of three deposition parameters on film stress have been investigated and identification on the film stress was analysed using XRD-$\sin^2\Psi$ method. The effect of kinetics movement of Cu atoms to the residual film stress was studied and verified on the adhesion strength. The adhesion improved with an optimized working pressure due to the film stress minimization during the deposition step.

The surface condition of $Al_2O_3$ substrate prior to bonding has also been elucidated. Adhesive forces between materials are affected by the environmental factors, surrounding medium and composition. M.B. Ranage [2] has mentioned that the particles in microelectronics are deposited from air, liquids or from human resources, in the size from 0.1 μm to several micrometres. Development of an effective cleaning method is mandatory for a robust bonding. The interaction between Cu and $Al_2O_3$ is believed to be affected by the surface cleanliness, as well as the modification of surface chemistry after treatments. Different surface cleaning techniques and treatment sequences were studied to understand their effect on Cu film adhesion with polycrystalline $Al_2O_3$ substrate. Excellent adhesion strength of more than 34 MPa has been achieved by argon plasma cleaning which is an abrupt increase compare to 6.1 MPa without plasma cleaning. The reason behind such drastic improvement is the effective removal of the surface contaminants as well as the creation of surface dangling bonds.

With further analysis, the study was extended on bonding mechanism was extended in terms of surface roughness, porosity density and surface morphology. The bonding mechanism and the area in contact between materials have been

analysed using polycrystalline $Al_2O_3$ with three different range of surface roughness. A comparative study was also carried out using monocrystalline $Al_2O_3$ substrates with surface roughness smaller than 0.5 nm in order to provide additional evidence on the obtained results. The study of bonding mechanisms and their quantitative contribution to the Cu-$Al_2O_3$ bonding were carried out. It was revealed that surface adsorption provides majority of contribution to the observed adhesion strength. Mechanical interlocking is another contributing factor behind the observed adhesion strength increase in the latter especially for the substrate with higher surface porosity. For the substrate with surface roughness of 350 - 500 nm, it has contributed up to 18.6 % to the Cu film adhesion with $Al_2O_3$ polycrystalline. Diffusion bonding mechanism may be operative only with post deposition annealing treatment. From the XPS measurement, it was observed that Cu atoms have diffused deeper into the substrate without chemical reaction between Cu and $Al_2O_3$.

The current works conducted have achieved superb adhesion strength beyond 34 MPa, this value has far exceeded the MIL-STD-883E of 10 MPa. The guidelines for enhanced Cu-$Al_2O_3$ adhesion were proposed in this thesis with uncomplicated and trouble-free processing step. Extra insertion of glue layer such as titanium, tantalum or chromium is not required in this proposed bonding system. More importantly, types of bonding mechanisms have been justified and quantified to understand their contribution in Cu-$Al_2O_3$ bonding system.

## ACKNOWLEDGEMENT

First of all, I would like to show my appreciation to my supervisor in Nanyang Technological University, Professor Chen Zhong for his kind advices, guidance and encouragement during my Ph.D study. His invaluable support has been keeping me on track throughout the project and his mentoring has enabled me to carry out my research work in a very smooth progress. I am very grateful to be Prof. Chen's student, thank you very much for his patience and understanding for making my progress in a more perspective view and increased the integrity of my efforts so far.

Secondly, I am very thankful to my ex-supervisor Associate Professor Wong Chee Cheong who has been guided me for the first 2 years of my study in NTU. I have been supervised by Prof. Wong at the beginning of my project; his style of guidance has strongly influenced me in every aspect of my life. He was trying to build up my confidence and practiced me to be a more sociable person. Without his supervision, I would not able to change my introvert and coward personalities. His precious suggestions and strict criticism has brought me a good starting point of my Ph.D's life.

I would also like to thank Assoc. Prof. Gan Chee Lip from NTU and Dr. Daniel Rhee MinWoo from Institute of Microelectronics (IME), A*STAR for their precious time to attend my presentations and provided me with loads of comments and ideas. Besides, the equipments support provided during my study are much appreciated. I could never complete my project in a stable and smooth path without their approval on the equipments.

I am so blessed with the GLOBALFOUNDRIES-EDB scholarship under the Joint Industrial Programme (JIP) awarded from GLOBALFOUNDRIES Pte. Ltd, so I am able to pursue my Ph.D in these 4 years without distressing on financial support. Moreover, I would also express my gratefulness to my supervisor in this company, Mr. Leong Kam Chew for assisting me in this project, teaching us about the process flow every week, and helping us in some documenting works in the company.

Meanwhile, I am so grateful with the generous help and valuable time contributed from my colleagues and staffs in NTU; IME and GLOBALFOUNDRIES specially to Dr. I Made Riko, Dr. Zviad Tsakadze, Dr. Liu Qing, Ms. Lee Pui Mun, Ms. Yeow Su Yi Susan, Mr. Phua Jian Rong Eric, Mr. Tan Jook Boon Eric, Mr. Tan Yong Kwang, Ms. Lim Bee Yen Adeline, Mr. Lim Jun Zhang, Mr. Lau Fu Long and Mr. Wahyuaji Narottama Putra. I would also like to show my thankfulness to all the laboratory technicians for the equipments training and give a hand whenever I need, and thanks to School of Materials Science and Engineering for the knowledge provided. A range of useful equipments in this school have made this project more fruitful.

Last but least, I wish to express my gratefulness to my lovely family, my soul mate and all of my friends who have been always stand by my side and bear on me throughout my study. I am awfully fortunate to have them in my life to motivate and encourage me especially during the difficult periods. Without their love, I wouldn't have been able to complete this task. Thank you very much from the bottom of my heart especially to my parents and my soul mate.

# TABLE OF CONTENTS

# LIST OF TABLES

# LIST OF FIGURES

## ABBREVIATIONS

| | |
|---|---|
| MCM | Multichip Module |
| MIL-STD | Military Standard |
| AFM | Atomic Force Microsopy |
| CTE | Coefficient of Thermal Expansion |
| MEMS | Microelectromechanical Systems |
| DCB | Direct Copper Bonding |
| DAB | Direct Aluminum Bonding |
| *rms* | Root Mean Square Surface Roughness |
| FIB | Focused Ion Beam |
| SEM | Scanning Electron Microscopy |
| XRD | X-ray Diffractometer |
| XPS | X-ray Photoelectron Spectroscopy |
| OWRK | Owen, Wendt, Rabel and Kaelble |
| TGA | Thermal Gravimetric Analyzer |
| ASTM | American Society for Testing |
| EDS | Energy Dispersive Spectrosocpy |

# CHAPTER 1 INTRODUCTION

## 1.1 Background

Bonding can be classified based on the scale of study. For the smallest scale of bonding, it can be defined as the binding between ions, atoms or molecules. For larger scale of bonding, it involves the attachment between the bulky items or the adhesion between two surfaces. Bonding, joining or adhesion is very general in our life; it always plays an important role in applications such as mechanical, electrical, biological or chemical. However, achieving an intimate contact with outstanding adhesion strength between materials is not an easy task to be accomplished. When materials (metal-metal, metal-ceramic, metal-polymer, or polymer-ceramic etc.) are bonded together, problems at interface (Fig. 1-1) such as buckling [3] , cracking [4], formation of voids [5, 6], adhesive fracture and de-lamination [7] may occur. Several factors such as high residual stress (external or internal), presence of contaminants, geometry concern or misfit in the coefficient of thermal expansion are always in the discussion to prevent bond failure.

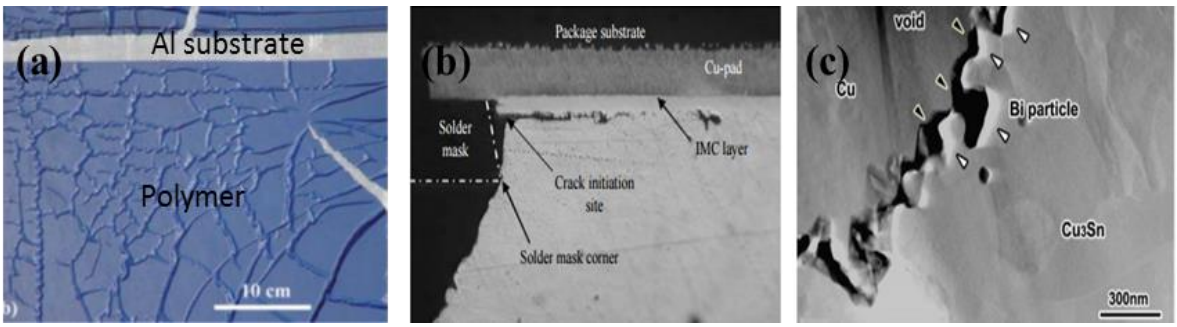


Figure 1-1: Types of bonding failures (a) buckling [3] (b) cracking [4] (c) void formation [5].

In the field of microelectronic packaging, multichip module (MCM) is a popular choice for devices to be deployed under extreme environmental conditions [8]. MCM is not a new topic, the basic science and the technologies of this area have been covered for more than 30 years [9]. However, in the quest of developing better reliability, low cost of production and excellent speed of performance, much more research is needed. One of the main reliability concerns is related to the adhesion between heterogeneous materials used in the package.

Electronic packages consist of different materials which are often joined together physically or chemically for specific functions. Attachment between wire and lead, lead and compound, die attach, IC and compound are crucial to maintain the system's reliability [10]. The issue of reliability from the substrate component is also an important concern for the system exposed to the environment accompanied with high temperature, high pressure and large vibration. Therefore, packaging technologies with good adhesion strength using advanced ceramic substrates for metallization is needed in these ruggedized electronic systems. Yet, interface complication is always a problem in the fabrication steps or service. In this project, a multidisciplinary approach is used to evaluate the adhesion between directly sputtered Cu films on $Al_2O_3$ substrate in the effort to develop more robust metallization scheme for microelectronic packages.

## 1.2 Proposal

### 1.2.1 Motivation and hypothesis

Due to the demands on simple fabrication, low processing temperature and low pressure for direct bonding, a Cu-$Al_2O_3$ system with excellent adhesion strength beyond the MIL-STD-883E (10 MPa) [11] for metallization scheme is proposed using DC magnetron sputtering deposition method. This bonding system can be made more robust by: (1) optimizing the bonding conditions in order to minimize the residual stress induced throughout the coating process, (2) implementing a standard treatment procedure to increase the surface cleanliness and the wettability of the substrate prior to bonding, (3) increasing the adhesion strength by varying the substrate surface structure, as well as having a good understanding about the bonding mechanisms at the interface through quantification analysis. This approach explicates a simple, easy and inexpensive way for ceramic metallization with no additional adhesion layer for Cu-$Al_2O_3$ bonding. To further assists the analysis of various factors affecting the adhesion, both polycrystalline and monocrystalline $Al_2O_3$ substrates have been studied in the current work.

### 1.2.2 Objectives and scope of work

This research project will be mainly focusing on the metallization of ceramic substrate for microelectronic packaging applications. The major target is to

enhance the adhesion strength and study the bonding mechanisms between sputtered Cu thin films and $Al_2O_3$ ceramic substrate by understanding the key factors behind the Cu-$Al_2O_3$ interface adhesion. Criteria such as low resistance conductive path and high mechanical strength must be considered in order to protect the device from the harsh environment. Such electronics can find applications in deep sea oil rigs, industrial chemical, nuclear plants, geological surveys, space vehicles, and military installations. This thesis reports mostly of the experimental study for the interface bonding between Cu thin films and $Al_2O_3$ substrate. The objectives of the thesis work are:

- Understand the key factors behind Cu-$Al_2O_3$ interface adhesion through qualitative and quantitative analysis
- Optimize the processing parameters leading to achieve Cu-$Al_2O_3$ adhesion strength of more than 10 MPa as required by the MIL-STD-883E standard
- Provide guidelines for microelectronic packaging in ceramic metallization without the use of adhesion layer

The scope of the work covers the following areas:

- **Effect of the processing parameters**

The sputtering parameters or conditions are crucial for interface bonding between heterogeneous materials. This could be varied for different bonding systems. In this study, factors such as deposition pressure, deposition time and post

annealing temperature have been investigated. The optimization of the bonding parameters will lay foundation for subsequent studies.

By altering the deposition pressure, transformation of the residual stress during the sputtering process is studied. Different stress state (tensile stress or compressive stress) may affect film growth mechanism at the interface region. Besides deposition pressure, post annealing step has been applied to exam the Cu diffusion at high temperature.

- **Importance of surface pre-treatments**

Various types of surface treatments either is in-situ or ex-situ have been investigated. Surface pre-treatment is a well-known technique for adhesion enhancement. However, this topic has not been studied quantitatively. This is particular important for the reported Cu-$Al_2O_3$ system because it represents a popular metallization scheme for many high-end device applications. Due to the inertness of ceramics, there is an intrinsic low adhesion with metal thin films.

Surface treatments such as heating, plasma bombardment and acid etching were evaluated and checked on their effectiveness to the interfacial adherence. Surface analysis has been carried out before and after the treatment in order to check on their impact on the film adhesion. Besides surface chemical analysis, it is known that bonding quality between materials can be reflected by the material's wetting behavior. For this reason, it is imperative to evaluate the change of wetting state and surface energy with diverse cleaning conditions and study their behaviors toward the adhesion strength for Cu-$Al_2O_3$ bonding. This could help to acquire

insights into the subject of surface chemistry in order to develop a better contact between heterogeneous materials.

- **Role of substrate surface roughness**

Surface roughness is always a very important topic for interface bonding. Failure of interfacial joining can be caused by significant adhesion deterioration at the contact point [12-14]. In some cases, surface roughening is used to increase the interface contact area for adhesion improvement [15-17]. The complexity of the surface structure has a broad range of scales in height and spatial distribution. For a substrate with high surface roughness, there will be a large deviation between the effective area and the image projected area. Hence, information on real contact between metal film and substrate is needed to understand the key factors for a good bonding.

Polycrystalline $Al_2O_3$ substrates with different range of surface roughness have been used to check their interface adherence with Cu thin films. The effective area of the substrates was calculated using MATLAB in order to study its effectiveness to the adhesion enhancement. Besides adhesion improvement, it is equally important to study the bonding mechanisms between Cu thin films and $Al_2O_3$ substrate. In this study, the bonding mechanisms have been investigated and their contributions to the entire system have been quantified.

## 1.3 Organization of the Thesis

For summarization, this thesis consists of six major chapters and has been arranged in the subsequent manner followed by a brief description.

Chapter 1 introduces the background information of this project with the motivation provided in order for the author to develop few approaches to conquer the problems encountered. Objectives and scope of work will be included at the end of this chapter to provide a comprehensible aim of this project.

Chapter 2 is the literature review section of the thesis. It consists of an overall review for this research project on the following topics: failure mechanisms in microelectronics packaging; adhesion and de-lamination in microelectronics; surface finish prior to bonding; metal-ceramic bonding and types of bond strength measurements.

Chapter 3 presents the simple fabrication process of the test sample using the DC magnetron sputtering equipment. It also studies several fabrication factors affecting the bonding between Cu thin films and $Al_2O_3$ substrate.

Chapter 4 shows the concern of surface cleanliness and surface properties of the substrate prior to bonding. Different types of surface pre-treatments have been employed to exam their effectiveness to the adhesion strength for Cu-$Al_2O_3$ bonding. The changes observed before and after the treatments will be analyzed and discussed.

Chapter 5 demonstrates how the effective contact area to be calculated based on the data extracted from the AFM analysis. A MATLAB coding was developed to calculate the total effective area of the polycrystalline substrates with different surface roughness. Types of bonding mechanisms for Cu-$Al_2O_3$ bonding and their contributions will be elucidated.

Chapter 6 summarizes the overall findings in this project and concludes with important results from chapter 3 to chapter 5. Several recommendations for future work are included.

# CHAPTER 2 LITERATURE REVIEW

Microelectronic packaging is an influential section for the microelectronic industry. With the trend of miniaturization and advanced level of integration [18], importance of design, manufacturing and fabrication processes are always the focal points for improved reliability in microelectronic packages. To ensure good overall performance of the system, few fundamental aspects include mechanical, electrical, chemical and thermal characterizations must be incorporated for every step of processes. In the next section, an overview of the packaging failures will be discussed together with some examples.

## 2.1 Failure Mechanisms in Microelectronic Packaging

Topics of reliability, performance and life span are very crucial and cannot be neglected in microsystems, especially in the market of microelectronic packaging. Two approaches have been implemented (a) design systems packaging up front for reliability and (b) acceleration testing to check on the product's performance over a period of time [19]. It is always true that all of these approaches are expensive, complicated and time consuming in every step of manufacturing and testing. However, a range of possible failures can be predicted and solved by using these approaches before moving forward for further processes or until the end of the production.

From the earlier study, the failure mechanisms encountered can be minimally classified into two main categories which are overstress failure mechanism and wearout

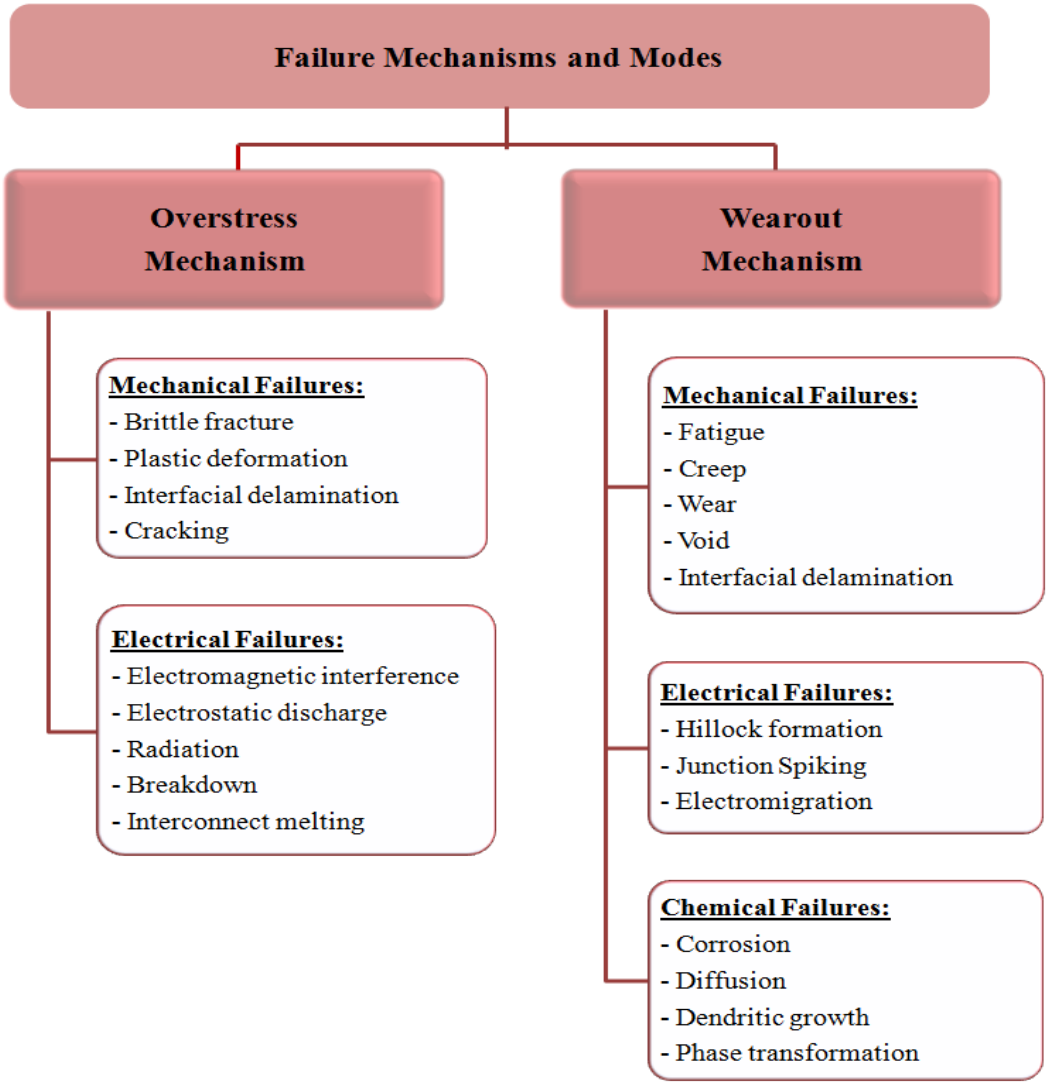


Figure 2-1: Types of failure mechanisms and modes in microelectronic packaging [19].

failure mechanism. For overstress failure mechanism, it happens when the level of stress created is much higher than the component's capacity. On the other hand, wearout failure mechanism is a different kind of deterioration takes place gradually even if it is under a low stress situation. From the mechanisms mentioned, the failure might be initiated electrically, mechanically, thermally, or chemically as depicted in Fig. 2-1 [19, 20]. As stated in Fig. 2-1, problem of delamination at the interface area can be considered as the major dilemma in the packaging system, it could happen either in low stress condition or high stress condition. Precautious steps have to be implemented in order to prevent or minimize failure to take place.

### 2.1.1 Mechanical and thermomechanical failure mode

From the business point of view, there are high demands on short-time-to-market and cutback of production cost. This will greatly affect the design margin and the device quality. In addition, it will increase the probability of various failures to occur and is leading to more troubles on the subject of reliability requirements. According to the conducted survey, discovery on the mechanical failure mode and thermomechanical failure mode have been accounted about 65% in microelectronic packaging [20]. In particular, mechanical failure mode is the bottleneck for the technology now, as well as in the future.

Mechanical or thermomechanical failure modes are mostly driven by CTE mismatch, stress concentration, deformation, fatigue, creep etc. Studies have been

conducted to resolve this problem in the packaging system. Several case studies regarding mechanical failure mode are described below.

Case study 1: Residual stresses [21-26]

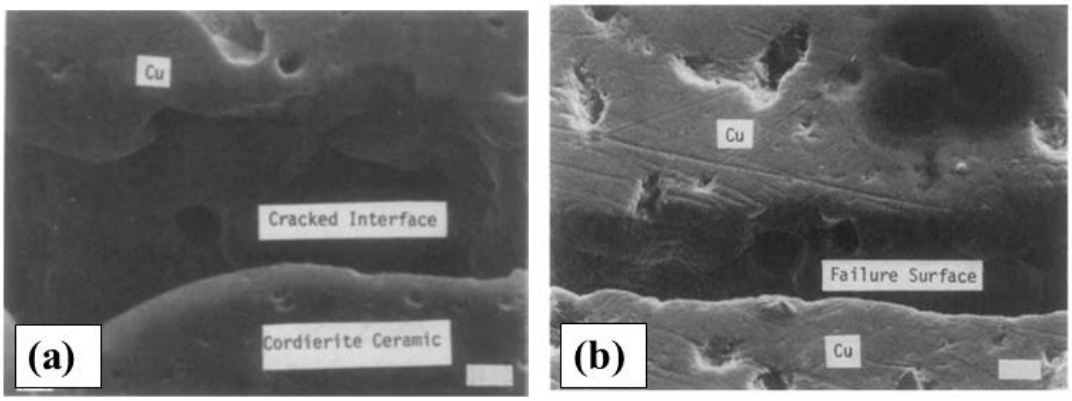


Figure 2-2: SEM images of (a) cracked interface for Cu-Cordierite bonding and (b) surface failure of Cu [21].

Residual stress is the internal stress generated within a material and under a condition with no external force applied. Occurrence of residual stress is normally by temperature gradient of a material during heating and cooling, plastic deformation during processing or volume change through phase transformation. In thin film application, there are plenty of failures that have been reported due to the induced residual stress, either is intrinsically or extrinsically. Extrinsic stress is also known as thermal stress, which created by the CTE mismatch between coated thin film and substrate material. As for intrinsic stress, it is the stress induced during the processing step, leading to an impact on the film growth and nucleation. Likewise,

development of stress can also be affected by other factors such as ion implantation, doping, diffusion etc.

From C.H. Hsueh and A.G. Evans [21], the cracked interface was reported between Cu-cordierite ceramic (Fig. 2-2) initiated by the residual stresses. The bonding between materials was done at high temperature with a stress relaxation situation. The cooling process was considered to be completed when the sample has reached 300 K. With the indentation technique introduced, a residual stress of 1500 MPa was measured at the interface. Development of high residual stress was mainly due to the CTE misfit (Cu alloy: $17x10^{-6}/\ ^{o}C$; Cordierite ceramic: $2x10^{-6}/\ ^{o}C$) upon cooling between these materials. Besides, it also shows that the elastic properties, the yield strength and the work hardening rate of Cu will also affect the total stress of the bonding system.

Case study 2: Moisture absorption [3, 27-32]

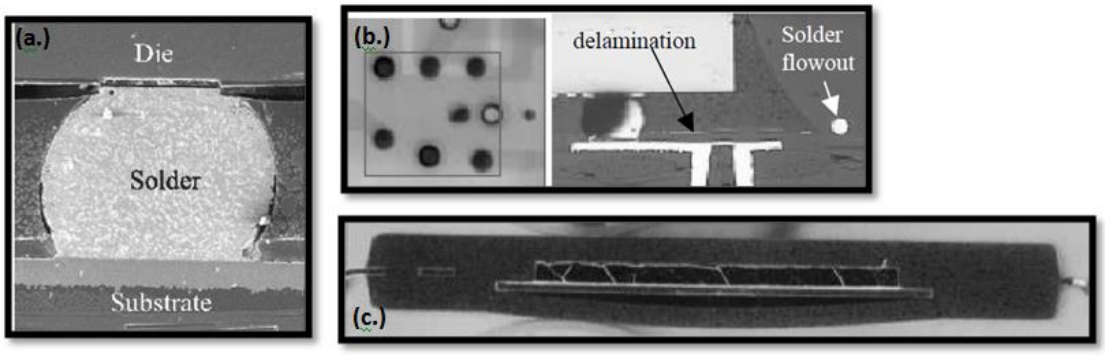


Figure 2-3: Consequences of moisture attacked: (a) hygro-swelling in flip chip assembly [33] (b) detachment of solder during reflows [29] (c) package bulging caused by the vaporized moisture[33].

Presence of moisture might induce different types of failure mechanisms and affect the overall performance of the packaged devices. The moisture effect can be simply explained into three failure mechanisms: (i) hygroscopic stress via swelling (ii) existence of vapor pressure at reflow temperatures (iii) deterioration of material with high humidity level [20, 29, 33]. Under a humid environment, water absorption in the package is relatively high. The entrapped moisture might condense in every part of the package especially at the interface. During the reflow or heating stage, there will be an increase of vapor pressure caused by the vaporization process and is leading to the failures. Several failure modes such as interface debonding, bulging, and swelling were discovered and illustrated in Fig. 2-3.

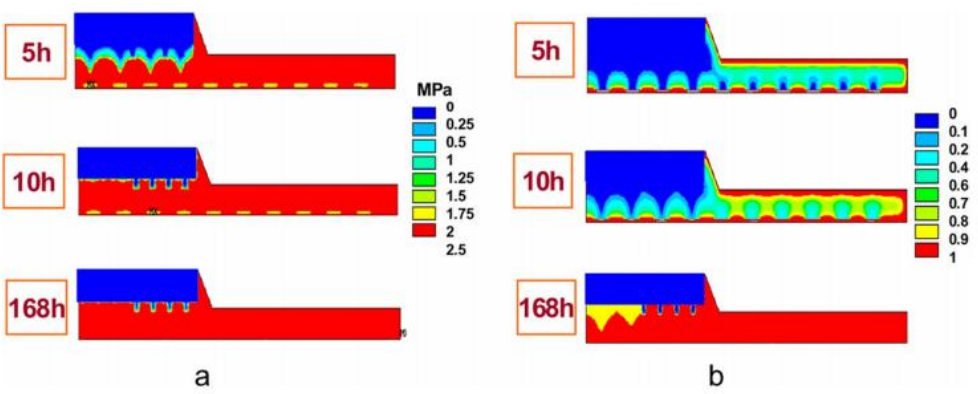


Figure 2-4: Moisture sensitivity level of the flip chip package at 220 °C by ANSYS: (a) distribution of vapor pressure and (b) distribution of moisture diffusion [32].

In a paper reported by X. Fan et al. [32], interfacial adhesion and vapor pressure inside the flip chip package were strongly affected by the moisture absorption during the reflow process. At the early stage of reflow process,

distribution of vapor pressure increased with moisture diffusion until it has reached the saturation stage after 10 hours of heating as illustrated in Fig. 2-4. It explained that the vapor pressure saturation was generated much faster during reflow compared to moisture absorption. No further increment of the vapor pressure was detected even though there was an additional intake of moisture. On the other hand, degradation of adhesion at the interface was experimented with the moisture absorption although there was saturation on the vapor pressure as shown in Fig. 2-5. The delamination will take place when the adhesion strength was lower than the vapor pressure level.

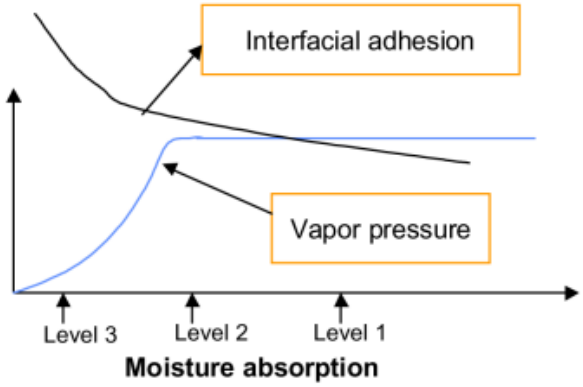


Figure 2-5: Correlation between moisture absorption to the vapor pressure and interfacial adhesion [32].

Case study 3: Deformation [34-38]

Deformation refers to the shape change or varies in size of an object. Deformation of a body or a material might be affected by external forces, inner

load of the body or the extreme environment conditions. In addition, it also depends on the type of materials, the size and the geometry. With different conditions applied, deformation might be in reversible mode (elastic deformation) or irreversible mode (plastic deformation). Upon reaching the ultimate strength of a material, fracture will take place with excessive applied load.

In the paper written by F. Laura [37], liquid crystal polymer (LCP) substrate with high flexibility was used to investigate the reliability of a flip chip joint using an anisotropic conductive adhesive. The bonding was done under two different joining pressures; low bonding pressure at 60 MPa and high bonding pressure at 120 MPa. Severe deformation was observed with high bonding pressure as shown in Fig. 2-6 (b) compared to sample assembled at low pressure in Fig. 2-6 (a). The pads were submerged down into the LCP layer and are leading to reliability issue.

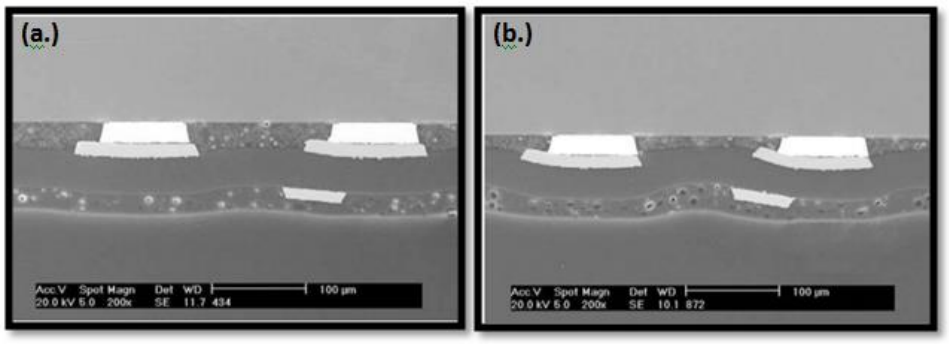


Figure 2-6: LCP film deformation with bonding pressure at (a) 60 MPa (b) 120 MPa [37].

### 2.1.2 Electrical failure mode

According to the Moore's law introduced by G. E. Moore, he had mentioned that emerging of transistors in an integrated circuit doubles in every two years. Accordingly, issue of miniaturization of microelectronic has been the main theme of research and development. With the requirements of high speed performance, multi-functionality, multi-technology, as well as shrinking down of the device's size, failures from the point of electrical are getting more complicated.

There are two main parts for the electrical function in a packaged device, include signal distribution and power distribution [39]. The functionalities in the electrical aspects depend on the wiring, interconnection, material properties and geometrical shape of the material.

Case study 1: Electromigration [40-44]

For interconnects, the driving force for electromigration is due to the momentum transfer of the electrons causing the atomic diffusion under applied electric field. Transportation of metal atoms (ions) towards the positive end of the conductor is leading to the formation of void at the negative end of the material. At the side of atoms depletion, the resistivity will increase gradually and is resulting in interconnect failure. At the other side of the conductor, deposition of atoms is generated and is leading to hillock formation type of failure. Current density, temperature, grain structure, stress distribution, surface roughness, surface

structure and alloying are the contributory factors for electromigration in an electronic system.

For advanced flip chip technology, there is a need to increase the number of input-output for interconnects. Hence, the size of the solder ball has to be reduced to meet the requirement. However, it could lead to the matter of reliability especially electromigration. From T.Y. Lee et al. [45] , experiments were done to analyze the electromigration behavior of solder joints and solder strips. A flip chip solder joint was formed by attaching the silicon chip to the FR4 substrate using eutectic Sn-37 % Pb interconnects with diameter of 125.0 μm. The bonding was carried out at an annealing temperature of 120 °C and power supply up to $2.0 \times 10^4$ A/cm$^2$ for 70 hours and 324 hours. After long hours of current stressing, electromigration was discovered in the structure indicated in Fig. 2-7 (b) and (c). At the anode side of solder ball (bottom region), hillock failure was formed. Void formation was also clearly revealed on the cathode side (top region).

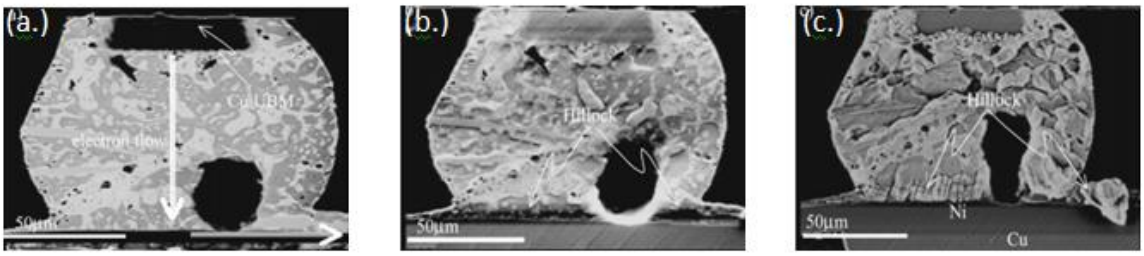


Figure 2-7: Cross-sectional images of eutectic Sn-37 % Pb solder ball (a) before current stressing (b) after 70 hr of current stressing (c) after 324 hr of current stressing at 120 $^o$C and $2 \times 10^4$ A/cm$^2$ [45].

Case study 2: Electrostatic discharge (ESD) [46-50]

Static charge is known as imbalance electrical charge condition of a material. Electrostatic discharge is a phenomenon whereby the static charge transfers between two materials with different potentials under rapid electricity flow. It can be transferred via direct contact mechanism or through an induced electric field. The ESD process can be divided into 4 stages: (i) charge generate (ii) charge transportation (iii) electrical conduction and (iv) device breakdown [51]. There is a possibility of direct, indirect or hidden damage to the device [50]. It will also cause permanent damage to the integrated circuit if the voltage is extremely high especially to the metallization layer, gate oxide and junctions.

In the paper reported by J. Ruan et al. [48], the authors have investigated the ESD failure mechanism on aluminum nitride-based capacitive RF MEMS switches via transmission line pulsing (TLP) method. The experiment was carried out with constant impedance of 50 Ω and the voltage scale in the range of 260 V to 420 V. The original top view of the device was shown in Fig. 2-8 (a) and degradation of the device after the stress testing was indicated in Fig. 2-8 (b). The device has operated continuously until it was fully destructed. From the measurement taken, the feature of the capacitive contact was strongly affected by the TLP stresses.

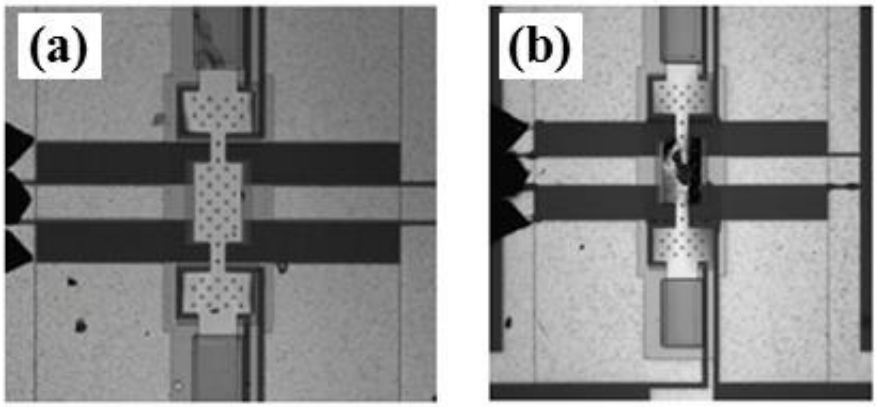


Figure 2-8: Top view of AlN-based capacitive RF-MEMS switch (a) before EDS test (b) after EDS test [48].

### 2.1.3 Chemical failure mode

Besides mechanical and electrical failure modes, failures occurred chemically in a packaged system are increased drastically especially under the extreme environment. Corrosion, diffusion, electrochemical reaction or the dendritic growth of chemical reactions are generally caused by the factors of humidity, temperature, voltage or stress. Problem of cracking, de-bonding, breakdown thru interconnect, trace or via are the consequences from chemical failure mode.

Case study 1: Corrosion [52-56]

Corrosion can be considered as the most common type of failure in chemical processes. It is a natural destructive process in which the metal is being

oxidized and transformed into an oxide with higher stability. The deterioration is more significant when the material is being attacked by the elements in an aqueous phase of condition containing dissolved ions through chemical or electrochemical reaction [18, 57]. Weakening of material properties in the aspect of strength, hardness, ductility and toughness is leading to crack or pit formation. Besides metals, other materials such as ceramic and polymer will also corrode under certain situation. Galvanic corrosion, erosion, stress corrosion, concentration cell, pitting, crevice, fretting, etc. are some of mechanisms in corrosion failure.

In the corrosion study carried out by C. W. Tan et al. [54], the bonding behavior of copper ball onto aluminium-based bond pad was measured using interfacial shear test. The experiment was conducted at 121 °C under a very humid environment. Up to 192 hours of testing, an excellent interfacial shearing force of 157.4 gf was achieved due to the strengthening effect from Cu-Al intermetallic formation. But, there was a drop on the shearing force after 288 hours and the interfacial shear force has decreased to 97.6 gf at the end of the testing (576 hours). Cracking at the interface was observed after 384 hours and increased with the testing time; it was mainly due to the stress corrosion cracking induced by the concentrated CuO at outer bond interface. After 576 hours, 100% concentration of Cu-O compound was detected and is leading to an observed detachment failure for Cu-Al bonding in Fig. 2-9.

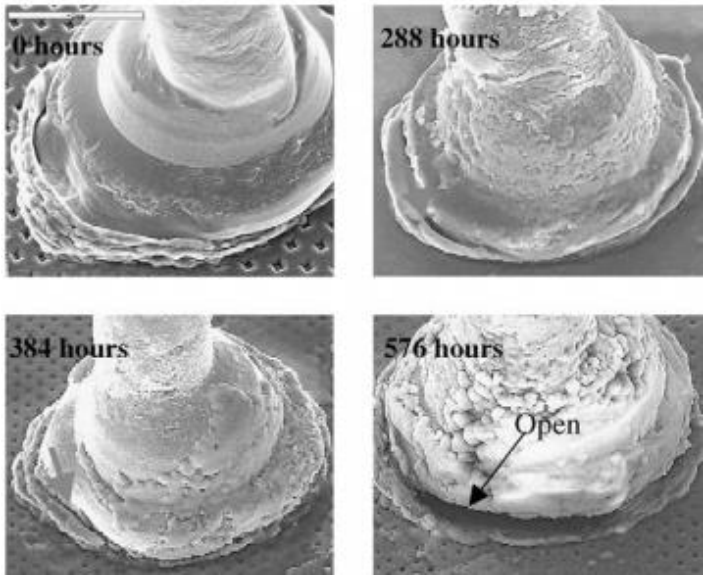


Figure 2-9: Degree of corrosion with testing time [54].

Case study 2: Diffusion [58, 59]

Diffusion is defined as a mechanism involving the mass transportation of substances (ions, atoms or molecules) according to the concentration profile of the materials. Diffusion between materials is commonly used to generate new chemical product for further improvement, and it is normally conducted at elevated temperature or high pressure. In microelectronic packaging, formation of intermetallic compounds via diffusion reaction plays an important role in the reliability study and joint integrity [18]. However, well controlled of the thickness, the growth between phases and the changes of the microstructure are still very tedious in the process. Without proper control, it will strongly affect the performance of the system in terms of stiffness, ductility, fracture resistance of the material.

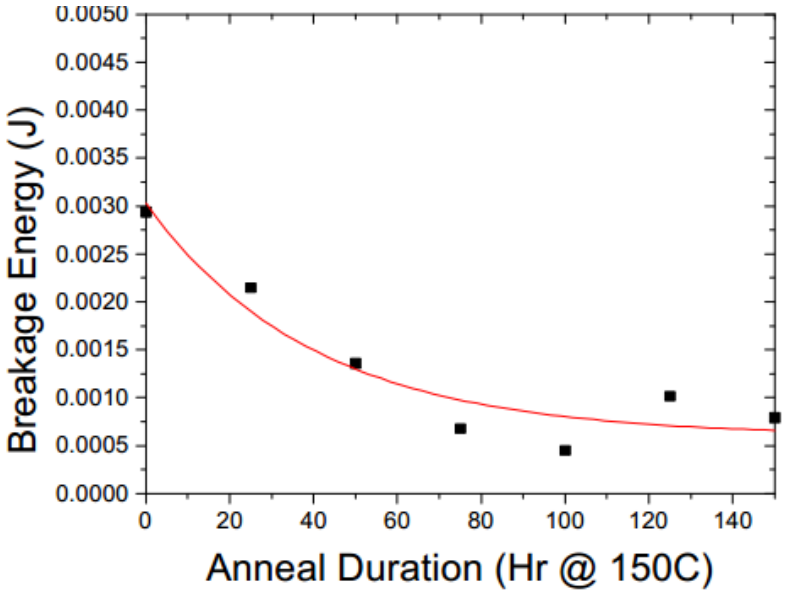


Figure 2-10: Decrease of breakage energy with annealing time [58].

An intermetallic compound Cu/Ni/Au/PbSn was investigated by Zribi et al. [58] to test on the mechanical properties of BGA solder joint on FR4 substrate. The substrate was first plated with Au with different thickness. The solder joints were then thermally aged at 150 °C for long hours under the inert gas atmosphere after solder reflow. Tensile-shear mechanical testing was then carried out at different annealing durations as illustrated in Fig. 2-10. From the mechanical measurement, decrease of adhesion strength (breakage energy) with the aging time from 0 to 150 hours was observed. The toughness reduction was caused by the growth of ternary alloy $(Au_{0.5}Ni_{0.5})Sn_4$ at the $Ni_3Sn_4$ /solder interface. In this study, high solubility of Au tends to dissolve into the solder during reflow and forms $AuSn_4$ intermetallic alloy. Migration of $AuSn_4$ started with the aging step at 150 °C, it moved to the interface region and affected the bonding of BGA assemblies.

## 2.2 Adhesion in Microelectronic Packaging

Assemblies of layers from heterogeneous materials are on high demand to accomplish different special functionalities in the application of microelectronic packaging. Nevertheless, the physics and the science of adhesion are still an extremely challenging topic to the engineers in the aspects of design and process. The weak linkage of the object is mostly influenced by the thermomechanical properties of the materials (CTE, Young's modulus, melting temperature, strain hardening etc.) [10, 60-62]. In addition, factors such as intrinsic stress created throughout the deposition [1, 63, 64], impurities on the surface [65], chemical damage during the process [66], as well as the geometry of the bonded surfaces [15, 67] are the driving forces to initiate the interface breakage. The schematic in Fig. 2-11 illustrates the preliminary stage for the failures to take place in a coating system [68]. Well control and precautious steps have to be incorporated in order to make sure the device can be fabricated smoothly from the beginning of the process until the end of the production.

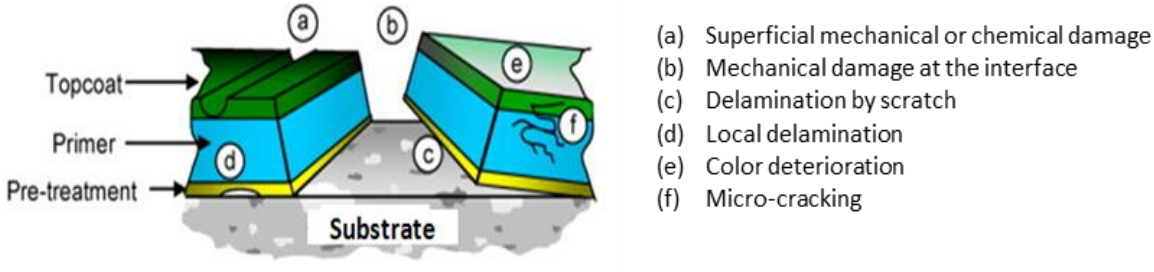


Figure 2-11: Different types of failures in a multilayer bonding scheme [68].

### 2.2.1 Substrate technology

Substrate is important for assembly of different electrical components. The requirements for the substrate technology have been incrementally increased by the ongoing development of the packaging industry especially for MCM application. Some fundamental properties of the substrate must be well considered to ensure the good performance of the system [39]:

(a) Smaller CTE mismatch between materials

(b) Good thermal conductivity

(c) High mechanical stiffness

(d) Stable in high temperature environment

(e) Low electrical permittivity

Table 2.1 Organic and inorganic types of MCM substrates

| **Organic-inorganic Substrates** | **Inorganic Substrates** |
|---|---|
| Epoxy-Glass | Glass-ceramic |
| Maleimide-Styril | Mullite + Silica + Alumina |
| Polyimide-Glass | Aluminum Nitride |
| Epoxy-Kevlar | Alumina + Borosilicate |
| | Low TCE Polyimide |
| | Alumina |
| | Silicon Nitride |
| | Berryllium Oxide |

For substrate selection, there are two main categories, including organic materials and inorganic materials as listed in Table 2.1. The extraordinary properties of ceramic substrates ($Al_2O_3$, AlN, SiN etc.) have attracted intensive interest for metallization in microelectronic packaging application. Besides of superb stability in the aspects of mechanical, thermal and chemical, it is also a non-toxic, and inexpensive material with high hardness and good wear resistance [69-73]. Its superior properties are recommended for microelectronic devices to further improve the reliability and able to operate under harsh environment.

However, metal film adhesion with ceramic substrate is intrinsically low due to the poor wetting of metals on ceramics. Intimate contact between these two materials is difficult to achieve and maintain. Various joining methods such as eutectic joining [62, 72-76]; ion beam dynamic mixing[77]; casting bonding [62]; spraying [78, 79] etc. have been explored to obtain optimized bonding. An adhesion layer of materials such as titanium [70, 80], chromium [80, 81] or zirconium [39] is deposited for adhesion improvement. However, the adhesion causes higher cost and may bring in additional reliability concerns. An ideal solution would be direct deposition without the adhesion layer.

### 2.2.2 Metallization

Aluminium (Al) has been widely used for metallization layer for the past 30 years. By increasing the electrical conductivity, reducing the overall capacitance, as well as lowering the power utilization, Copper (Cu) has been brought up as the

current favorite in the field of microelectronic [39, 82, 83]. Furthermore, higher melting point of Cu (1085 °C) compared to Al (660 °C) is leading to a better resistance to the problem of electromigration and capable to operate under the high temperature environment.

Besides electrical properties, the chemical properties of materials are a discussion topic in metallization scheme. Al and Cu tend to oxidize when removed from the vacuum atmosphere. The oxidation rate of Cu is slower and normally takes place at the temperature above 350 $^{o}$C. Conversely, Al will react with oxygen vigorously compared to Cu[82]. There is no pure Al exists in nature due to the extreme strong bonding at the interface.

Silver (Ag) and gold (Au) have also been listed as another two favorable options. They are also known as noble metals (d-block) in the periodic table in the group of 11. The resistivity of Ag (1.60 μΩ-cm) and Au (2.27 μΩ-cm) are comparable with Cu (1.72 μΩ-cm) [84]. Gold is an excellent corrosion protector for the devices; but the adhesion of gold to any material is always a tough issue to be solved, it is also a fast diffuser which might destroy the device effortlessly. As for Ag, even though the conductivity is slightly higher than Cu, the speedy diffusion of Ag make it not a good choice in the processing and the corrosion rate of Ag is very high [85]. Based on the characteristics and the material properties, Cu is chosen as the most suitable candidate for metallization material in this study.

### 2.2.3 Considerations for good adhesion

Some precautious steps have to put in mind in order to prevent debonding or delamination during processes. A diagram as depicted in Fig. 2-12 [10] is used to summarize the concern of adhesion-delamination in microelectronic and MEMS. In order to secure a strong bonding at the interface, it is crucial to have a good fundamental understanding for all the components and elements in a bonding system. With the knowledge attained, it is more accessible to the design stage and the material selection steps. It is important to select suitable materials with good compatibility in a packaging system. Simulations under various conditions can also be done during the design stage to scrutinize the possibility of interfacial failures.

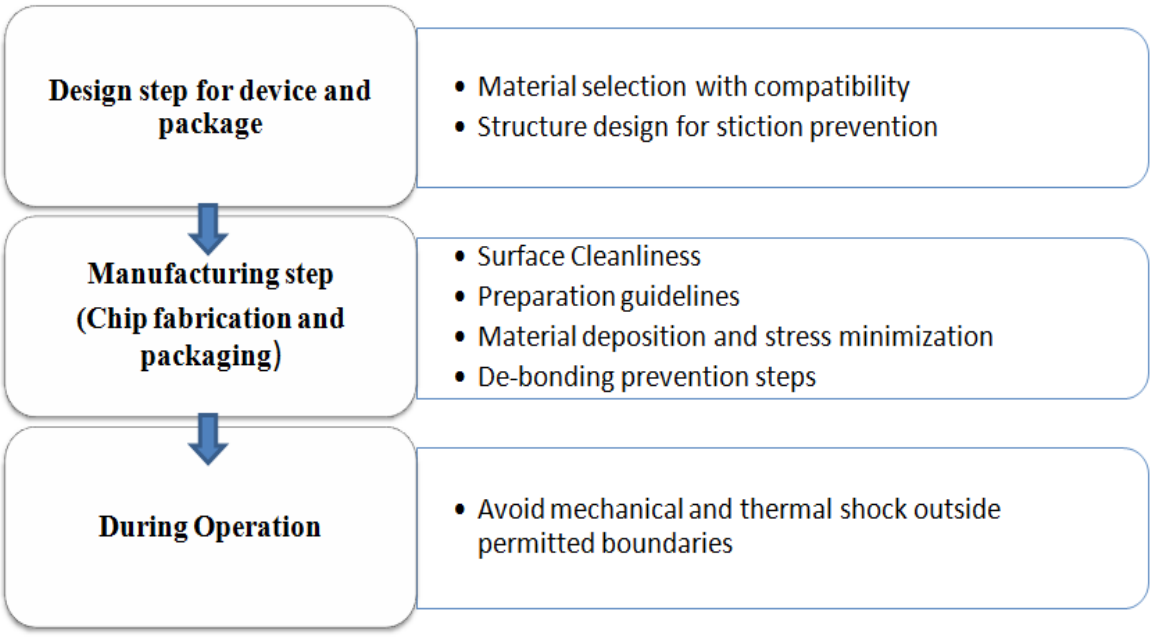


Figure 2-12: Debonding prevention in microelectronic and MEMS [10].

There is no assurance at which the problem of delamination is not going to happen in the subsequent steps even though the material selection and the design steps have been settled. During manufacturing, proper guidelines have to be included and standardized for the coating procedures such as surface pre-treatment and coating parameters. Good control throughout the deposition process is crucial to determine the total residual stress in a bonding. Different types of testing such as mechanical, electrical and thermal has to be incorporated during the operation stage in order to investigate the functionalities of device under different conditions. In summary, considerations throughout the process are vital to accomplish the appointed performance.

### 2.2.4 Bonding mechanisms

Adhesion mechanisms between two objects are important to achieve excellent bonding. Bond formation between heterogeneous materials is basically developed by several adhesion theories:

(a) Adsorption: It is a process whereby the adsorbate (ions, atoms or molecules) will transport to and adhere on the substrate surface without penetrating inside the bulk material. The contact between the substances is determined by the wetting behavior of the adsorbent.

(b) Diffusion: Kinetic movement of atoms or molecules from the region of low concentration to the region of high concentration. The extent of diffusion at

the interface is the key factor to determine the adhesion strength of the bonding.

(c) Chemical bonding: Creation of bond chemically through the interaction between atoms or molecules. The bond formation may result from covalent bonding, ionic bonding, hydrogen bonding, or metallic bonding.

(d) Physical locking: Non-planarization of the substrate surface induces mechanical interlocking bonding mechanism between two materials especially at the porous regions. Larger area in contact is attributed by the rough surface of the substrate material. However, detachment or other failures may be initiated by the excessive surface roughness.

(e) Intermediate layer: An extra layer with different material is inserted in between film and substrate in a bonding system. This thin layer in nano-scale is normally used to improve the adhesion between materials.

## 2.3 Surface Modification Prior to Bonding

An interface symbolizes the interaction between two individual forms of matter when they are in contact. The interface formation can be assembled either from similar or dissimilar materials and phases. The layer in contact is dependent mostly on the material properties which might be influenced by surface modifications as listed below [86]:

(a) Compatibility

(b) Surface Texture

(c) Interfacial electrical properties

(d) Wear and tear

(e) Corrosion

(f) Wettability

Hence, surface science is an important topic for adhesion or bonding. The surface condition or the surface state for the materials being bonded can be described with several aspects: (i) original geometrical shape of the subject to be bonded (ii) mechanical surface finish (iii) chemical surface finish and (iv) physical surface finish. For bonding with a complex geometrical shape, material with high flexibility is needed to adapt the surface structure of the substrate. The smoothness of materials can be modified by mechanical surface finish such as etching or polishing method. For chemical surface finish condition, the surface chemical state can be modified to improve the interfacial bonding through chemical reaction between materials. Physical surface finish is caused by the defects on the surface such as grain boundaries, pores, grooves, etc.

### 2.3.1 Surface roughening

The joint created between materials can be portrayed by the basis of their geometrical shapes at the interface. When they are in contact, strong bond is

formed via a full connection on the entire region of the bonded materials [87]. Therefore, surface roughening is suggested in some cases in order to increase the substrate's flexibility to adapt the shape of the material being bonded.

From Kim et al. [15] and C. Yang et al. [17], topography of polyimide substrates have been modified by increasing the surface roughness using plasma pre-treatment at the power of 125 W and 200 W respectively . The main purpose was to reduce the flatness of substrate in order to develop a better bonding for metal-polymer structure through mechanical interlocking bonding mechanism. Hence, surface compatibility or surface texture is the major factor influencing the bonding geometrically.

### 2.3.2 Polishing

It is not perfectly accurate that rougher surface helps to enhance the interface bonding. In some cases, extreme uneven surface might cause more failures to happen such as cracking, reducing the conductivity of the system, and scattering related problem etc. Surface polishing either mechanically or chemically is a good way to reduce the high irregularities of the surface structure to a certain extent.

For mechanical polishing method, solid particles with high pressure are used in the process with the presence of chemically inert solution to flatten the substrate. However, the vigorous interaction between particles and substrate might create scratches on the surface and degrade the interfacial adhesion. On the other hand,

chemical polishing can only apply to certain types of materials [87] and the toxicity level is undesired. The choice of mechanical or chemical polishing depends on the type of materials, desired surface morphology, processing cost, and so on.

### 2.3.3 Chemical finishing

For chemical finishing, modification of a material's outer surface is done by adding a layer of chemical constituents or removing the compounds from the surface for various functionalities. For chemical etching, it is commonly adopted to eliminate the organic or inorganic impurities on the substrate surface [88, 89]. In addition, it is used to remove the sacrificial layer of certain materials such as oxide layer from the silicon wafer prior to coating. The chemical solutions used depend not only on the material properties, factors such as concentration of the etchant, time and temperature are also the crucial considerations. A good and accurate control is necessary to prevent any undesired circumstances or damages [90].

The second approach of chemical surface finish is to form a specific layer of chemical constituents on the surface for adhesion improvement between materials through the chemistry reaction at the interface. This layer of adhesion promoter is capable to modify the wetting behavior (hydrophilic or hydrophobic) of the surface to be bonded. In the photolithography process, a chemical named hexamethyldisilazane (HMDS) is normally utilized to enhance adhesion of photoresist to the wafer and to increase the degree hydrophobicity of the wafer's

surface. HMDS can be applied in the phase of liquid or gas during the priming stage [91].

## 2.4 Adhesion Measurements

In the field of semiconductor, adhesion is always a crucial topic for discussion. A proper and reliable methodology is necessary to measure the interfacial adhesion strength. Over the years, a variety of measurements have been developed. The approaches used can be classified with different categories such as qualitative or quantitative; destructive or non-destructive [92]; in the unit of force (N), stress ($N/m^2$) or energy (N/m) [93]. There is no standard method to measure the interfacial adhesion for a coating system. Selection of testing method generally depends on the test structure. For an ideal measurement, three criteria should be considered: (i) quantitative analysis integrated with numerical data (ii) simple preparation with readily accessible equipment (iii) relevance data with the final application [92]. Several types of testing techniques are selected and summarized in Table 2.2.

Table 2.2: Summarization of different adhesion measurements

| Type of test | Method | Measurement | Unit | Destructivity |
|---|---|---|---|---|
| **Qualitative** | Scotch tape | - | - | Destructive |
| | Abrasion | - | - | Destructive |
| | Impacting | - | - | Destructive |

| | | | | |
|---|---|---|---|---|
| **Quantitative (Semi)** | Grinding | - | - | Destructive |
| | Scratch | Force | N | Destructive |
| | Tensile | Stress | $N/m^2$ | Destructive |
| | Shear | Stress | $N/m^2$ | Destructive |
| | Peel | Energy | N/m | Destructive |
| | Four Point Bending | Energy | N/m | Destructive |
| | Indentation | Energy | N/m | Destructive |
| | Brazil Nut | Energy | N/m | Destructive |
| | Surface acoustic waves | Young Modulus | - | Non- destructive |
| | Dynamic modulus | Young Modulus | - | Non- destructive |

### 2.4.1 Tensile test

This is the most primary mechanical technique for adhesion measurement. It is also known as pull test or tension test. Quantitative measurement of this method enables the users to analyze the amount of force (N) required to detach the coating from the substrate material. This can be done by increasing the loading force in the direction normal to the testing specimen as illustrated in Fig. 2-13 (a) under a constant pulling rate Results can be obtained in the unit of stress (Pa) by dividing the specimen area (eq. 2.1).

$$\sigma = F/A, \quad (2.1)$$

where $\sigma$ is the uniaxial stress, F is the normal force applied and A is the area of the specimen.

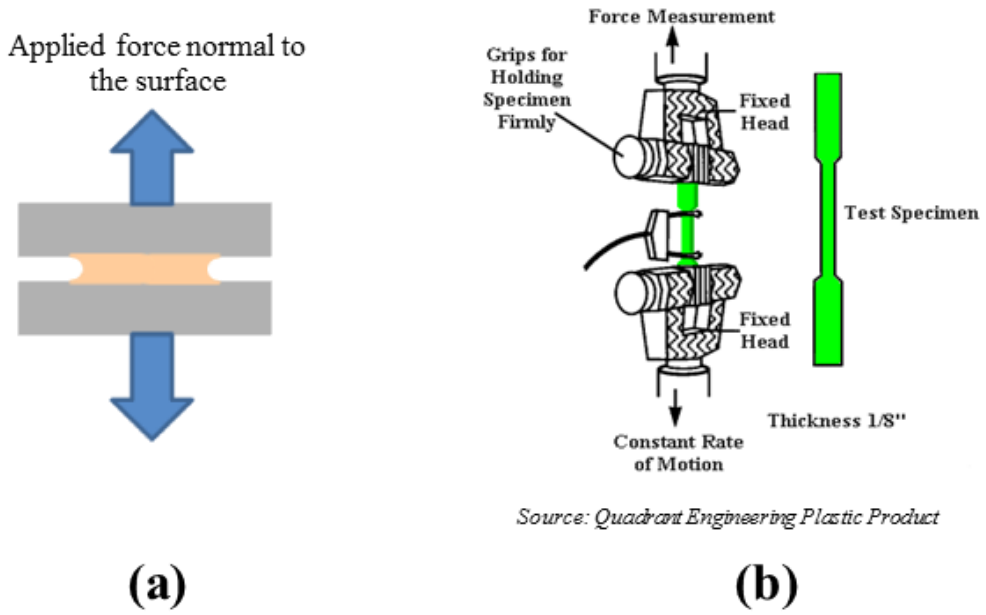


Figure 2-13: Tensile test configuration (a) adhesion test (b) elongation test.

Besides interfacial strength measurement, this method can also be applied to a wide variety of materials (ductile, brittle, rigid or flexible) with specific dimensions for better accuracy. For material with high ductility and elasticity, elongation analysis of the material can be done using dog bone-shaped structure as illustrated in Fig. 2-13 (b). A stress-strain diagram can be plotted and checked on the material properties such as elastic deformation and plastic deformation, as well as the Young's modulus of the tested material.

The preparation step of this technique is very straightforward, and various brands of tensile testers are commercially available [93]. There are two main weaknesses of this method. Firstly, broad scattering of the analyzed data affects the precision of the result. A number of tests have to be repeated for the samples

under the same conditions coupled with statistical analysis in order to increase the repeatability of the data [92]. Secondly is the issue of alignment between studs and sample. The problem of misalignment during the gluing process and the amount of glue applied will strongly affect the final result. Precautious and patient are very imperative for this test methodology. However, tensile test is still the most trustworthy and consistent technique among the adhesive force measurements [94].

### 2.4.2 Shear test

Compare to direct tensile test, this technique is considered less favorable for bond strength measurement. The direction of shear force is different from tensile test. The force is applied in the direction parallel with the sample as shown in Fig. 2-14 at constant velocity. For shear test, it is usually conducted for the coating system whereby there is an adhesive layer in between two materials and provided the upper material is thick enough for shearing. The force required to break the sandwich system per unit area is calculated as shear stress in eq. 2.2.

$$\sigma = P/S, \tag{2.2}$$

$$\text{Ɛ} = x/h, \tag{2.3}$$

where $\sigma$ is shear stress, Ɛ is shear strain, S, P, x and h are the bonding area, shear force, displacement and thickness of the adhesive layer respectively.

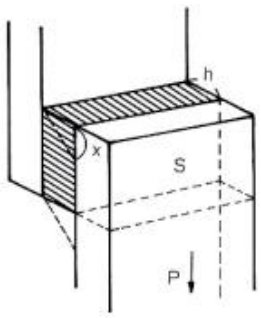


Figure 2-14: Shear test geometry [92].

This technique is not recommended for direct thin film coating on substrate due to the thickness limitation. Although the preparation step is easy; the uniformity and viscosity of the adhesive will greatly affect the accuracy of the result. In addition, constant pressure during bonding is needed for every test samples.

### 2.4.3 Peel test

Peel test with different configurations are illustrated in Fig. 2-15. Both tensile loading and shear loading are included while performing this test, the ratio obtained from these loadings is known as loading mode-mixity [92]. This test method is suitable to measure the adhesion energy of a flexible coated film, provided the film is easy to be stripped off from the substrate. Factors such as thickness of the film, material properties of the substrate and the film, peeling rate and peeling angle are needed to be considered on the final data compilation [95]. It

has been reported by Kim et al. that the peeling strength of a coating system was different with thickness although there was no changes on the true interfacial adhesive strength [96].

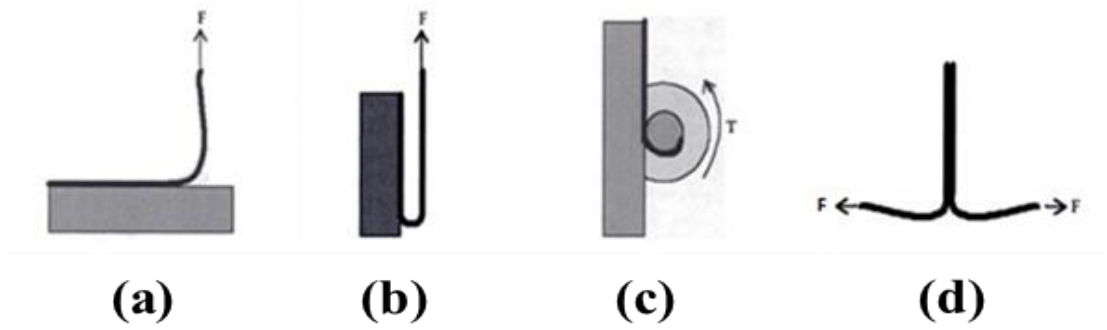


Figure 2-15: Four different types of peel test measurements: (a) $90^{o}$ peel test (b) $180^{o}$ peel test (c) climbing drum test (d) T-peel test [92].

There are two ways to conduct the peel test, either is directly holding the coated film or peeling from the backing material on top of the film. However, the accuracy for the backing approach is poorer due to unstable failure at the peeling surface [92]. The second disadvantage of this method is that the peeling strip of the specimen is not easy to initiate and it might be varied for different samples. However, users can accurately control the delamination rate and the locus of failure by this method.

### 2.4.4 Scratch test

Scratch test (Fig. 2-16) is also known as stylus test or scribe test [97]. It is an adhesion technique used to determine the failure occurred at the point of critical loading by moving the diamond stylus along the surface tangentially [98]. For bulk material, cohesive failures such as plastic deformation or cracking can be observed. For coated material, detachment of coating material from the substrate can be analyzed under the higher load regime.

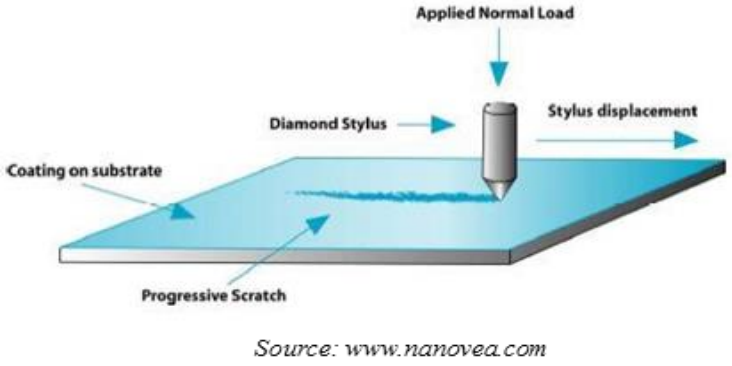


Figure 2-16: Schematic illustration of progressive scratch test [97].

There are two approaches for scratch test: (i) constant load test with a stable speed (ii) progressive load test with a constant loading rate. The critical load can be studied through the microscopic inspection, the fluctuation along the scratch by the frictional force recording, the acoustic emission detection by noticing the elastic waves created from the cracks, or the scratch depth sensing due to the rapid change

of depth. Nonetheless, study of scratch path using microscope observation is still the most consistent and reliable approach in the scratch analysis.

According Benjamin and Weaver in 1960 [99], the shearing force used to detach a coating system can be calculated based on the critical load needed (eq. 2.4).

$$F = \frac{a\,P}{\sqrt{r^2 - a^2}}, \text{ where } \quad a = \sqrt{\frac{W}{\pi\,P}}. \tag{2.4}$$

where $F$ is the shearing force per unit area, a is the radius of stylus contact circle, r is the radius of the stylus tip, P is the hardness of the substrate, and W is the critical load .

However, this calculation method is not fully supported for all types of bonding. It can only be applied on the specimen with fully detachment at the interface [100]. For a very soft coating material, it might stick around the stylus tip and amass at the side of the scratch path. In addition, the high indentation force during the test will also give rise to the residual stress at the interface and is leading to the deformation of the deposited film and the substrate.

### 2.4.5 Four point bending test

Beam bending test is commonly used to measure the flexural strength of a material. Besides bending strength analysis, four point bending test (Fig. 2-17) is employed to quantify the interfacial adhesion strength between materials [101, 102]. For adhesion measurement, a preset cut has to be drawn in order to produce a constant bending moment between the inner pins. Debonding failure will be initiated when there are two mechanical forces applied at the specific distance from the pre-crack region. The interface fracture energy or the energy release rate of the bonded system can be calculated using eq. 2.5.

$$G_c = \frac{21\left(1-v^2\right)P^2l^2}{16EB^2h^3} \tag{2.5}$$

where $G_c$ is the critical energy release rate, $v$ and E are the Poisson's ratio and Young's modulus of the substrate , P is the loading force, l is the distance between the loading pins and the supporting pins, B is the sample width and h is the thickness of the substrate.

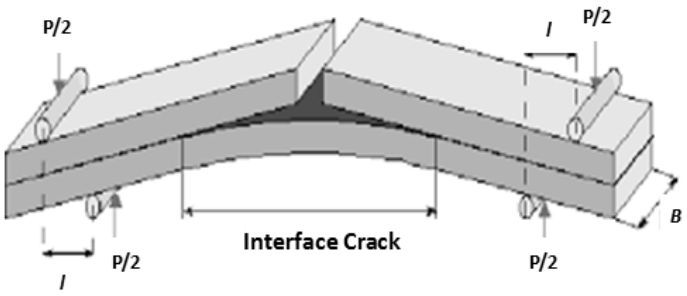


Figure 2-17: Schematic of four point bending test [102].

For this type of measurement, factors such as the notch depth, the testing speed, the size of the sample, and separation between the pins will give an impact on the data scattering. An experiment has been carried out by R.Shavie et al. [102] using Si-low k dielectric bonding system. In order to increase the percentage of precision, a notch at about 80 - 90% of the thickness from the top layer with the working speed at 0.06 to 0.08 μm/s was recommended.

## 2.5 Ceramic Metallization

Although ceramic metallization is a well known and highly developed topic in various applications, for example electronic and semiconductor, aerospace and military, medical and life science, power generation, oil and gas etc.; it is still a subject of interest in industrials and research institutes. There are three main characteristics for metallization: (i) high reliability with strong bonding (ii) reduction of cost and time during process (iii) waste lessening for eco-friendliness.

Over the years, works have been carried out in order to optimize the interfacial bonding between metal and ceramic substrate. Besides the factors such as variation of bonding parameters, transformation of the bonding structure under different conditions or altering the surfaces to be bonded, a number of bonding methods have been extensively studied. Table 2.3 summarizes some reported metallization schemes and adhesion test methods used. Discussion on different types of bonding is made next.

Table 2.3: Metallization methods on ceramic substrates

| Method | Material | Measurement | Observations |
|---|---|---|---|
| [75] Eutectic | Cu-$Al_2O_3$ | 90° peel test<br>12.1 kg/cm | - High processing temperature<br>- Special controlled of oxygen partial pressure |
| [62] Casting | Al-$Al_2O_3$ | 90° peel test<br>13.0 kg/cm | - High processing temperature |
| [76] Cold gas spraying | Al-$Al_2O_3$ | Tensile test<br>31.0 MPa | - High spraying pressure<br>- Problem of uniformity<br>- Used of adhesion layer |
| [103] Plating | Ni(p)-$Al_2O_3$ | Tensile test<br>51.6 MPa | - Problem of oxidation<br>- Void formation at the interface |
| [104] Transient liquid | Al-$Al_2O_3$ | Shear test<br>64.0 MPa | - High bonding temperature<br>- Used of interlayer with many components<br>- Precise controlled on the wt% |

| | | | |
|---|---|---|---|
| [105] Sputtering | Cu-$Al_2O_3$ | - | - Used of adhesion layer |
| [77] Ion beam dynamic mixing | Cu-AlN | - | - Used of adhesion layer |
| [106] Pulsed high energy density plasma | Cu-$Al_2O_3$ | - | - Unstable at high temperature<br>- Difficult to synthesize<br>- Needs of high voltage |
| [107] Co-firing process | W-AlN | Tensile test 3.8 $kg/mm^2$ | - High processing temperature |
| [107] Screen Printing | Ag/Pd-AlN | Tensile test 1.9 $kg/mm^2$ | - High processing temperature |
| [108] Screen Printing | Au-Lead Borosilicate Glass | - | - High processing temperature<br>- Toxic |

### 2.5.1 Eutectic bonding

This bonding method is not a new technology for ceramic metallization. In 1976, direct bonding of metal to the ceramic material using eutectic temperature was first discovered by Burgess and Neugebauer [109]. For direct copper bonding (DCB) [60, 62, 72-75, 110-112] using eutectic bonding technique is well established in MCM packaging for the metallization scheme.

Theoretically, DCB is formed when the temperature has reached in the range of 1065 °C to 1085 °C, which is the eutectic temperature for the molten eutectic to be coexisting according to the Cu-O phase diagram as presented in Fig. 2-18. For direct bonding to $Al_2O_3$ substrate, a piece of Cu foil is placed on top of the substrate before placed it in the furnace. With controlled amount of oxygen gas, a liquid is formed at the interface when the heating temperature is above 1065 °C; this layer of liquid will then form a layer of copper-oxygen eutectic skin in between Cu and $Al_2O_3$. Consequently, formation of strong bond can be achieved when the system is cooling down to room temperature. The final product produced at the interface either is $CuAl_2O_4$ or $CuAlO_2$. According to reports in [72, 75, 109], the oxygen concentration or partial pressure is the key factor to determine the interfacial adhesion strength of the system.

Yuichi Yoshino [75] has inspected on the role of oxygen for DCB system. He discovered the adhesion strength of the bonding was strongly affected by the dissolved-oxygen concentration at the interface. In this experiment, 90° peel test with peeling rate of 50.0 mm/min was used for the adhesion measurement. The partial pressures of the oxygen used in the experiment were 3, 5 and 8.5 Pa. From the peel measurements, he has reported the peeling strength was reduced with higher oxygen partial pressure, which might be due to the voids and excessive oxide formation. The peeling strengths were 12.1 kg/cm, 8.2 kg/cm and 6.7 kg/cm respectively.

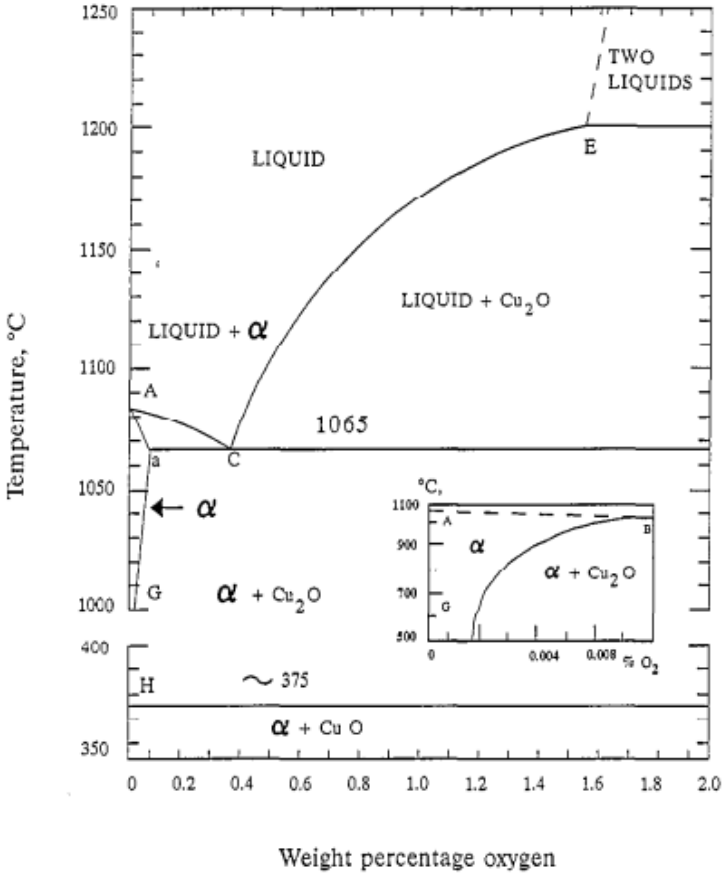


Figure 2-18: Cu-O phase diagram [113].

As for the directly bonded Cu to AlN substrate, the preparation step is more complicated compared to the $Al_2O_3$ substrate. Pre-oxidizing of AlN to create a layer of $Al_2O_3$ on top of AlN is needed before the eutectic bonding [74, 114]. This can be done by either chemical reaction at low temperature or oxidation at high temperature [72]. Besides high temperature prerequisite, elevated technical asset is needed for this method. Due to the complexity and high cost, alternative bonding techniques are needed to replace the eutectic bonding method.

### 2.5.2 Casting bonding

As mentioned, direct bonding of metal layer to the ceramic substrate is a well-established method since 30 years ago. For directly bonded aluminum (DAB), there are some limitations. Firstly, the strong interfacial bonding is affected by the oxide layer on the aluminum [62, 115, 116] on either $Al_2O_3$ or AlN substrate. Second factor is due to the poor compatibility between materials [115].

X.S Ning et al. [62] used casting bonding method to join an Al block with purity of 99.99 % onto a 96 % $Al_2O_3$ plates as illustrated in Fig. 2-19. The Al block was inserted into the carbon die before being pushed it into the ceramic plate. The carbon die with the Al block was then heated under the nitrogen atmosphere at 1023 K in order to reduce the oxygen level and to melt the Al block. The melted Al was then pushed into the ceramic plate using a piston. The bonding process was completed after the solidification process at room temperature. $90^o$ peel test was used for the interfacial adhesion measurement. The measured adhesion strength was above 13 kg/cm for this type of bonding coordination.

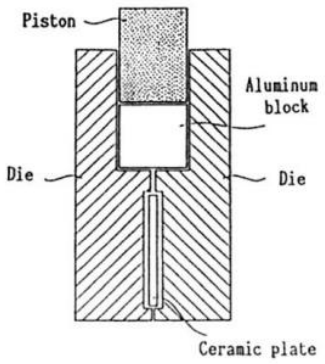


Figure 2-19: Schematic illustration of casting bonding for Al-$Al_2O_3$ bonding system [62].

### 2.5.3 Cold gas spraying (CGS)

Spraying is an alternative way to deposit a layer of metal film to the ceramic substrate. There are two types of spraying energy: thermal energy [117-119] and kinetic energy [78, 79, 120-122]. For thermal spray coating, the generated molten spray particle either is in the form of completely melted or partially melted under the high velocity condition. Bond formation can be successfully done when the particle is in the contact with substrate and rapidly quenched. The creation of the molten particles can be done via combustion blaze or plasma jet [123] and it can be applied on wide range of materials such as polymers, metals, or oxide materials.

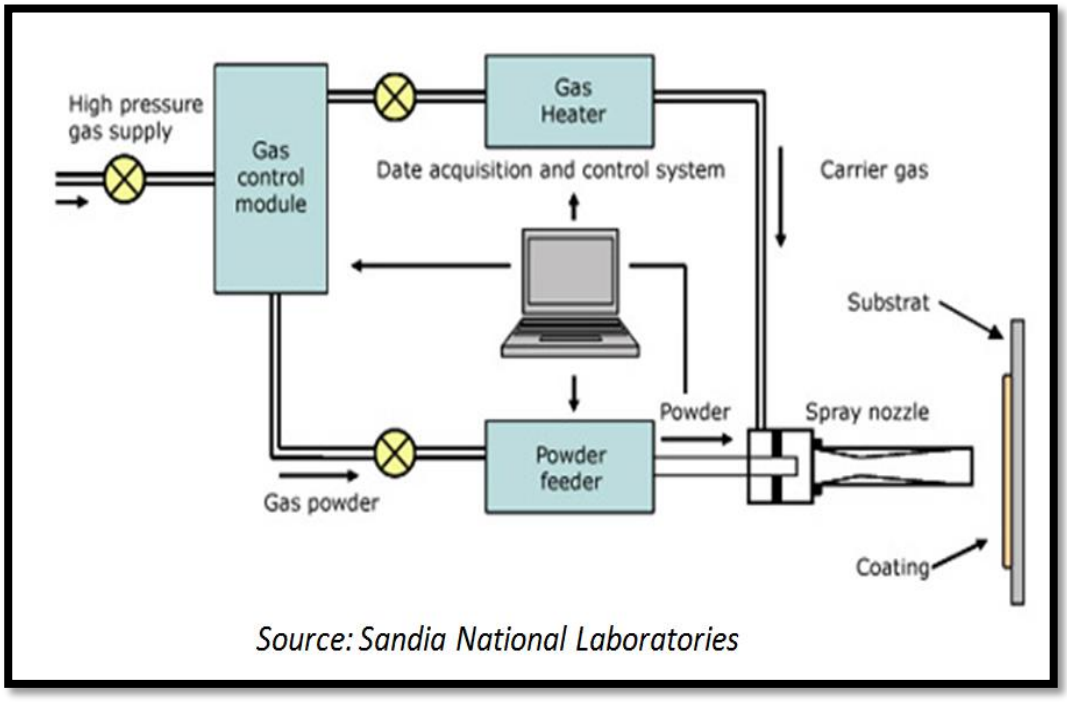


Figure 2-20: Diagram of cold spraying process [118].

Cold gas spraying (Fig. 2-20) utilizes the kinetic energy to accelerate and to project the particle onto the substrate surface. The bond quality is strongly dependent on the plastic deformation of the injected particles. With this method, a very dense coating can be easily achieved by the tremendous velocity inside the chamber.

B. Wielage has investigated the cold gas spraying method to produce an electronic circuit board by spraying the Cu powder onto the $Al_2O_3$ substrate [78]. Water atomized Al powder was coated in between the Cu layer and the $Al_2O_3$ substrate for adhesion enhancement. The process was done at 300 $^oC$ and the velocity in the range of 0.15 m/s to 0.30 m/s. The adhesion strength achieved was 31 ± 4 MPa. There was an increment up to 58 ± 6 MPa after annealed at 300 °C for 10 hours. From Fig. 2-21 (a), high density of Cu film and Al layer was clearly revealed, but with poor uniformity. From the STEM image in Fig. 2-21 (b), boundaries of the sprayed Al particles were observed and the problem of delamination was also discovered at the interface.

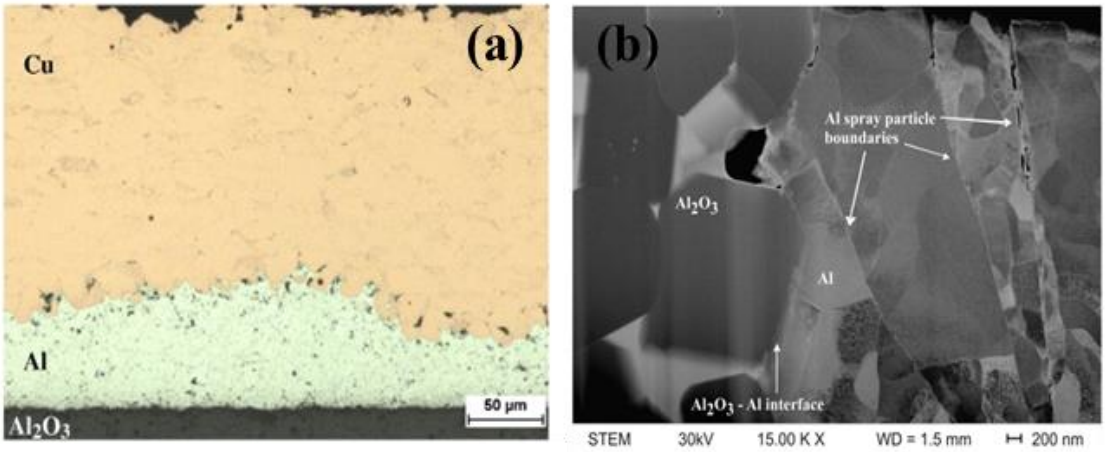


Figure 2-21: Cross sectional images of (a) Cu-Al-$Al_2O_3$ bonding system by CGS method (b) STEM image of Al-coating on the $Al_2O_3$ plate [78]

### 2.5.4 Transient liquid phase bonding (TLP)

Transient liquid phase bonding consists of the characteristics for both of the diffusion bonding and brazing bonding methods [104, 124, 125]. This joining technique used a thin interlayer to provide a strong bonding between two parent materials. The interlayer has to be first melted, diffused into the parent materials and followed by dissolution at which the thickness of the liquid is wider than the interlayer at the original state. The diffusion rate is relied on the diffusivity of the materials and the heating rate during the bonding process. Isothermal solidification starts to take place until there is no liquid and the process ends with homogenization in order to produce a structure with indistinguishable concentration profile. The simplified kinetics of the TLP joining is shown in the schematic in Fig. 2-22. Good adhesion strength is achievable by this method, but it is very time consuming and high production cost.

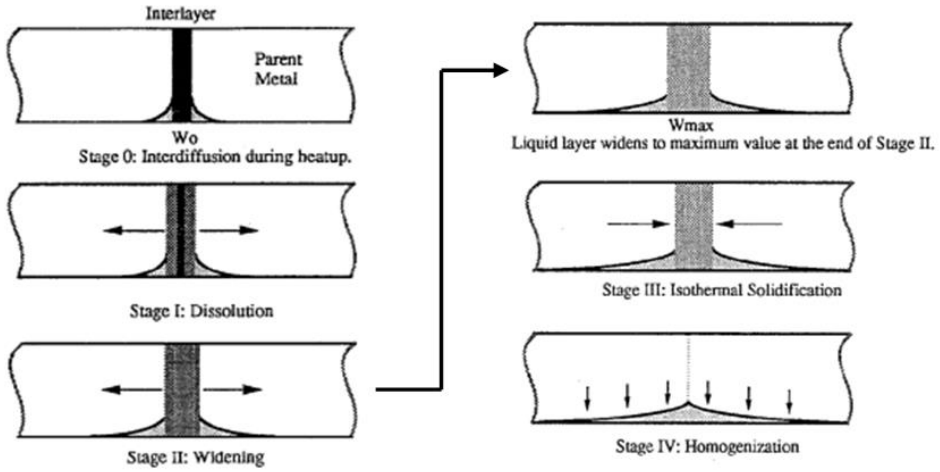


Figure 2-22: Bonding kinetics of transient liquid phase joining technique [126].

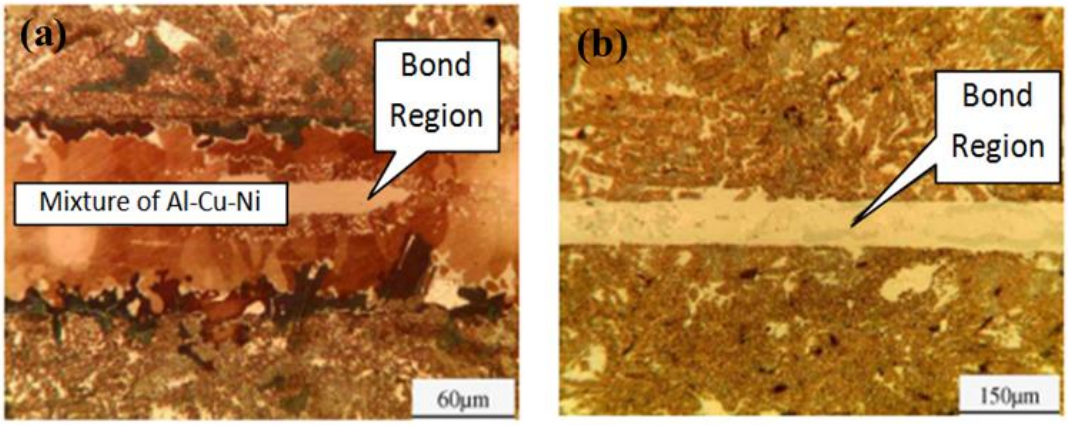


Figure 2-23: Cross sectional views of Al-$Al_2O_3$ bonding system using Cu-Ni-Cu interlayer with bonding time at (a) 60 min and (b) 75 min [127].

Joining of Al to $Al_2O_3$ with Cu, Cu-Ti and Al-Cu interlayer in the bonding system was performed by G. F. Zhang et al. [104]. Difference weight percentages of Cu and Ti components were used to check on their effect to the shear strength and the wetting behavior of the sandwich system. Precise controlled on the wt% was necessary to optimize the interfacial adhesion strength. From J. C. Yan et al. [127], the Al-$Al_2O_3$ bond was done by using Cu-Ni-Cu interlayer at 580 $^{o}$C for 30 – 90 min in a vacuum furnace. Increase of shear strength with bonding time was observed. The highest shear strength of 102 MPa was achieved with 90 min of bonding time. The width reduction in Fig 2-23 might be due to the interdiffusion bonding between Al, Cu and Ni.

### 2.5.5 Physical vapor deposition (PVD)

Physical vapor deposition is a process by which a thin film of material is deposited on a substrate surface by physical reaction. Evaporation and sputtering are the two main deposition techniques in physical vapor deposition (Fig. 2-24). It

is commonly used for building IC interconnects, microelectronic devices, conductive coating in the range of few nanometers to micrometers.

There are three main types of evaporators including filament, RF heating and electron beam. For evaporation deposition, the source material is evaporated under high temperature condition. The vapor particles are transported from its source to the substrate under low pressure atmosphere. Thin film is formed on the substrate surface after the condensation process. Thin film with high purity can be deposited by this technique, but the step coverage of the film is very poor.

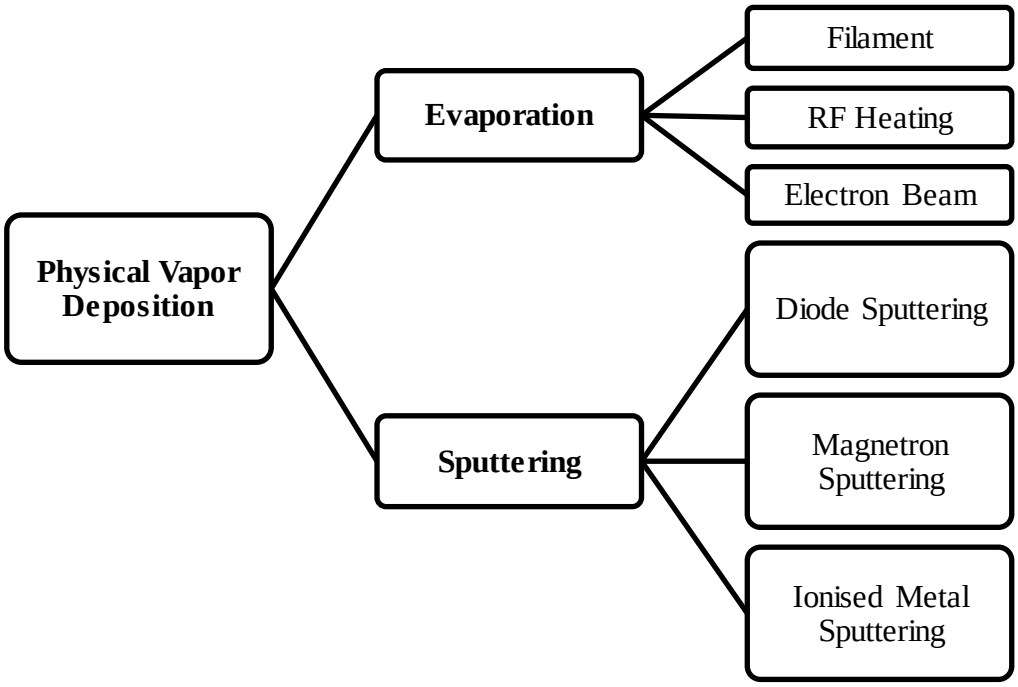


Figure 2-24: Physical vapor deposition technology.

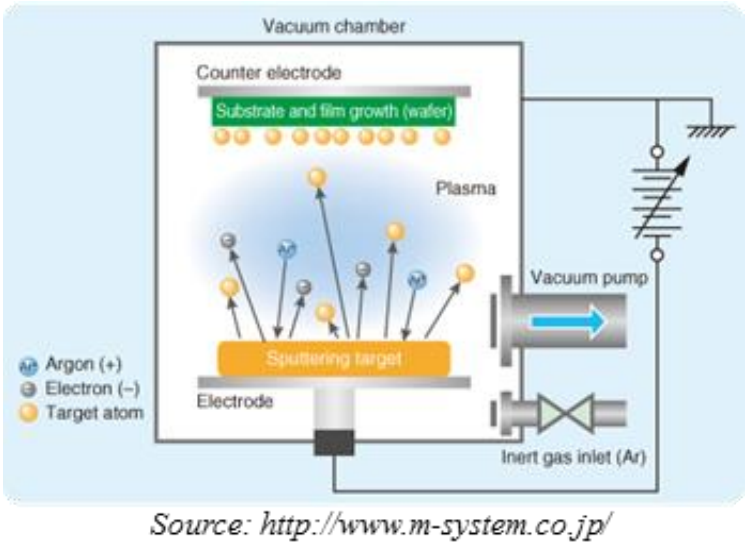


Figure 2-25: Schematic diagram of sputter deposition [128].

Sputter deposition (Fig 2-25) is a physical process whereby high energy particles strike on a target material with high purity, and dislodge atoms physically. The sputtered atoms migrate through a vacuum and eventually deposit on the substrate surface. The film properties can be modified by the sputtering conditions such as substrate temperature, working pressure, applied power, deposition temperature, target structure, target-to-substrate distance and so on. For example, D. Desideri et al. [128] has characterized the Cu thin film coated on glass-ceramic and glass by DC magnetron sputtering. Cu thin films with some hundreds of nanometers were coated in the pressure range of 0.13 to 6.6 Pa. The films obtained show similar structural and electrical characteristics on both glass-ceramic and glass substrate by applying the same working pressure. When the deposition

pressure increases, there was a large increase in resistivity caused by the grain boundary scattering.

Sputter deposition has been a good option for various applications with the following advantages: (i) able to deposit and maintain complex alloy (ii) capable to deposit high temperature and refractory metals (iii) good uniformity and film quality (iv) in-situ treatment step to provide better surface cleanliness prior to deposition (v) similar composition of deposited film from the source material.

## 2.6 Chapter Summary

The reliability and the overall performance of a device are greatly dependent on the processes during fabrication. The packaged devices have to be well operated and maintained its stability mechanically, electrically and chemically. From different types of failure mechanisms and failure modes, mechanical failure mode has been accounted for the highest percentage compared to other failure modes in microelectronic packaging application. In addition, interface debonding has been considered as the most critical issue in multilayer packaging system. Elevated stress state, high humidity and presence of defects are some of the major factors for mechanical failure to take place. It is important to implement the precaution steps during the design stage and the manufacturing step. In addition, surface modification such as etching, polishing or chemical finishing can also be incorporated in order to maximize the compatibility between materials, as well as improve the film adherence onto the substrate.

The bonding methods employed will also have significant impact on the interface adhesion between heterogeneous materials. The kinetics mechanism of the technique used for ceramic metallization will affect the overall bonding mechanism between metal film and substrate material. With a proper bonding technique and precise mechanisms introduced, an excellent adhesive strength can be achieved. Other considerations such as film uniformity, in-situ treatment prior to bonding, creation of defects during bonding, complexity of the fabrication step, etc. must also considered for proper bonding between materials.

For metallization on ceramic substrate, sputter deposition is a viable approach as it is compatible with existing semiconductor process, and does not require extremely high temperature as some other bonding techniques do. This technique is going to be used for the study of adhesion between Cu thin films and $Al_2O_3$ substrate in this thesis report.

# CHAPTER 3: EFFECT OF PROCESSING PARAMETERS TO THE COPPER-ALUMINA ADHESION STRENGTH

## 3.1 Introduction

Thin film deposition is an important topic for manufacturing, production and research applications. Applications are found in medical, telecommunication, microelectronic, optical, metallurgical and semiconductor industrials. Generally, there are two main categories of deposition: chemical vapor deposition and physical vapor deposition. Chemical vapor deposition is a process by which the film is coated through a chemical reaction on the substrate surface. Physical vapor deposition is relied on the physical motion such as mechanical, thermodynamic, and electromechanical to produce thin film on the substrate [129]. The deposition techniques are varied in the film quality and the degree of sophistication. For a given application, the ideal technique depends on the purpose of deposition, the substrate surface structure and the film thickness.

In microelectronics packaging, thin film deposition is one of the basic building blocks. This presents a great challenge to the system's reliability, especially under the extreme conditions. For metallization scheme, the unique properties of ceramic substrates have been extensively studied. A thin layer of metal film is coated onto the ceramic substrate using different bonding techniques

in order to optimize the joining conditions at the interface. However, the methods used have encountered problems such as film uniformity, fabrication steps complexity, high processing temperature, additional materials, interface failures etc.

Direct Cu-$Al_2O_3$ bonding was carried out in this study without additional steps and materials. It was done using sputtering deposition technique with DC magnetron sputtering mode. Coating can be done on large area and substrates with complex surfaces. The deposition rate is controlled by the time and the working power in order to maintain the film stoichiometry. Besides film thickness, quality (physical and chemical properties) of the deposited film such as film stress, film density, grain size, orientation etc. can also be modified by the sputtering parameters. In this study, effort has been made to improve the interfacial adhesion between Cu thin film and polycrystalline $Al_2O_3$ substrate by changing the deposition time, the working pressure and by employing the in-situ post deposition annealing step. The purpose of this study is to investigate the residual stress induced throughout the deposition process and its effect on the interfacial adhesion strength. Generally, there are two main types of residual stress components: (i) intrinsic stress and (ii) extrinsic stress [10, 21, 64]. Intrinsic stress is the residual stress induced during the processing steps. For example, there was a change of stress state from compression to tensile for sputter deposited molybdenum film on silicon substrate in a pressure range of 6 – 12 mTorr and the stress state will be different during the incorporation of nitrogen gas for molybdenum nitride film formation [63]. Extrinsic stress is affected by the mismatch of coefficient of

thermal expansion (CTE) between dissimilar materials. This can be avoided by selecting materials with smallest CTE mismatch. In a worst case scenario, high stress level may cause the problems of delamination, cracking, buckling, peeling or fracture and subsequently reduces the lifetime of the device.

## 3.2 Experimental Setup

### 3.2.1 Sample preparation

The polycrystalline $Al_2O_3$ substrates (purity of 96%) in the size of 4" (diameter) × 0.6 mm (thickness) were purchased from Semiconductor Wafer, Inc. The substrates have been polished to surface roughness (*rms*) of 10 – 150 nm by chemical and mechanical polishing method (CMP). Before deposition, the substrates were diced into small pieces by DISCO DFD 6361 with a speed of 1.0 mm/s. The cut substrates were in the dimensions of 3.0 mm × 3.0 mm × 0.6 mm. The sample cutting step was advised to be done prior to the deposition in order to prevent film cracking or film delamination. After that, cleaning step was conducted using organic solvent such as acetone and isopropyl alcohol under ultrasonic agitation at room temperature. The samples were then dried in an oven at 70 °C for 3 min.

The substrates were transferred to the sputtering chamber immediately after the surface cleaning step. Deposition of Cu thin film onto the $Al_2O_3$ substrates was

performed using PRO Line PVD 75 (Kurt J. Lesker Company). Before coating process started, the chamber was first evacuated by roughing pump and turbo pump in sequence in order to achieve the pressure of at least $5.0 \times 10^{-5}$ Torr. The ignition of plasma commences when the desired working pressure has been reached. The deposition power was fixed at 300 W. Argon gas was allowed to flow into the chamber continuously by adjusting the gas flow at a given flow rate. Before film deposition, target was pre-sputtered by closing the shuttle for the following purposes: (i) Removal of contaminants, (ii) Cleaning up the oxidized surface. (iii) Establishing an equilibrium state for the system with sufficient time provided. The pre-sputtered step was executed at 50 W for 5 min. Subsequently, the power was increased to 300 W for Cu film deposition. The substrate-to-target separation was set at 20.0 cm with the substrate holder constantly rotated in clockwise direction under the speed of 20.0 mm/s. After the deposition process, the target was shielded by the shutter and the power was turned off to 0 W. The flow of argon gas will then discontinued before venting. Finally, the chamber was vented by turning on the nitrogen gas valve and the specimens were taken out from the chamber when it has reached the atmospheric pressure.

*3.2.1.1 Different deposition pressures*

Investigation on the effect of working pressure to the interfacial strength was conducted by changing the deposition pressures: 1 mTorr, 5 mTorr, 10 mTorr, 15 mTorr and 18 mTorr. The deposition was all done at room temperature. Plasma

ignition is impossible when the deposition pressure is smaller than 1 mTorr. For this equipment, 18 mTorr is the maximum working pressure.

### *3.2.1.2 Different deposition times*

Three different deposition times (25 min, 50 min and 100 min) were used to control the thickness of Cu thin film. The deposition process was carried out under the working pressure of $1.5 \times 10^{-2}$ Torr and the deposition rate of about 0.3 nm/s. It was completed at room temperature.

### *3.2.1.3 Post deposition annealing*

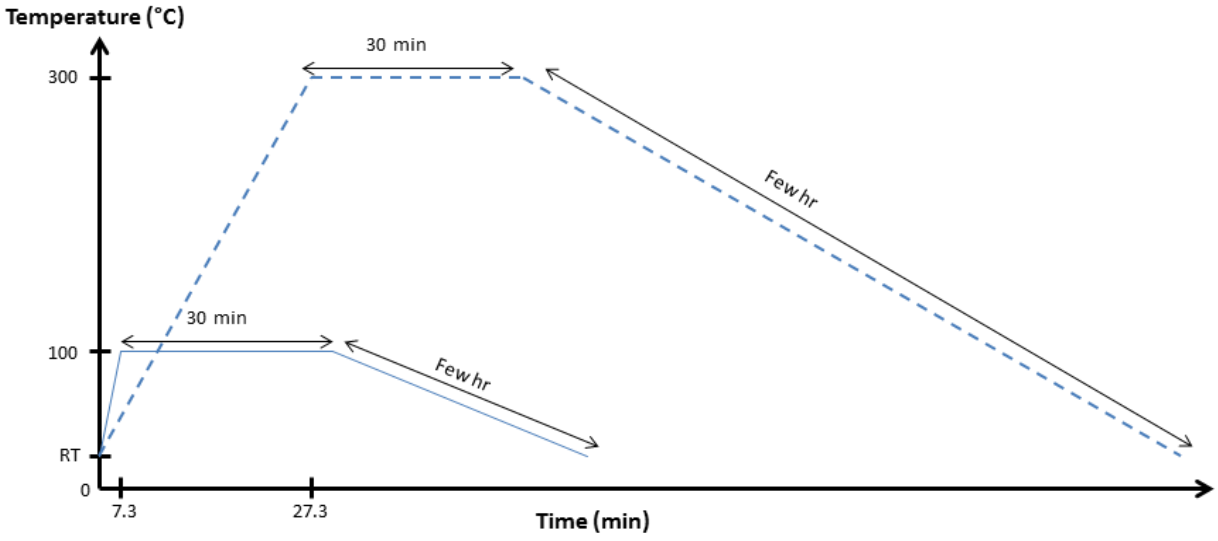


Figure 3-1: In-situ post deposition annealing profile for Cu-Polycrystalline $Al_2O_3$ bonding

After Cu film deposition process, the post annealing step was performed directly inside the sputtering chamber under vacuum condition to prevent oxidation. Two annealing temperatures (100 $^{o}$C and 300 $^{o}$C) were tested. The specimens were heated from room temperature to 100 °C and 300 °C with the heating rate of 10 °C/min (Fig. 3-1). A 30 min of dwell time was included. The specimens will be removed from the chamber when it has cooled to room temperature.

### 3.2.2 Materials characterization and adhesion measurement

Thickness of the deposited Cu thin film was checked using Alpha-step IQ surface profiler from KLA-Tencor. The profile of this measurement was conducted using step height analysis and the average value was taken based on three selected points. The deposition rate at different deposition parameters was then calculated from the measured thickness. The cross-sectional images of the specimens was captured using dual beam focused ion beam (FIB) built-in with in-lens scanning electron microscopy (SEM) from FEI Nova$^{TM}$ Nanolab DualBeam$^{TM}$ 600i. A trench was cut from the sample surface and tilted into a correction angle at 52° under the scanning voltage of 5 kV. The crystallographic structure of the sample was characterized by X-ray diffractometer (XRD) Shidmazu thin film in 2θ mode with the scan range from 10° to 80° and the scanning speed at 2 °/min. The operating voltage and current were set at 40 kV and 30 mA respectively with a secondary monochromator under Cu Kα radiation.

The XRD- $\sin^2\Psi$ method was used to determine the residual stress of sputtered thin film under different conditions. Psi angle ($\Psi$) is the tilt angle diffraction plane and the surface normal of the sample. The measurement was performed using Bruker D8 Discover XRD system with Cu $K\alpha_1$ radiation ($\lambda$ = 1.54 Å). The voltage was set at 40 kV while the current was fixed at 40 mA during the experiment. An apparent peak position will be selected for the stress analysis after a set of scanning at the fixed incident angles, $d^{\Psi}_{hkl}$. With the correlation between lattice strain and psi angle ($\Psi$) in the range of 0° to 50°, the residual stress created in a polycrystalline film will be computed from the LEPTOS 7.03 software.

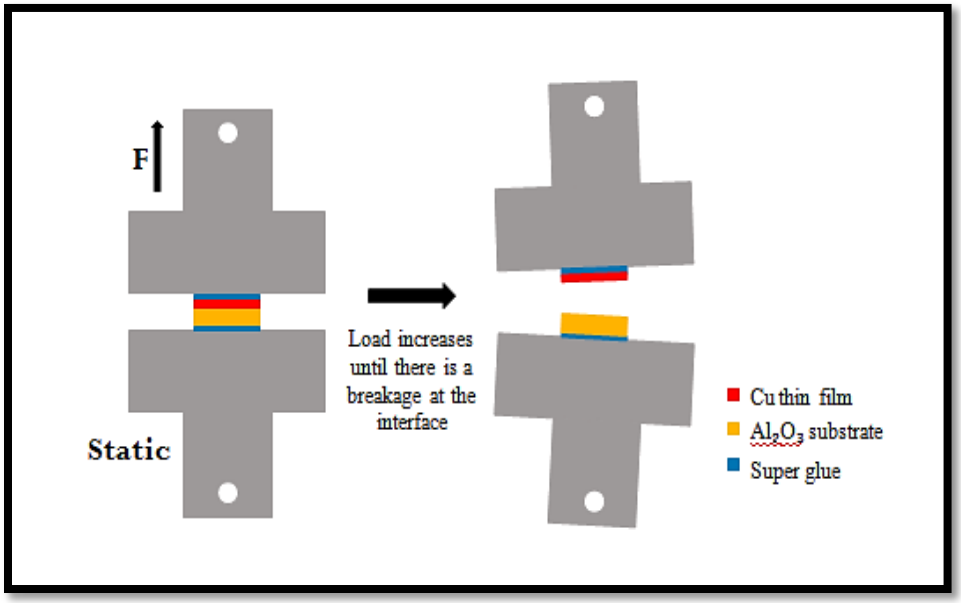


Figure 3-2: Schematic illustration of tensile test.

The debonding test was performed using Instron tester 5567 under tensile mode of testing. The interfacial measurement was illustrated in Fig. 3-2. After the deposition step, the specimen was pasted onto the test fixture using super glue (Selleys Supa Glue, Australia). The specimens were then sent for adhesion test under ambient condition with a load cell of 500 N. The testing speed was fixed at 10.0 μm/s. The adhesion strength was calculated from the average value of 10 pieces of specimens.

## 3.3 Results and Discussions

### 3.3.1 Effect of deposition time

Different Cu film thickness was obtained by changing the deposition time under the same sputtering conditions. The sputtering times are 25 min, 50 min and 100 min with the thickness measurement as shown in Fig. 3-3. For working power at 300 W, thickness of the deposited film increases as a function of deposition time with the deposition rate at about 0.3 nm/s.

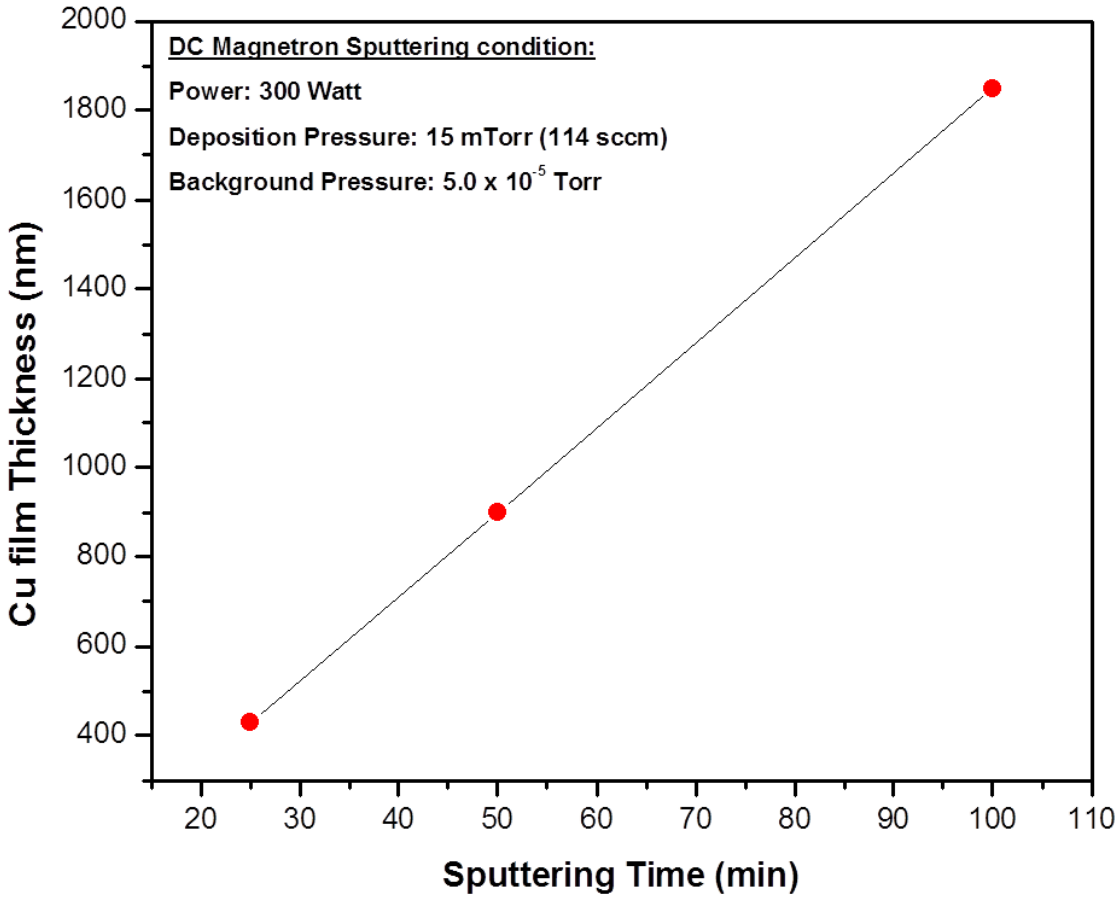


Figure 3-3: Thickness of Cu thin film as a function of sputtering time.

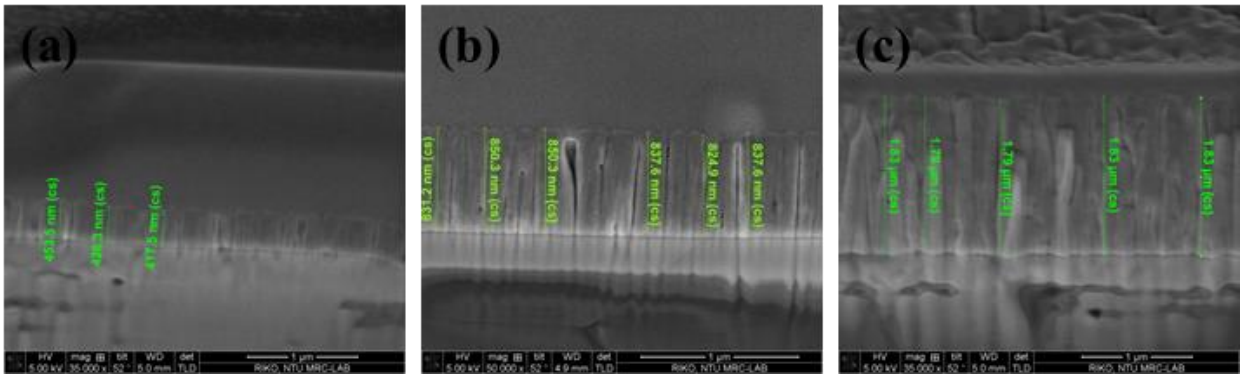


Figure 3-4: SEM cross-sectional images of Cu-polycrystalline $Al_2O_3$ bonding with different deposition times (a) 25 min (b) 50 min and (c) 100 min.

The cross sectional images of Cu-polycrystalline $Al_2O_3$ bonding were presented in Fig. 3-4 for different sputtering times. The Cu thin films were firmly adhered on the $Al_2O_3$ substrates with no failure indication such as delamination, cracking or buckling at the interface. Based on the film growth conditions, the columnar shape of microstructure was evidently revealed on Fig. 3-4 (a) and (b). Enlargement of columnar grains was observed by lengthening the deposition time. The average columnar diameter increased from 0.26 μm (25 min) to 0.54 μm (50 min) in the direction perpendicular to the substrate surface. As for sample coated at 100 min (Fig. 3-4 (c)), the columnar structure with distinguishable column boundary was not clearly observed. Transformation of film structure from columnar shape to a columnar-dendritic mixed microstructure was discovered as the film becomes thicker. It is believed the microstructure transformation is affected by the kinetics mechanism of sputtered atoms for the ordering evolution in the aspects of grain growth or crystallographic texture with prolong deposition period. According to G. Abadias et al. [130], microstructure evolution by film thickening is mainly governed by two mechanisms. The first mechanism is caused by the growth rivalry between the crystals orientating in different facets for the purpose of overall free energy minimization from the surface or at the interface. With the phenomenon of grain competitive growth, the texture orientation, microstructure and topography of a coated film will change incessantly by increasing film thickness. The second mechanism is induced by the migration of grain boundary or the recrystallization process. The recrystallization process takes place when the substrate is heated at high temperature or at the situation where

there is an ongoing strong ion irradiation. In addition, I. Petrov et al. [131] has also reported the ion bombardment during the deposition process will strongly affect the orientations of the coated film.

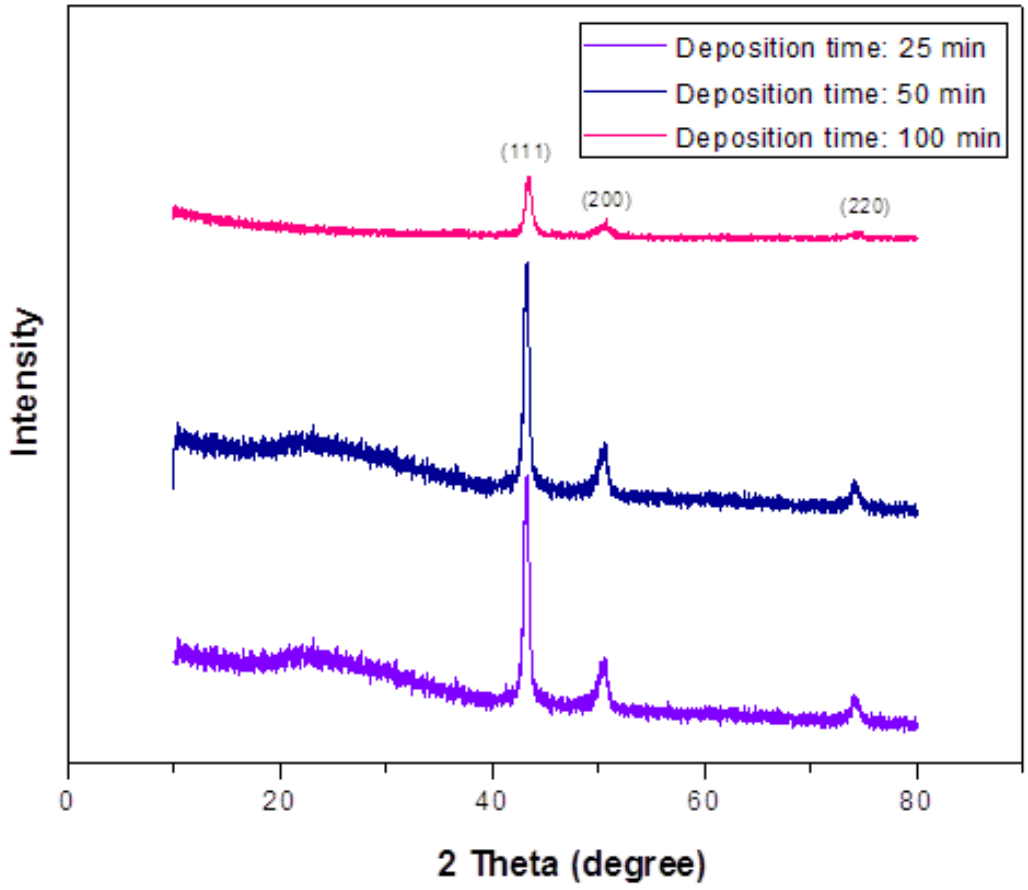


Figure 3-5: XRD pattern of deposited Cu thin film on amorphous glass slide with different deposition times

The crystallographic study of the sputtered Cu thin film was shown in Fig. 3-5. Cu film was also deposited on a piece of glass slide to avoid the peaks from polycrystalline $Al_2O_3$ substrate. Given that glass slide is an amorphous material; there will be no XRD peak from this material. For Cu film with smaller thickness (25 min and 50 min), the XRD signal of amorphous glass was detected. The three

peaks were attributed to the Cu thin film with orientations of (111), (200) and (220). For 25 min and 50 min of deposition times, it displayed a preferred orientation at (111) while the (200) and (220) are relatively low. The same can be said for the sample coated at 100 min.

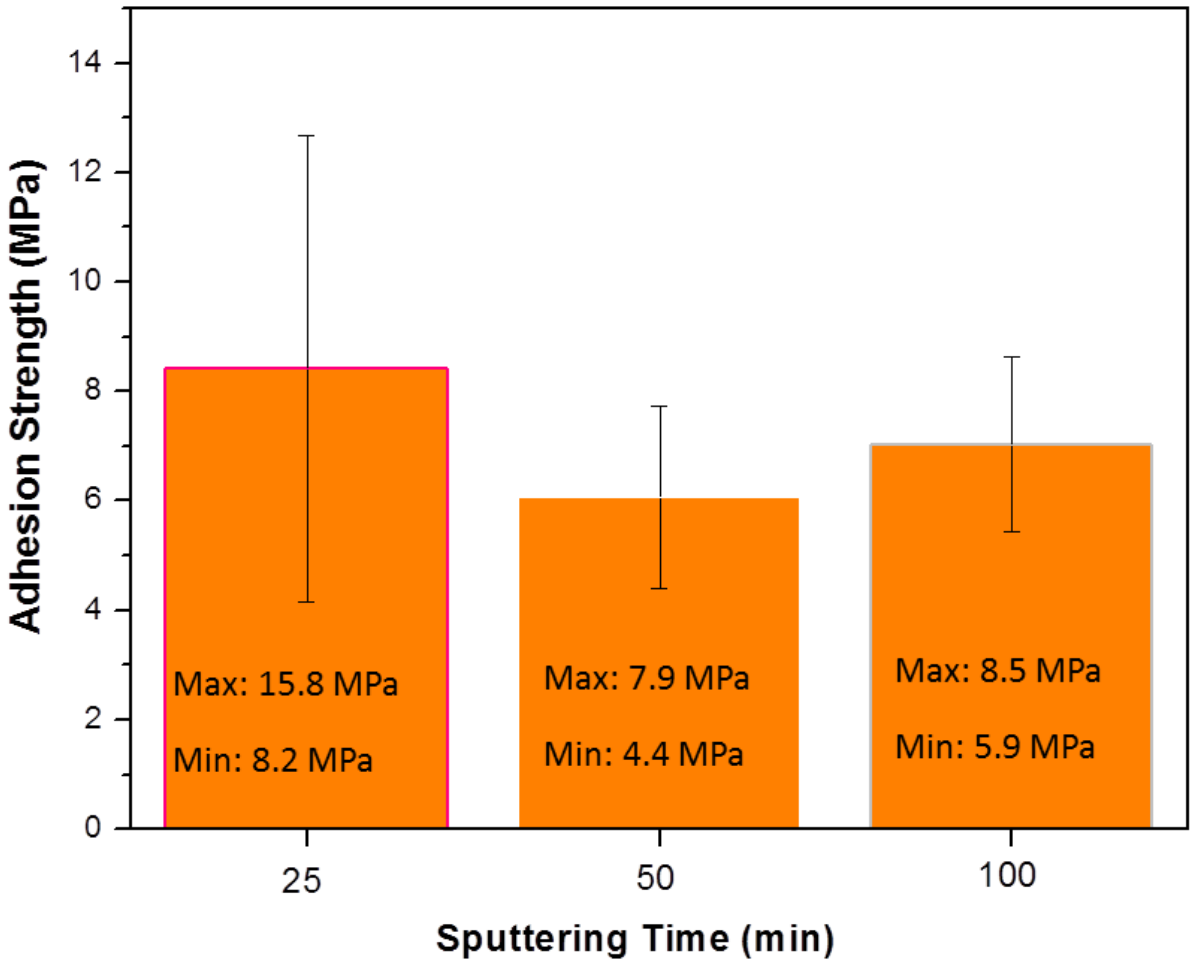


Figure 3-6: Effect of deposition time to the adhesion strength between Cu thin film and polycrystalline $Al_2O_3$ substrate.

G. Abadias et al. [130] has stated the stress field of a film is not dependent on the film thickness. The mobility and the kinetics movement of adatoms have the primary role with increasing film thickness. X.H. Liang et al. [132] found that

stress field of a film will be weaker, and can be even neglected when the coated film is getting thicker. There is no direct relationship between stress state and film thickness, but favorable execution on microstructure; texture and orientation are considered vital in thin film technology applications for better lifetime performance.

As shown in Fig. 3-6, the sample coated at 25 min shows an average adhesion strength of 8.4 MPa with the standard deviation of 4.3 MPa. For the samples with similar film microstructure, a decrease in the adhesion strength with film thickness was observed. However, the large error bar from the thinner film might be affected by the substrate surface roughness. In this study, 25 min of sputtering time is not appropriate especially for polycrystalline $Al_2O_3$ substrates with very high surface roughness. We believe the entire surface of the substrate is not able to be coated and results in interface failure. For 100 min of sputtering time with different film microstructure, increase of adhesion strength was insignificant (< 1 MPa) compared to 50 min of sputtering time. Hence, 100 min of deposition time is not recommended by the following reasons: (i) long time consuming (ii) high consumption of electricity (iii) speedy usage of the sputtering target (iv) generation of heat for extensive deposition period. The heat generated is not only circulating around the chamber; it will also affect the temperature of the substrate during deposition. For better consistency, 50 min of deposition time is selected for future study.

### 3.3.2 Effect of deposition pressure

The deposited thin film was measured for residual stress after deposition under different working pressures. The state of stress (tension or compression) and its magnitude might eventually affect the film adhesion. This work is important especially for sputtering deposition technique due to the high impact energy from the irradiated ions or atoms, where microstructure evolves during deposition.

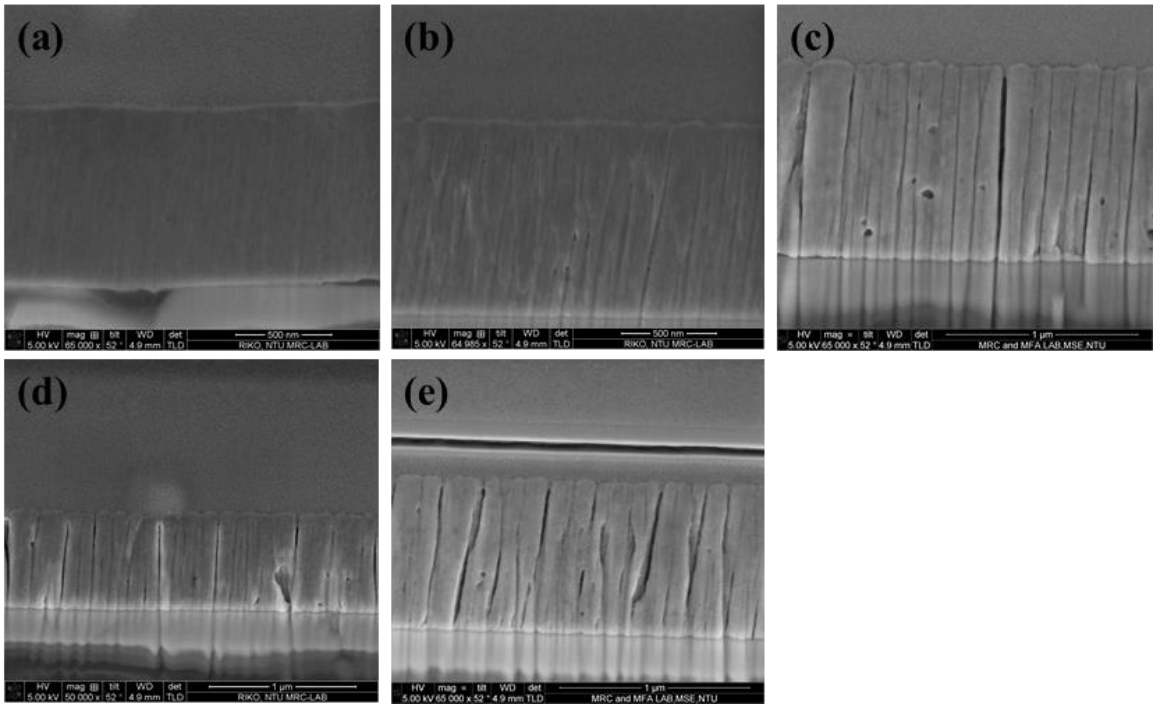


Figure 3-7: FIB-SEM cross-sectional micrographs of Cu-polycrystalline $Al_2O_3$ bonding with different deposition pressures: (a) 1 mTorr (b) 5 mTorr (c) 10 mTorr (d) 15 mTorr and (e) 18 mTorr.

The effect of deposition pressure to the adhesion strength between Cu thin film and polycrystalline $Al_2O_3$ substrate was examined by changing the working pressure from 1 mTorr to 18 mTorr. From Fig. 3-7 (b) to (e), no failure was

detected at the interface. However, it is noticed that there was a sign of delamination for the sample coated at 1 mTorr (Fig. 3-7 (a)). It is believed the interface failure is caused by the high residual stress during the sputtering process. Decrease in Cu film density with deposition pressure was observed. It changed from a denser film at low deposition pressure to a porous columnar film at higher deposition pressure. Presence of voids between columnar grains has been enlarged with the working pressure.

The evolution of the film structure is due to the factors such as kinetics movement, mobility and collision mechanism of sputtered atoms from target to substrate. The circulation of argon gas ions is not only applied for atoms injection from the target material, it is also used to moderate the speed of movement for the atoms at a controlled distance. Extremely high or low pressure will strongly affect the film quality and properties. At a very low deposition pressure, there is lesser amount of particles. Higher ion energy by least collisions is leading to elastic bombardment of adatoms. The active adatoms will then be transferred to the substrate with high surface mobility. The film densification is suggestive of the impinging particles at low deposition pressure by increasing the kinetic energy of the adatoms onto the substrate surface. When the deposition pressure increases, there is a reduction in the adatoms mobility. Due to the frequent collisions, the scattering effect and the decrease of mean free path have weakened the kinetic energy of the arrival atoms. The coalescence process is more kinetically limited and is leading to the observed columnar grains with significant void boundaries.

The mean free path of Cu can be calculated with the equation below:

$$\lambda = \frac{RT}{\sqrt{2}\pi P d^2 N_A}, \quad (3.1)$$

where R is the universal gas constant =8.3145 J/molK, T and P are the temperature and pressure respectively, d is the diameter of molecule, $N_A$ is the Avogadro's number =6.0221 × $10^{23}$/ mol and $\pi$=3.14159.

Table 3.1: Effect of deposition pressure to the mean free path of Cu atoms

| **Deposition Pressure (mTorr)** | **Mean Free Path (cm)** |
|---|---|
| **1** | 7.72 |
| **5** | 1.54 |
| **10** | 0.77 |
| **15** | 0.51 |
| **18** | 0.43 |

According to the kinetic theory of molecular gases, the mean free path of a molecule at constant temperature has a value that is inversely proportional to the pressure. In Table 3.1, it shows a decrease on the mean free path from 7.72 cm to 0.43 cm as the deposition pressure increases. In addition, the directed momentum loss mean free path determines the rate of loss of kinetic energy and direction of particles travelling through a gas, and it is a controlling parameter in establishing

the energy of bombardment during film growth. In this study, the target-substrate distance is about 20 cm and this value is higher than the calculated mean free path. Sputtered atoms undergo many collisions before arriving to the growing film surface especially at high deposition pressure. Hence, the kinetic energy transfer from the plasma to the growing film surface is enhanced as the sputtering pressure decreases. Due to high particle energy at low deposition pressure, the atomic peening mechanism is the net effect of film densification delivered by the energetic particles; certain amount of lattice damage could be induced too. This gives rise to films showing high residual stress and poor interfacial adhesion between Cu thin films and $Al_2O_3$ substrate.

For the sample deposited at high deposition pressure, a large fraction of sputtered atoms collide with residual gas molecules on their way to the substrate. Consequently, the arrival energies of these sputtered atoms are suspected to be much lower than their initial energies. Films grown with such low arrival energies tend to have an appreciable density of voids or defects since arriving atoms do not have sufficient mobility to move into ideal lattice sites. A volume change which affected by the vacancy concentration of the film is suspected. High stress state is eventually developed due to the film shrinkage effect and resulted in low adhesion strength.

Besides film microstructure analysis, investigation on the residual stress under different deposition pressures was carried out using non-destructive XRD $\sin^2\Psi$ method. In this study, the lattice plane of (220) with $2\theta$ angle at 74.129° ($\Psi$ = 0°) was selected after the XRD $2\theta$ broad scanning (Fig. 3-8). The strain of the

chosen plane was then measured by rotating the psi angle (Ψ) from 0 ° to 50 °. The analyzed result was plotted in the form of strain-$\sin^2\Psi$ as illustrated in Fig. 3-9 and the normal stress induced was calculated automatically using LEPTOS XRD fitting software in the following way (eq. 3.1).

$$\epsilon_{\phi,\Psi} = (d_{\phi,\Psi} - d_o)/ d_o = \sigma [ (1+\nu)/ E] \sin^2\Psi, \quad (3.2)$$

where $\epsilon_{\phi,\Psi}$ is the lattice strain for a given plane, $d_o$ and $d_{\phi,\Psi}$ are the unstressed and stressed lattice spacing respectively, σ is the residual stress of the film, $\nu$ is the Poisson ratio with the value of 0.34 and E is the Young's modulus for Cu with the value of 137.174 GPa.

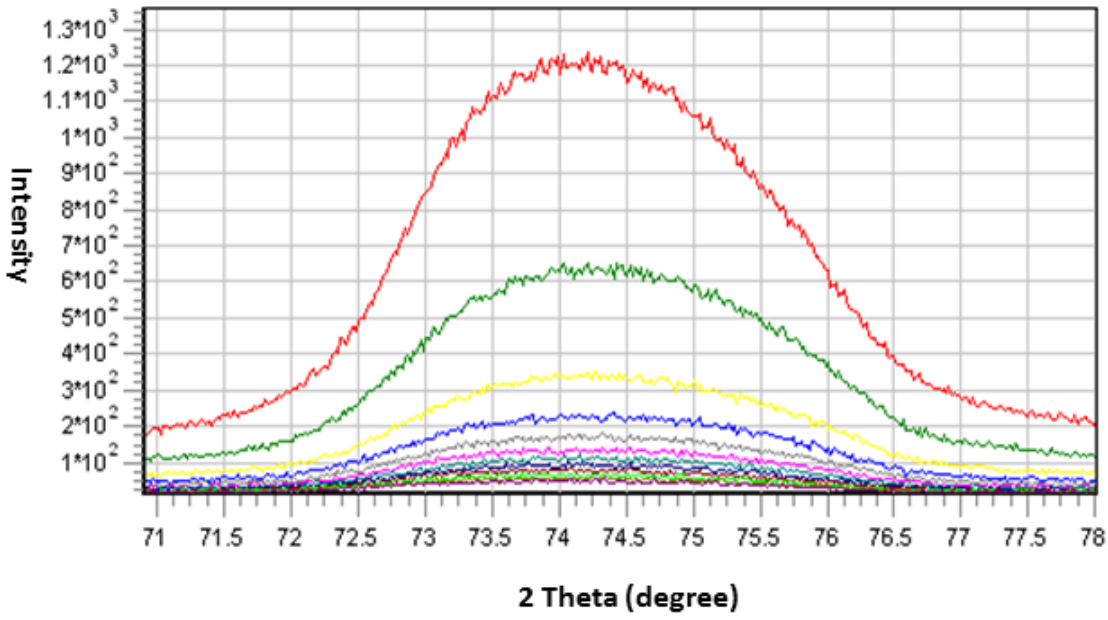


Figure 3-8: XRD pattern on (220) plane with psi angle (Ψ) changing from 0° to 50° for sample coated at 1 mTorr.

From Fig. 3-9, the positive slope in strain-$\sin^2\Psi$ graph indicates the presence of tensile film stress. This trend was applied to other deposition pressures from 5 mTorr to 18 mTorr. Regardless of the deposition technique and the coating conditions, the residual stress induced could also be affected by the mismatch of coefficient of thermal expansion (CTE) of the materials. When the CTE value of metal film is higher than substrate, tensile state of stress will be created from the film. Compressive film stress is induced when the CTE value of metal film is lower than substrate. In this study, the CTE of polycrystalline $Al_2O_3$ is $8.0 \times 10^{-6}$ /K and Cu film is $17.0 \times 10^{-6}$ /K. Higher CTE value of Cu is leading to tensile film stress at room temperature. However, since the film was deposited without heating, the stress contribution from CTE mismatch is negligible. The measured stress in this case is contributed by the intrinsic stress of the film.

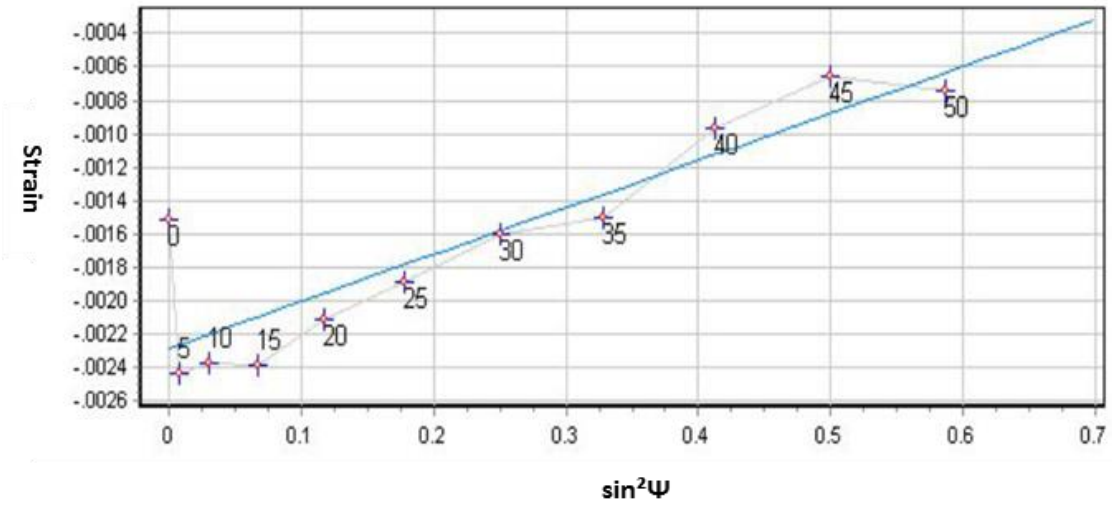


Figure 3-9: Graph of strain-$\sin^2\Psi$ for sample coated at 1 mTorr

A deposition technique with proper controlled is necessity for stress minimization. In Fig. 3-10 and Table 3.1, the correlation study between deposition

pressure and adhesion strength, as well as the induced residual stress was evaluated. It is believed the mechanical stress of a film is affected by the ion bombardment during the deposition process. At 1 mTorr deposition pressure, this group exhibits the weakest adhesion strength of 4.3 ± 1.3 MPa with maximum film stress at 276.5 MPa. The adhesion strength between Cu thin film and polycrystalline $Al_2O_3$ increased with deposition pressure up to 10 mTorr. The reduced film stress to 45.3 MPa at 10 mTorr is leading to the observed adhesion enhancement.

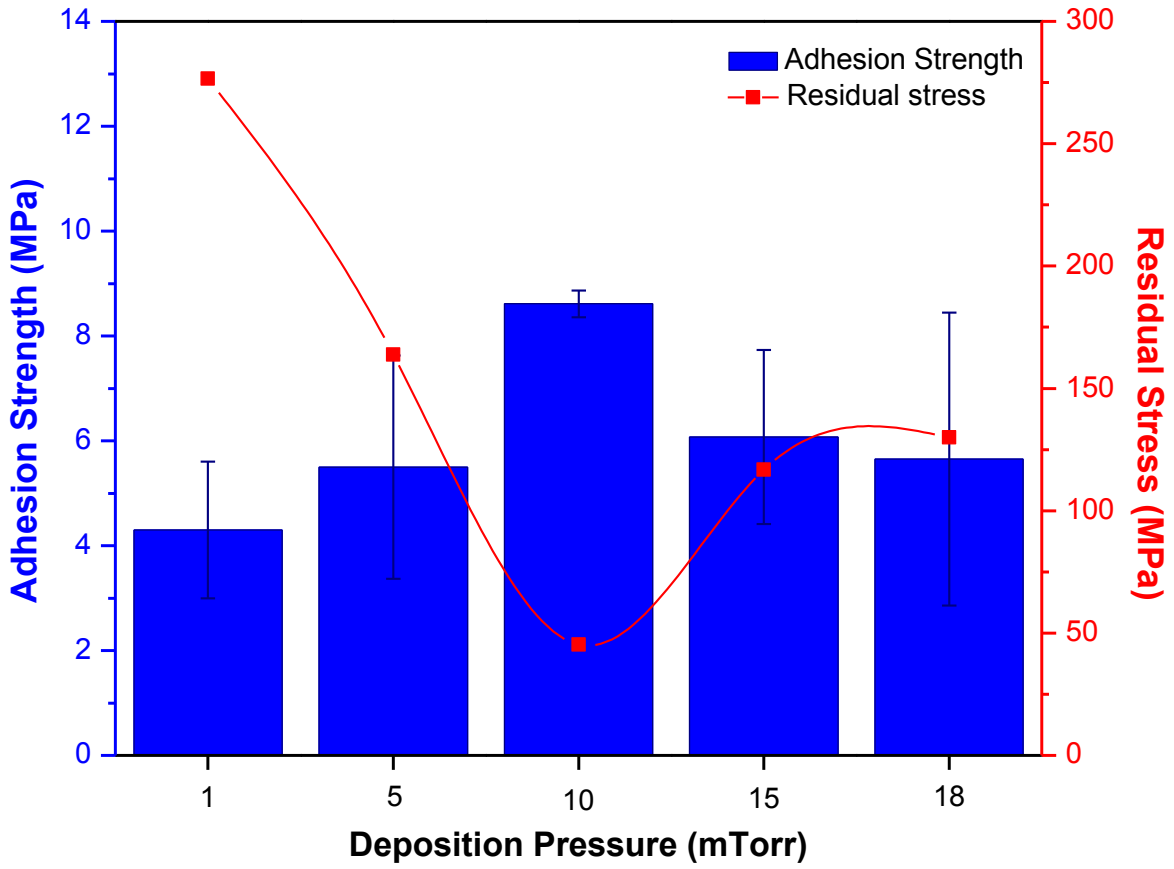


Figure 3-10: Tensile strength measurement for Cu-polycrystalline $Al_2O_3$ bonding as a function of deposition pressure and residual stress.

At low deposition pressures, densification of film microstructure is responsible for the observed high residual stress. It is believed the atomic peening effect by energetic ions or atoms is the key factor for film densification [63]. Development of columnar growth structure is restricted by the striking effect of energetic particles, and is leading to the observed high tensile stress.

After the optimized pressure at 10 mTorr, decrease of adhesion strength at 15 mTorr and 18 mTorr were observed in Fig. 3-10 and Table 3.2. At low deposition temperature, little surface diffusion is developed for thin film. The vacancy concentration is expected to be higher than at equilibrium. There is a volume change which affected by the vacancy concentration of the film, and eventually is leading to residual stress of the film. The stress change depends on the vacancy volume and the site of annihilation. At higher deposition pressures, presence of voids and the size of columnar grains increase with the Ar pressure due to the kinetics movement of adatoms. R. Huang et al. [133] has reported that the grain growth process is tend to reduce the amount of grain boundaries in order to eliminate the excess volume of the film. The annihilation of the vertical boundaries may result in an in-plane change of film dimensions. In such case, high mechanical film stress is developed due to the film shrinkage effect. Interface failure occurs if the columnar structure is not capable to maintain the high mechanical stress in the film. Hence, moderate kinetic energy at 10 mTorr is finalized as the optimum pressure for Cu-$Al_2O_3$ bonding in this study.

Table 3.2 Change of adhesion strength and film stress with deposition pressure

| Deposition Pressure (mTorr) | Film Stress (MPa) | Adhesion Strength (MPa) |
|---|---|---|
| **1** | 276.5 | 4.3 ± 1.3 |
| **5** | 163.8 | 5.5 ± 2.1 |
| **10** | 45.3 | 8.6 ± 0.3 |
| **15** | 116.7 | 6.1 ± 1.7 |
| **18** | 129.9 | 5.6 ± 2.7 |

### 3.3.3 Effect of post deposition annealing

Annealing used to be a process to relieve stresses of a bonding system [10]. The stress may be originated by intrinsic stress formed during film deposition, or the stress due to the CTE mismatch during cooling. High stress condition might also be relieved through delamination, cracking, buckling or fracture. According to Waters. P. [3], strain energy is accumulated by the amount of stress induced. Interface failure will take place when the strain energy release rate has exceeded the interfacial toughness of the film.

In this study, in-situ post annealing step was carried out directly after the deposition process. The samples were heated at 100 °C and 300 °C for 30 min from room temperature with a heating rate at 10 °C/min. Annealing temperature beyond 300 °C was not included in order to prevent re-crystallization of Cu film [134, 135]. Problem of thermal shock was avoided by slow cooling process under inert gas atmosphere.

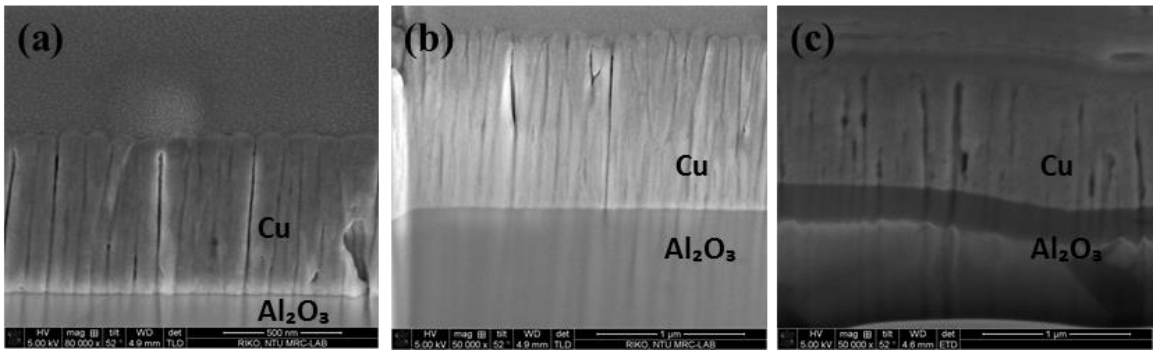


Figure 3-11: Cross sectional images of Cu-polycrystalline $Al_2O_3$ bonding (a) at room temperature (b) annealed at 100 °C for 30 min and (c) annealed at 300 °C for 30 min.

Change of film microstructure was observed in Fig. 3-11. Transformation of Cu film from columnar grains to a more densified morphology at 300 °C was clearly revealed. For the sample annealed at 100 °C for 30 min (Fig. 3-11 (b)), film structure evolution was initiated from the interface region. It continues to grow from bottom to top by densifying the columnar structure gradually. At 300 °C in Fig 3-11 (c), there was an increase of film density by reducing the void boundaries. At elevated temperature, we believe the Cu atoms are able to diffuse and fill up the porous boundaries between the columnar grains. Besides the atomic diffusion, annealing step might also help to accelerate the coalescence process of the Cu thin film.

There was a decrease of film stress from 116.7 MPa (room temperature) to 53.3 MPa (300 °C for 30 min) after the annealing. Corresponding to the residual stress reduction, the adhesion strength between Cu thin film and polycrystalline $Al_2O_3$ substrate shows an increase of 18 % from 6.1 MPa to 7.2 MPa. The adhesion

enhancement is attributed to the reduction of residual stress, as well as the improve contact with substrate surface. Besides, Cu atoms with high mobility are suspected to have moved into the depth of the substrate through diffusion bonding. Discussion on diffusion bonding will be further elaborated in Chapter 5. In addition, there is a possibility of residual stress reduction by the out diffusion of Ar gas atoms entrapped during film deposition, especially when the working pressure is high. However, we believe the contribution from out diffusion of Ar gas during heating will be very small.

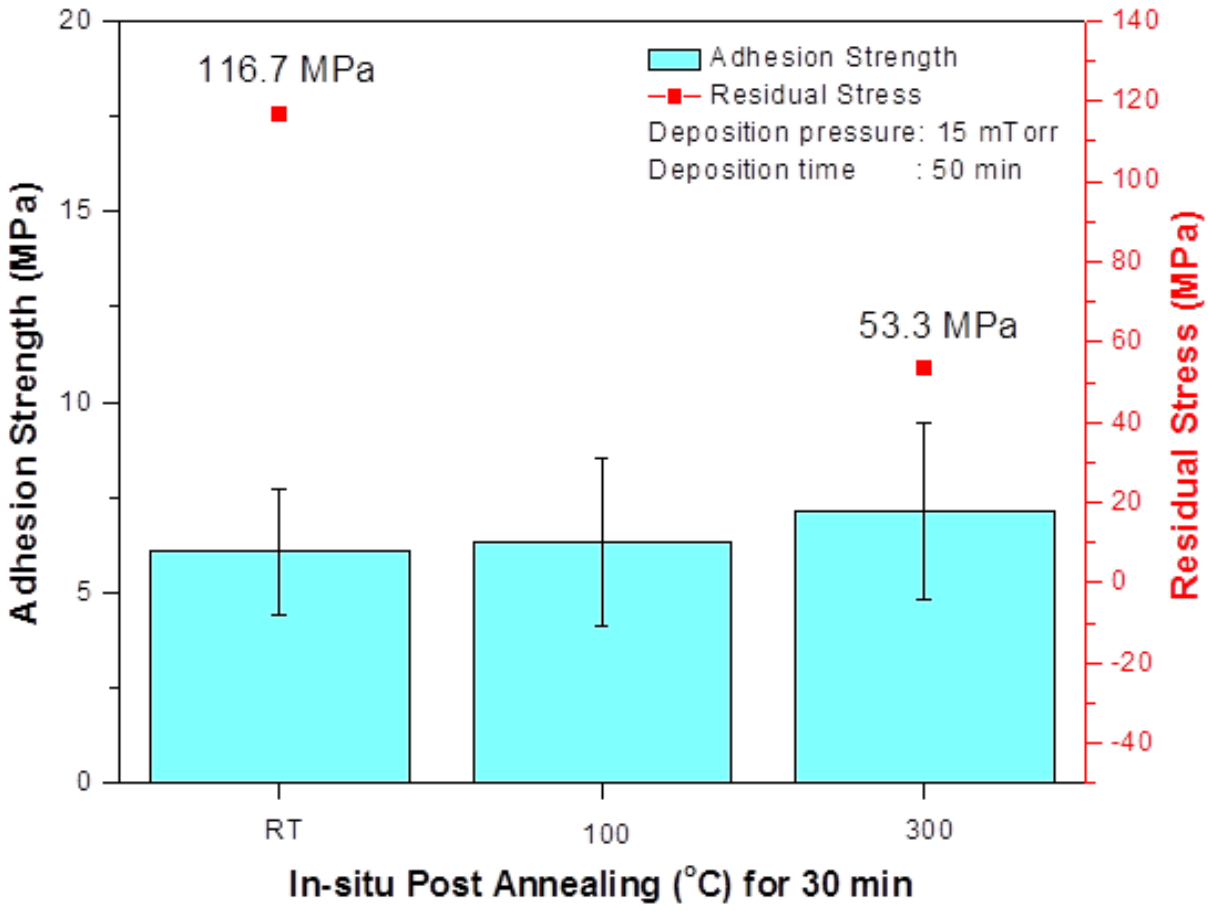


Figure 3-12: Effect of post deposition annealing to the residual stress and adhesion strength between Cu thin film and polycrystalline $Al_2O_3$ substrate.

## 3.4 Chapter Summary

Besides extrinsic stress, intrinsic stress induced for a bonding system will strongly affect the adhesion tendency between materials. For the purpose of stress minimization, different bonding parameters include deposition time, working pressure and post annealing were investigated for their effect on Cu film adhesion with polycrystalline $Al_2O_3$ substrate. The findings are:

(1.) There is a change of microstructure and crystallographic orientations with deposition time

(2.) No significant relationship between stress field and film thickness

(3.) Columnar film with higher degree of porosity is formed by increasing the deposition pressure

(4.) Kinetics movement, mobility and collision mechanism of adatoms are the factors for microstructure evolution

(5.) There is a change of adhesion strength and residual stress with deposition pressure

(6.) 10 mTorr is the optimized pressure for Cu-polycrystalline $Al_2O_3$ bonding with lowest film stress of 45.3 MPa and highest adhesion strength of 8.6 MPa

(7.) There is a transformation of film microstructure from columnar to a denser film after in-situ post deposition annealing (100 °C and 300 °C for 30 min)

(8.) There is an increase in adhesion strength for 18 % by residual stress reduction after post deposition annealing.

(9.) Diffusion of Cu atoms through the porous boundaries for adhesion improvement at elevated temperature

# CHAPTER 4: IMPORTANCE OF SURFACE PRE-TREATMENT

## 4.1 Introduction

In the past decades, numerous inorganic (alumina; aluminum nitride etc.) and organic-inorganic materials (polyimide-glass; epoxy-glass etc.) have been utilized as the substrates in electronic devices. In particular, the metallization of ceramics has long been a subject of interest due to its excellent thermal, mechanical and chemical stability, high hardness and good wear resistance [54, 69, 70, 72, 73]. This enables the manufacturers to fabricate microelectronic devices with better reliability which are able to work under harsh environment. In order to fully achieve the advantages, good adhesion between the metallization films and the substrate is crucial. However, since metals tend to have a higher surface energy than ceramics, it is difficult to form a strong bond between metal films and ceramic substrate.

An electronic package usually consists of different materials for different functions which are often connected via physical and/or chemical means. Debonding or delamination between these heterogeneous materials during fabrication or service is always a great concern for device reliability. Metallization on ceramic substrates is an important issue due to the intrinsic low adhesion caused by poor wetting of metals on ceramics. MIL-STD-883E standard (method 2027.2) [11] requires a minimum of 10 MPa for metallization on ceramic substrate. To

achieve the desired adhesion strength, many factors have to be considered to develop a better bonding between different materials. In the study of joining method, various techniques such as eutectic joining [62, 72-76], ion beam dynamic mixing [136], casting bonding [62], spraying [78, 79] etc., have been explored to obtain optimized bonding. Besides, insertion of an adhesion layer such as Titanium [52]; Chromium [52, 137] or Tantalum is often employed before the final metal film is deposited on a ceramic substrate. These methods either require a high processing temperature, or additional materials and steps.

There is a clear advantage to form metal films on a ceramic substrate without using an adhesion layer. In such a case, the surface condition is an important factor affect the adhesion strength. It is well known that a clean surface is very important to achieve high adhesion strength. Over the years, a variety of surface treatment methods have also been extensively developed for improving interface bonding. However, the topic related to the impact of surface pre-treatments to the Cu-polycrystalline $Al_2O_3$ bonding has not been systematically studied and little has been known for the effectiveness of individual surface treatment as many reports were focused on an optimum solution. In this paper, effort has been made to increase the adhesion strength between Cu thin film and polycrystalline $Al_2O_3$ by employing a few types of surface treatment prior to bonding as listed in Table 4.1. Copper thin films of around 1.0 ± 0.2 μm were sputtered on polycrystalline $Al_2O_3$ substrate without employing any adhesion layer. Different surface treatments are designed to be applied in different sequences to understand the contribution by each of these treatments.

## 4.2 Experimental Setup

### 4.2.1 Sample preparation

Preparation of polycrystalline $Al_2O_3$ substrates has been described in section 3.2.1. Before film deposition, the substrates were cleaned using different combinations of treatment as listed in Table 4.1.

Immediately after the surface treatment, Cu thin film was deposited onto the $Al_2O_3$ substrate using DC magnetron sputtering technique (PRO Line PVD 75, Kurt J. Lesker Company®). The sputtering chamber was pumped to a vacuum level below $5.0 \times 10^{-5}$ Torr before the coating process starts. After the desired vacuum pressure was reached, the deposition will be conducted under the power of 300 W with deposition pressure of $1.5 \times 10^{-2}$ Torr, and the deposition rate was about 0.3 nm/s. During the deposition, the sample holder was rotated at 20.0 mm/s in order to obtain a uniform film. The distance between the substrate holder and the sputtering target was maintained at 20.0 cm.

A comparison study was also conducted using monocrystalline $Al_2O_3$ substrate (Latech Scientific Supply Pte Ltd) with surface roughness (root mean square, *rms*) less than 0.5 nm. The purchased monocrystalline substrate in the orientation of $(11\bar{2}0)$ has similar surface energy with polycrystalline $Al_2O_3$ substrate. Surface analysis after treatment was investigated and compared based on the density of substrate surface pores.

### 4.2.2 Materials characterization and adhesion measurement

Investigation on the substrate's chemical state on the surface and subsurface (depth profiling) was carried out by a Kratos Axis Ultra X-ray photoelectron spectroscopy system under the vacuum state of $10^{-8}$ to $10^{-9}$. The binding energies of the elements were calibrated using CASA XPS processing software by referring the adventitious C 1s peak at 284.8 eV as internal reference. The surface energy of the substrate was measured using three different liquids: *viz.* distilled water, ethylene glycol and diethylene glycol with known surface energy. The surface energy of the ceramic samples was then calculated using the Owen, Wendt, Rabel and Kaelble (OWRK) method. X-ray diffractometer (Shimadzu) equipped with a secondary monochromator with Cu Kα radiation was used to determine the crystal structure of the substrate in the scan range from 20 to 80°. The amount of solvent residue was measured using a thermal gravimetric analyser (TGA-Q500) under a controlled atmosphere.

The adhesion measurement has been described in section 3.2.2. After tensile test, the separated surfaces were analysed using scanning electron microscopy JEOL JSM 6360 to examine the location of the failure. True adhesion strength was available only if the failure is between the Cu film and the $Al_2O_3$ substrate. If cohesive failure in the applied glue or adhesive failure between the glue and the Cu film is observed, the case will be highlighted. Under such circumstance, the actual strength between the film and substrate will be greater than the recorded strength value.

## 4.3 Results and Discussions

### 4.3.1 Adhesion strength after different surface treatments

As shown in Table 4.1, four different surface treatment steps are grouped into 4 categories (group 1 to group 4) and were applied to the $Al_2O_3$ substrate before film deposition. The treatments include solvent cleaning, acid washing, heat treatment, plasma cleaning, and they were organized into different sequences in order to evaluate their individual contribution to the film adhesion. Results are compared with as-received condition (denoted as group 0). The as-received polycrystalline $Al_2O_3$ substrates have a surface roughness (root mean square, *rms*) in the range of 10 – 150 nm after going through a chemical mechanical polish (CMP) process.

The interfacial adhesion strength between Cu thin film and polycrystalline $Al_2O_3$ substrate under different group of surface pre-treatments was shown in Fig. 4-1. The highest adhesion strength of 34.0 MPa and above has been achieved through plasma treatment (Group 2). This value has been far exceeded the MIL-STD-8883E of 10 MPa. Changes on the interfacial bonding are affected by: (i) removal of contaminants (ii) change of wetting behaviour and (iii) creation of surface dangling bonds. Discussion on the effect of surface pre-treatments to the interfacial bonding tendency will be further elaborated in the following sections.

Table 4.1 Types of surface pre-treatments, group into different sequences, and the resulting adhesion strength

| Treatment | Cleaning steps | Description | Average adhesion strength (MPa) |
|---|---|---|---|
| Group 0 | No | As-received sample | 5.4 ± 3.4 |
| Group 1 | Solvent cleaning | - Acetone 10 min with ultrasonication<br>- IPA 10 min with ultrasonication<br>- Dry at 70 $^{o}$C for 3 min | 6.1 ± 1.7 |
| Group 2 | Solvent cleaning → Acid etching | - Solvent cleaning as described above<br>- Piranha acid at 90 $^{o}$C for 15 min<br>- Rinse with distilled water<br>- Dry at 70 $^{o}$C for 3 min | 7.1 ±1.9 |
| | Solvent cleaning → Heat treatment | - Solvent cleaning as described above<br>- In-situ heating at 300 $^{o}$C for 30 min right before film deposition | 7.3 ± 1.8 |
| | Solvent cleaning → Plasma treatment | - Solvent cleaning as described above<br>- In-situ Ar plasma treatment at 50 W<br>a.) 2 min<br>b.) 10 min | 2 min: 25.0 ± 6.0<br>10 min: > 34.0 |
| Group 3 | Solvent cleaning → Heat treatment → Plasma treatment | - Solvent cleaning as described above<br>- In-situ heating at 300 $^{o}$C for 30 min<br>- In-situ Ar plasma at 50 W for 2 min | 16.9 ± 3.0 |
| | Solvent cleaning → Plasma treatment → Heat treatment | - Solvent cleaning as as described above<br>- In-situ Ar plasma at 50 W for 2 min<br>- In-situ heating at 300 $^{o}$C for 30 min | 5.3 ± 2.1 |
| Group 4 | Solvent cleaning → Plasma treatment → Re-contamination | - Solvent cleaning as described above<br>- In-situ Ar plasma at 50W for 10 min<br>- Exposed to air atmosphere for 10 days | 7.7 ± 7.0 |

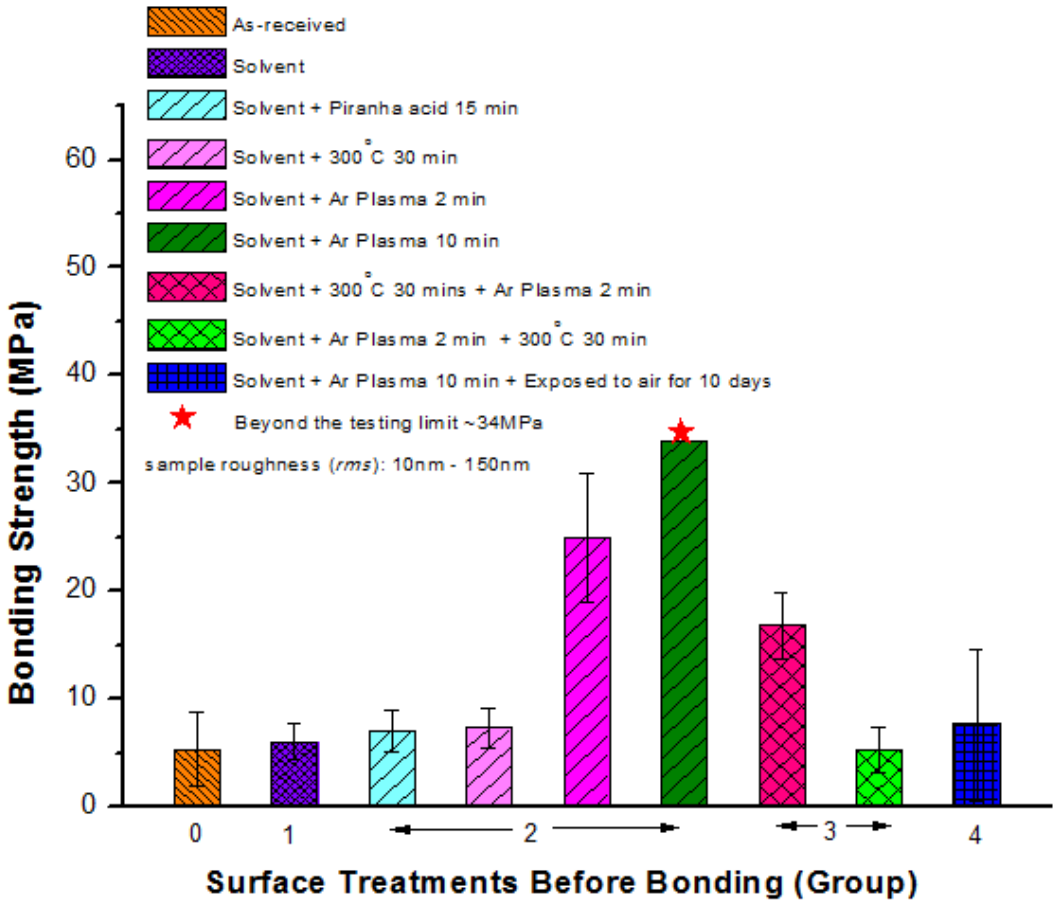


Figure 4-1: Effect of surface pre-treatment on the adhesion strength between Cu film and polycrystalline $Al_2O_3$ substrate.

*4.3.1.1 Group 0*

As shown in Fig. 4-1, the as-received sample shows an average adhesion strength of 5.4 MPa with the standard deviation of 3.4 MPa. This group exhibits very weak bonding with a large variation among different samples. The large error bar might be caused by 2 factors; (i) wide range of substrate surface roughness (ii)

uneven distribution of contaminants throughout the wafer fabrication, especially after the CMP process. The commercial polycrystalline $Al_2O_3$ substrates contain a relatively large number of pores on the surface. Although the degree of porosity has been reduced after the CMP, there are still many pores available to act as storage site for impurities or the residues left behind after the CMP process.

*4.3.1.2 Group 1*

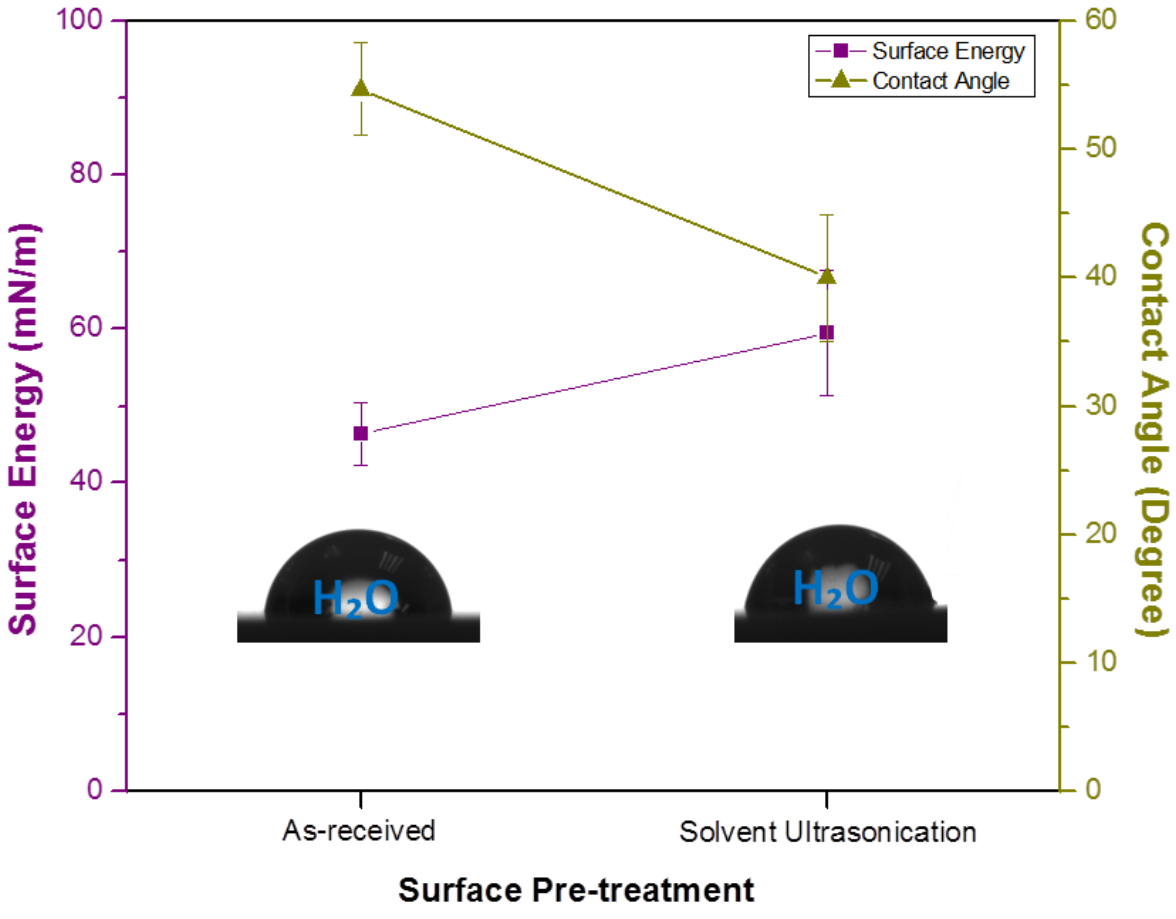


Figure 4-2: Surface energy and contact angle before and after the organic solvent cleaning.

The most common cleaning method to remove organic contamination is to use organic solvents such as acetone, and isopropyl alcohol with the aid of ultrasonication. The treatment (group 1) slightly improves the adhesion strength from 5.4 ± 3.4 to 6.1 ± 1.7 MPa. Analysis of the surface energy reveals a better wetting performance of the substrate as indicated by the measured surface energy from 46.3 to 59.5 $mJ/m^2$ and the contact angle from 54.7 to 40.0° (Fig. 4-2). However, we find that organic solvent cleaning is not effective for the improvement of Cu film adhesion to alumina substrate probably because it is not sufficient to totally remove the contaminants that adhere on the substrate's surface.

*4.3.1.3 Group 2*

Under treatment conditions in group 2 (Table 4.1), one more step was added after the solvent cleaning. The surface was either treated by piranha acid etching, or in-situ (i.e., right before sputtering without breaking the vacuum) heat treatment, or in-situ plasma treatment. In general, piranha solution was used to etch native oxide and organic residues on silicon wafer [53]. In the current work, the diced substrates were soaked in a 3:1 mixture of concentrated $H_2SO_4$ and $H_2O_2$ solution at 90 °C for 15 min, rinsed, and then transferred to the deposition machine. The acid etching shows very limited improvement as shown in Fig. 4-1. The same can be said for the heat treatment at 300 °C for 30 min inside the sputtering chamber. Notice that there was no change of the crystal structure (Fig. 4-3) and the surface morphology (Fig. 4- 4) of the substrate after the heat treatment, we believe

that there might be some residual solvents trapped inside the large number of pores after the initial solvent cleaning. To confirm this, a TGA measurement was carried out and the results are presented in Fig. 4-5. The weight loss was monitored for heating up to 300 °C with a heating rate of 10 °C/min. The substrate with solvent cleaning shows a significant weight drop as compared with the one without. Based on Fig. 4-5, solvent evaporation probably takes place from 23 to 200 °C corresponding to the drastic drop of weight in this temperature range. From Fig. 4-6, no indication of weight lost for monocrystalline substrate with and without solvent cleaning. It is believed the moisture is totally evaporated from the substrate surface without flowing into the bulk substrate. Besides contaminants, the substrate surface porosity is the trapping site for moisture. However, the removal of the residual solvents does not seem to be a key factor for the adhesion strength improvement as the strength only slightly improved.

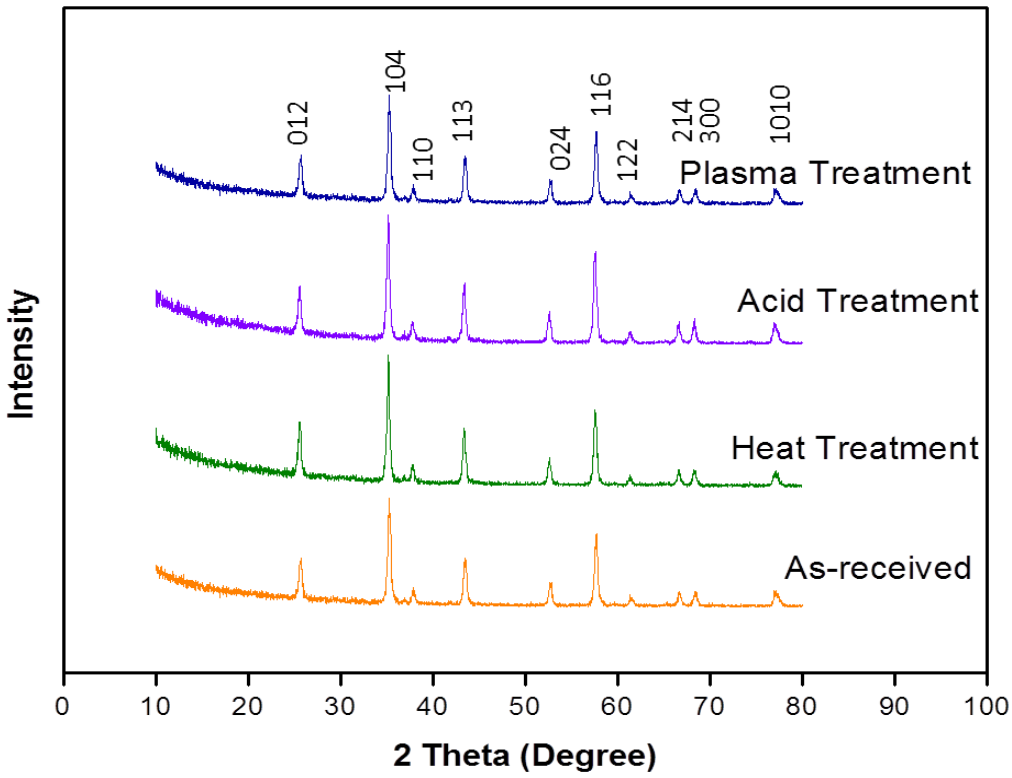


Figure 4-3: XRD analysis after different surface treatments.

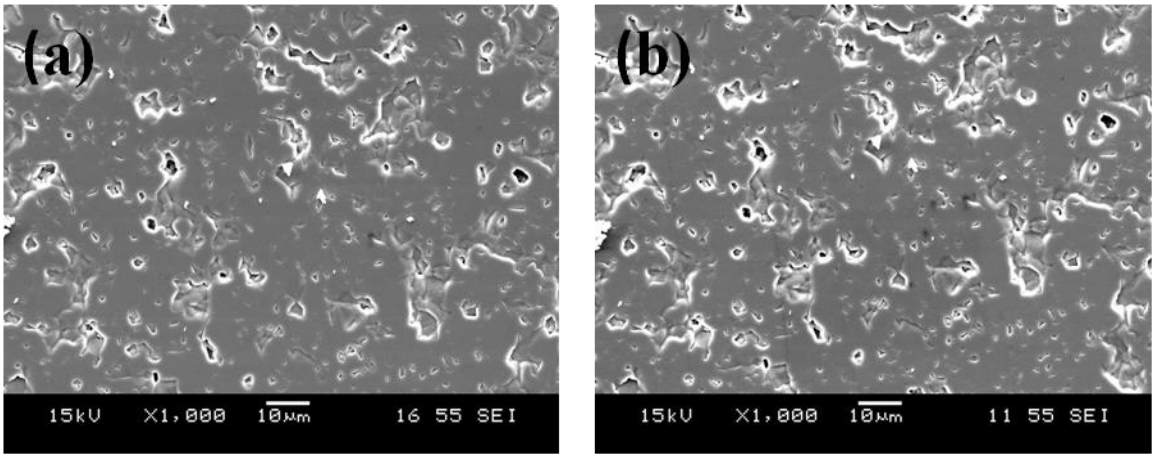


Figure 4-4: SEM images of polycrystalline $Al_2O_3$ (a) before and (b) after heat treatment at 300 °C for 30 min.

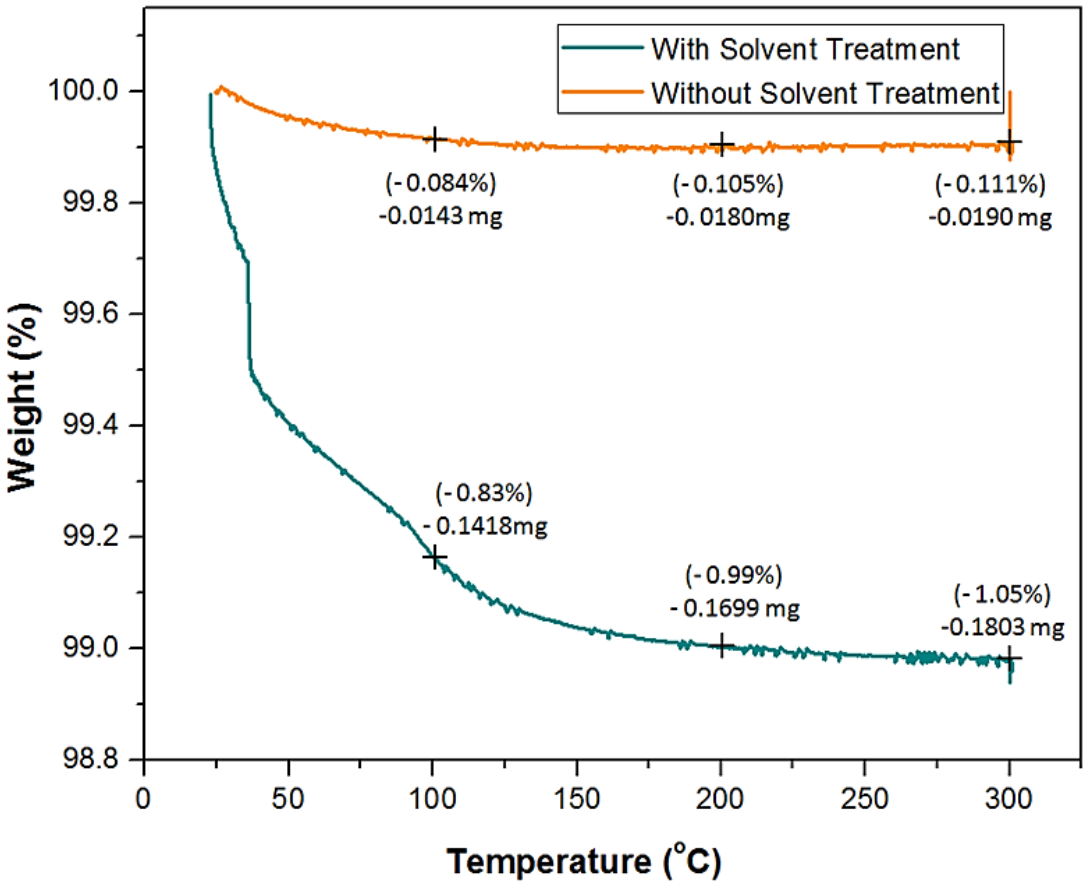


Figure 4-5: Weight loss analysis after heating up to 300 °C for polycrystalline $Al_2O_3$ substrates with and without solvent treatment.

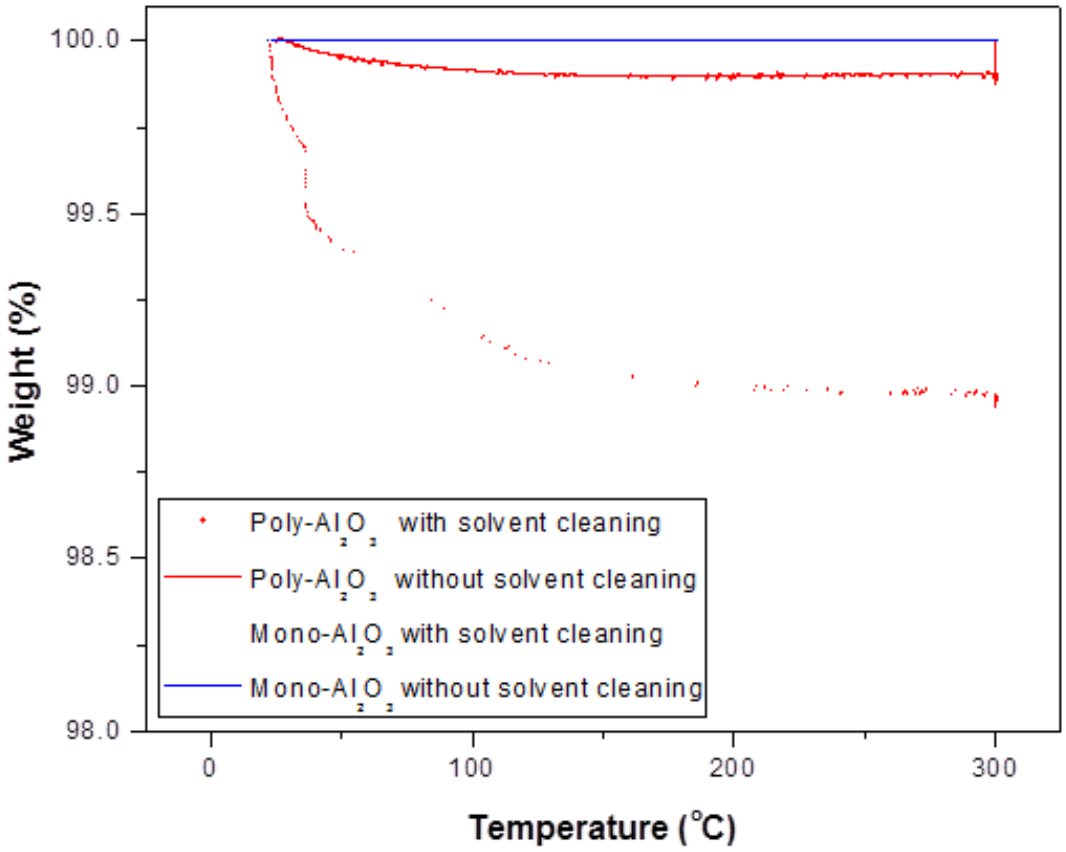


Figure 4-6: Weight loss comparison analysis after heating up to 300°C for monocrytalline and polycrystalline $Al_2O_3$ substrates with and without solvent treatment

Since both heating and piranha solution treatments have shown limited improvement, they are not recommended for adhesion enhancement in practice. On the other hand, plasma treatment has shown significant enhancement for the bonding system. From Fig. 4-1, in-situ Ar plasma cleaning under pressure of 15 mTorr with the power of 50 W has led to much improved Cu film adhesion with polycrystalline $Al_2O_3$. The strength has increased with the plasma treatment time from 2 min to 10 min. After 10 min of argon ion bombardment, the adhesion strength reached beyond 34 MPa (the star sign indicates the breakage is between

the glue and the film surface, indicating the copper film / $Al_2O_3$ substrate adhesion is no less than 34 MPa), which is at least a 6-fold increment from the as-received sample. This value has far exceeded the MIL-STD-883E requirement of 10 MPa.

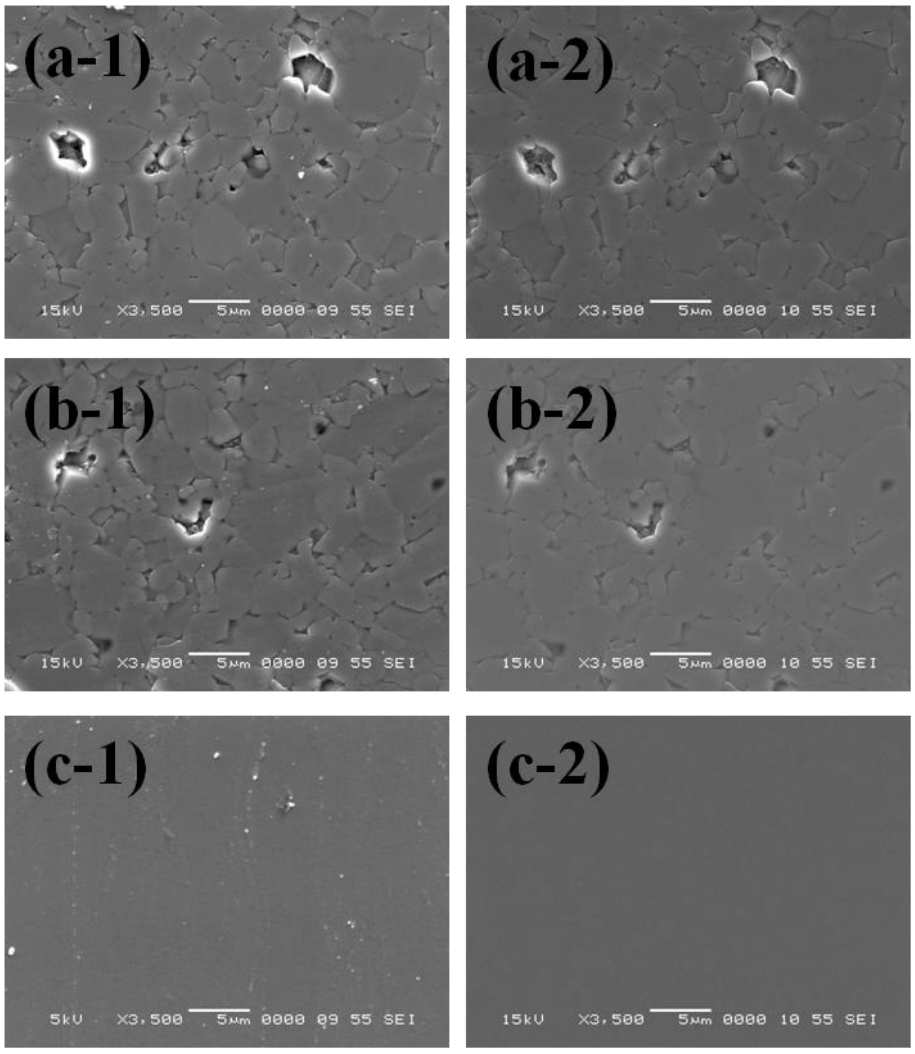


Figure 4-7: SEM micrographs of (a-1) polycrystalline $Al_2O_3$ before (a-2) after 10 min of Ar plasma cleaning at 20 W (b-1) polycrystalline $Al_2O_3$ before (b-2) after 10 min of Ar plasma cleaning at 50 W and (c-1) monocrystalline $Al_2O_3$ before (c-2) after 10 min of Ar plasma cleaning at 50 W.

Besides plasma cleaning time, investigation on the substrate surface chemical state was carried out before and after the argon ion bombardment using two different levels of power (20 W; 50 W) for 10 min. In this study, two types of substrates were also used for comparison: (i) very smooth monocrystalline $Al_2O_3$ (*rms* < 0.5 nm, orientation of $(11\bar{2}0)$) and (ii) polycrystalline $Al_2O_3$ (*rms* 10 – 150 nm). SEM inspection was made on the same area before and after the plasma treatment as presented in Fig. 4-7 to check the changes on the surface morphology and the substrate roughness. From Figs. 4-7 (a) and (b), reduction of surface charging effect after the Ar plasma bombardment was observed, and this phenomenon was more evident with higher plasma power at 50 W. The reduced surface charging is suggestive of a cleaner surface after the treatment by knocking off the organic and inorganic contaminants from the surface including the concaved regions. Yet, there was no significant increase in the surface roughness even after the bombardment process was carried out at 50 W. The monocrystalline $Al_2O_3$ has very flat surface and limited number of surface pores (Fig. 4-7 (c)). It is not surprising that this sample has the cleanest surface after Ar plasma bombardment at 50 W for 10 min.

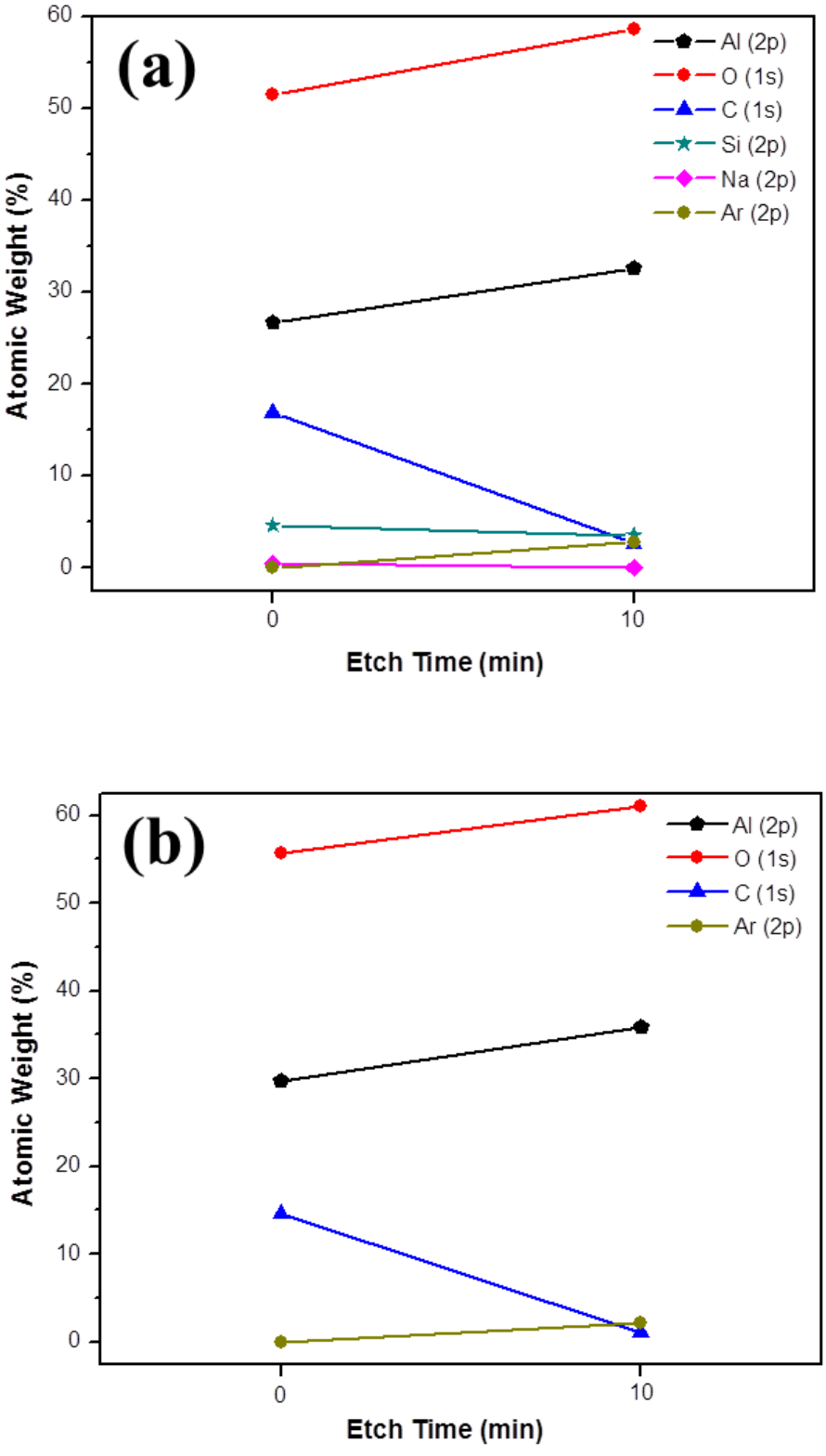


Figure 4-8: XPS analysis on the atomic weight percentage with plasma cleaning time and the impact of porosity to the impurities entrapped using (a) polycrystalline $Al_2O_3$ (b) monocrystalline $Al_2O_3$.

Table 4.2 Elemental compositions of polycrystalline $Al_2O_3$ substrate before and after plasma treatment for 10 min

| Elements | Elemental composition (At %) | |
|---|---|---|
| | **Before plasma treatment** | **After plasma treatment** |
| Al 2p | 26.7 | 33.7 |
| O 2p | 51.5 | 60.7 |
| C 1s | 16.9 | 2.8 |
| Na 2p | 0.4 | 0 |
| Si 2p | 4.6 | 0 |
| Ar 2p | 0 | 2.9 |
| Al/O ratio | 0.52 | 0.56 |
| Average adhesion strength (MPa) | $5.4 \pm 3.4$ | > 34.0 |

To support the above analysis on surface cleanliness, XPS was also carried out to quantify the amount of contaminants removed from the surface after the Ar plasma treatment. The organic contaminants have indeed been much reduced after 10 min of treatment as indicated by the reduction of carbon from 16.9 to 2.8 at.% as indicated in Fig. 4-8 and Table 4.2. In addition to the removal of carbon, other contaminants such as Na and Si were also found to be reduced to 0% in the polycrystalline substrate. Furthermore, the atomic weight percentages of Al (as indicated by the Al 2p peak) and O (O 1s) have also increased with the plasma cleaning time, which leads to an oxygen-rich surface after the plasma treatment. From the elemental compositions listed in Table 4.2, the ratio for Al/O increases

from 0.52 to 0.56 after plasma treatment. The increase of Al/O ratio could be another indication of removal of organic containments. Besides, we also believe the substrate porosity has an impact on the amount of entrapped impurities too. The atomic weight percentage and the impurity level were higher for the substrate with higher number of porosities. Hence, the removal of contaminants was more effective on flat surface as shown in Fig. 4-8 (b) as compared with rougher surfaces in Fig. 4-8 (a).

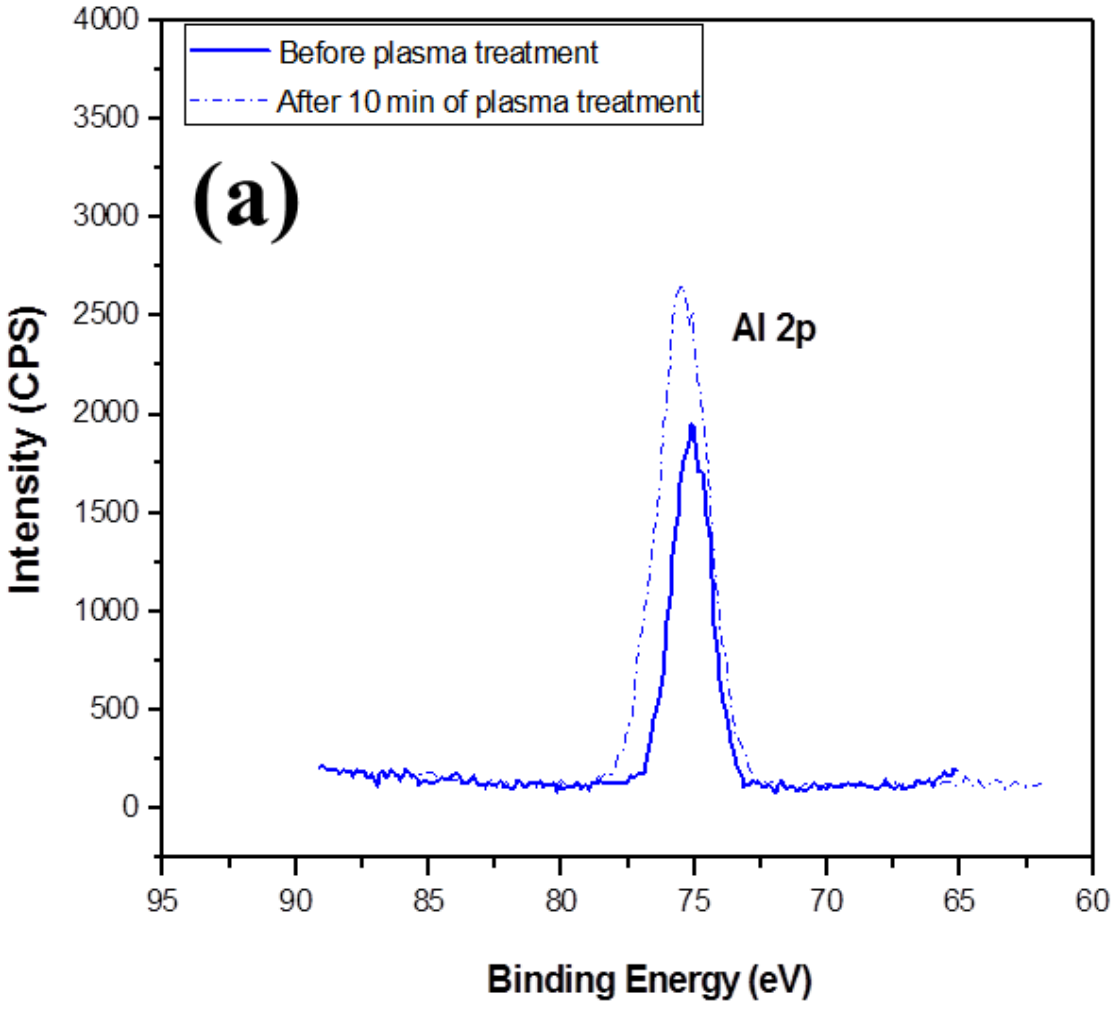

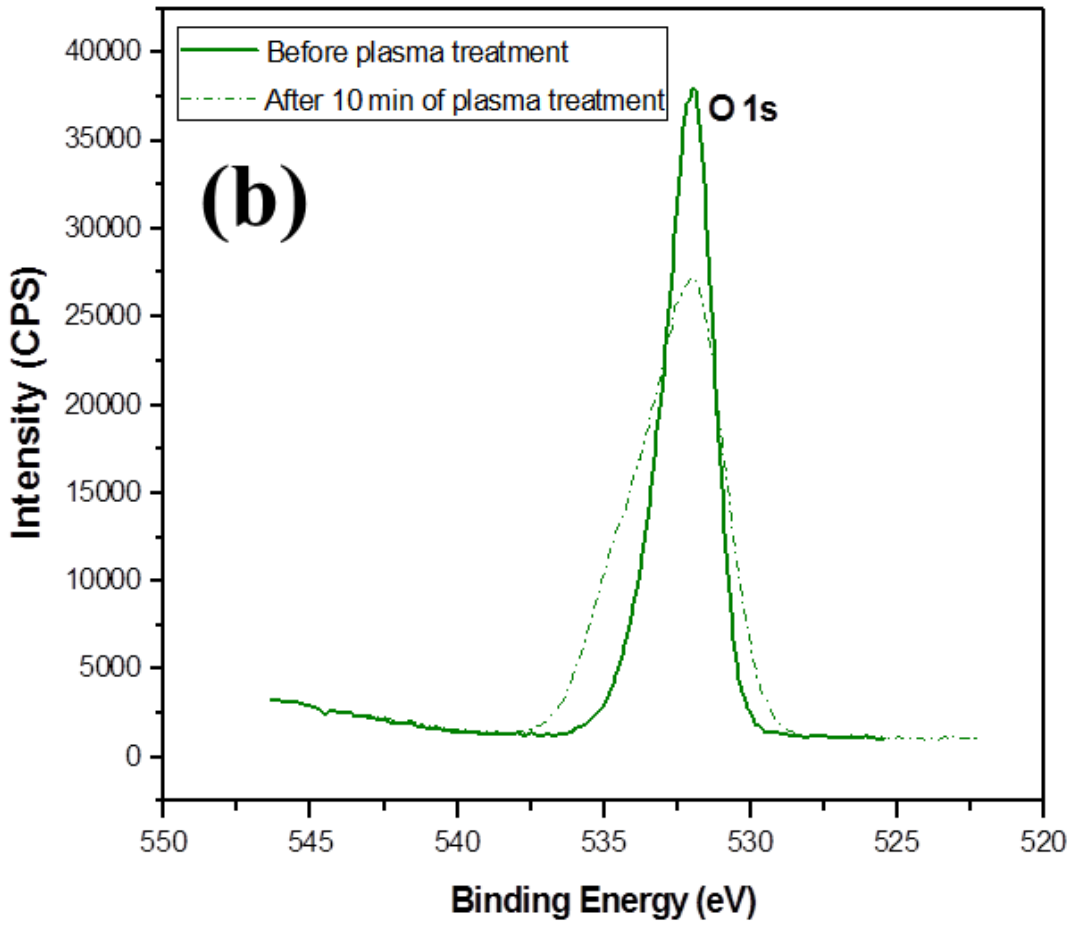


Figure 4-9: XPS spectra of polycrystalline alumina (a) Al 2p and (b) O1s peaks before plasma treatment and after 10 min of plasma treatment.

Besides the surface contaminant removal, the plasma treatment is believed to have broken the chemical bonds on the surface [138], leading to the observed enhancement in the adhesion strength. For XPS spectrum analysis in Fig. 4-9, higher Al/O ratio after plasma treatment is leading to the increased of peak intensity of Al 2p. A slight shift was observed for the Al 2p peak after plasma treatment. In general, XPS peak shift might be caused by the film thickness or the charging effect of the material [139]. In this study, however, both do not seem to

be responsible for the shift because (i) alumina is a thick substrate, so the film thickness effect is excluded; (ii) alumina is an insulating material regardless of the plasma. A possible cause could be the formation of dangling bonds after the plasma treatment, which requires further investigation in the future. There was a peak broadening at binding energy of 532.0 eV in core level for O 1s (Fig. 4-9 (b)). We postulate that the broadening might be due to the new bond formation with O, and detailed analysis will be provided next.

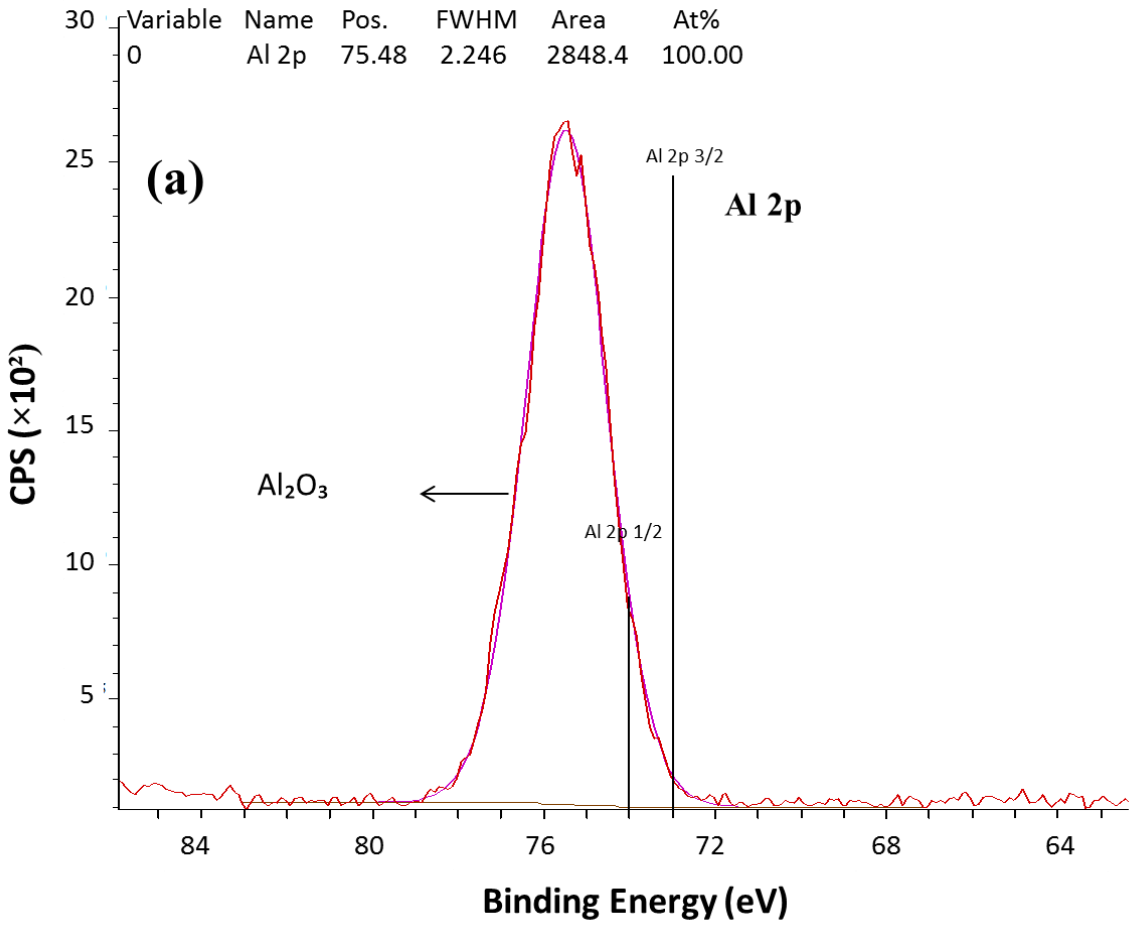

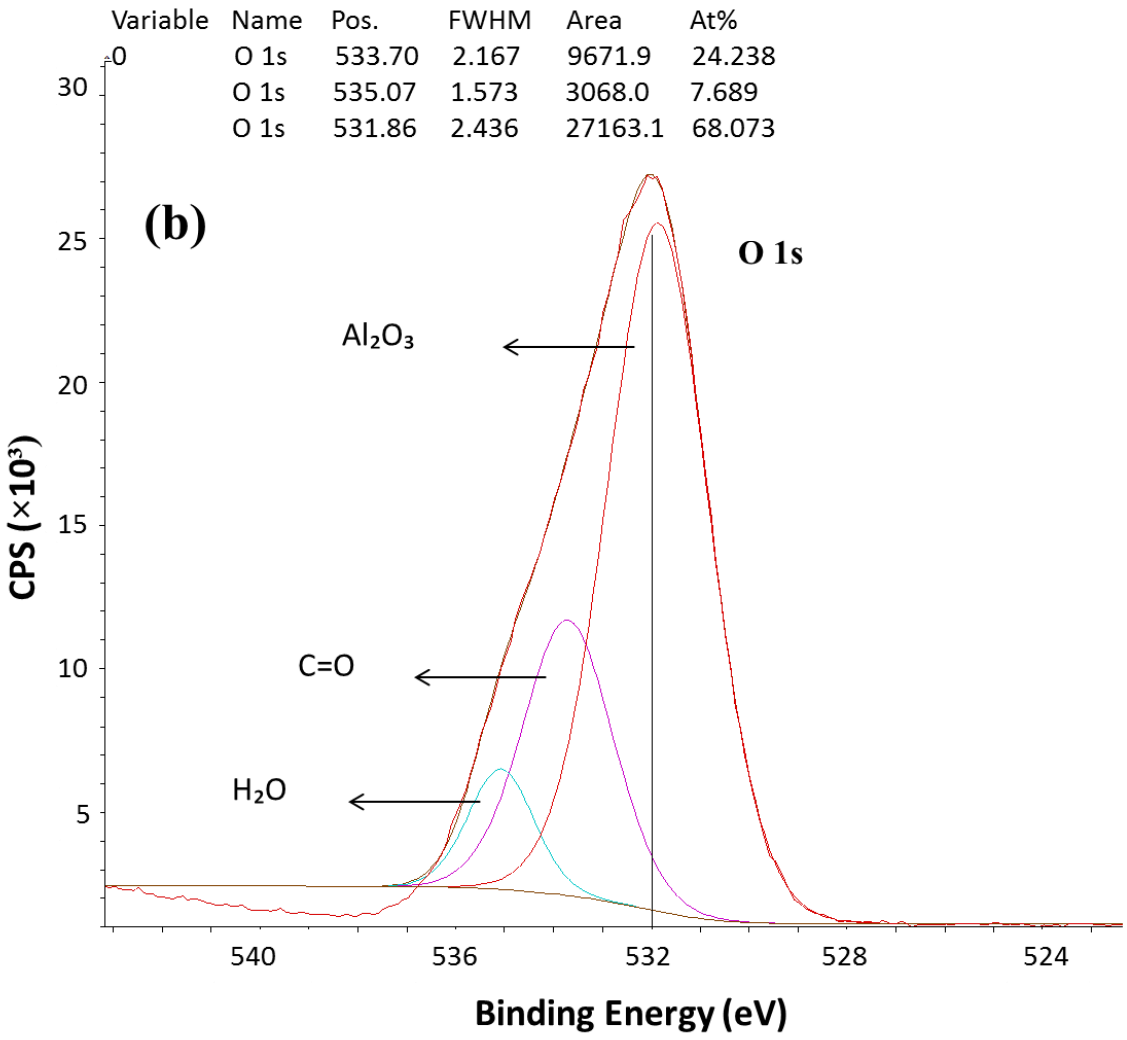


Figure 4-10: XPS peak fitting of polycrystalline alumina (a) Al 2p and (b) O 1s spectra after 10 min of plasma treatment.

Based on the XPS narrow-scan spectrum analysis in Fig. 4-10, the Al 2p and O 1s peaks after plasma treatment are well fitted by one and three binding energy components respectively. The single peak locates at 75.0 ± 0.1 eV [140] is attributed to Al 2p in $Al_2O_3$ (Fig. 4-9 (a) and Fig. 4-10 (a)) before and after plasma treatment. For the O 1s spectrum in Fig. 4-10 (b), three individual component

peaks at 531.86 eV (68.07 At %), 533.70 eV (24.24 At %) and 535.07 eV (7.69 At %) [140] are shown after deconvolution. The peak with lowest binding energy and highest intensity is assigned to $Al_2O_3$. Formation of C=O bond belongs to the middle peak. The one with highest energy is assigned to H-O bond in $H_2O$. It was reported that at low pressure condition, hydrogen gas can be considered as a residual element, and the dissociated H atom might interact with other species to form $H_2O$ or $C_xH_y$ [141].

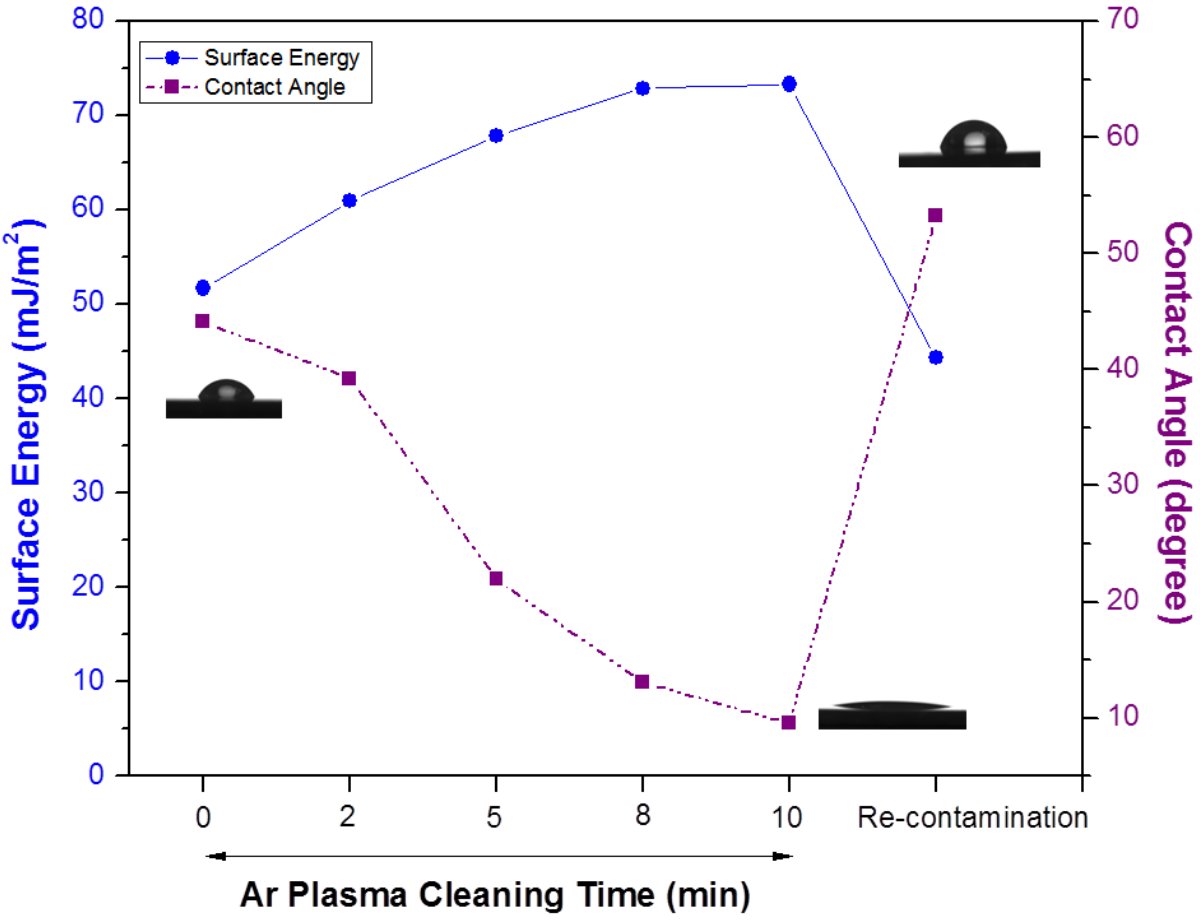


Figure 4-11: Change of wettability, surface energy and contact angle with plasma treatment time.

It was reported that for industrial application, adequate adhesion can be achieved if the surface energy is greater than 50 $mJ/m^2$ [138]. In the current work, surface energy has been measured before and after the plasma cleaning using contact angle measurement. Results on the surface energy and contact angle are shown in Fig. 4-11. It is clear that Ar plasma cleaning has improved the surface energy significantly, reaching 73.3 $mJ/m^2$ after 10 min treatment. Corresponding water contact angle is extremely low immediately after the plasma treatment. However, after exposure in ambience for 10 days, the surface contaminants came back, and the surface energy was reduced to 44.3 $mJ/m^2$. The substrate has lost the benefits introduced by plasma treatment and nearly returned to the original state.

The polycrystalline $Al_2O_3$ substrates were treated with various surface pre-treatments and the surface was then analyzed by contact angle measurement using three different liquids as described in section 4.2.2. For the substrate without any treatment, the contact angle of the original surface was > $90^o$ with poor wettability and hydrophobic condition (Fig. 4-2). For plasma treatment, it is believed the substrate surface was activated by Ar bombardment. The contact angle of plasma activated surface was less than $10^o$ after 10 min of Ar bombardment. It is suggested $Al_2O_3$ surface is very active with a large number of dangling bonds. From the contact angle measurement, a large number of hydroxyl groups may exist on the activated substrate surface after the droplet test.

Change of bond configuration by physical bombardment also contributed to the XPS peak broadening for O 1s spectra. Formation of O-H bond is observed after the surface has been activated by plasma treatment. Under a low pressure

condition, hydrogen gas is considered as a residual element. With the dangling bonds created on the substrate surface, the dissociated H atoms may interact with the O ions and form O-H bond on the surface as shown in Fig. 4-10.

It shows that plasma for a length of time is sufficient to enhance the number of dangling bonds for the $Al_2O_3$ substrate surface and improves the surface affinity to adhesion. The microscopic flatness of the substrate was not deteriorated by the plasma activation process (Fig.4-7). Hence, it can be considered to be an optimum treatment for Cu-$Al_2O_3$ bonding. The comparison has illustrated the importance of keeping the surface clean for strong film adhesion. It is therefore recommended that film deposition to be carried out immediately after the cleaning step inside the sputter deposition chamber without breaking the vacuum.

*4.3.1.4 Group 3*

To further understand the interplay between heating and plasma treatment, they are both applied after solvent cleaning (group 3, Table 4.1). Following the sequence of solvent cleaning, heating, and argon plasma treatment, the adhesion strength was 16.9 ± 3.0 MPa, which is much lower than the two-step treatment without heating (25.0 MPa after 2 min plasma treatment and > 34 MPa after 10 min treatment). The measured surface energy (Fig. 4-12) shows insignificant increase after the plasma treatment (from 50 $mJ/m^2$

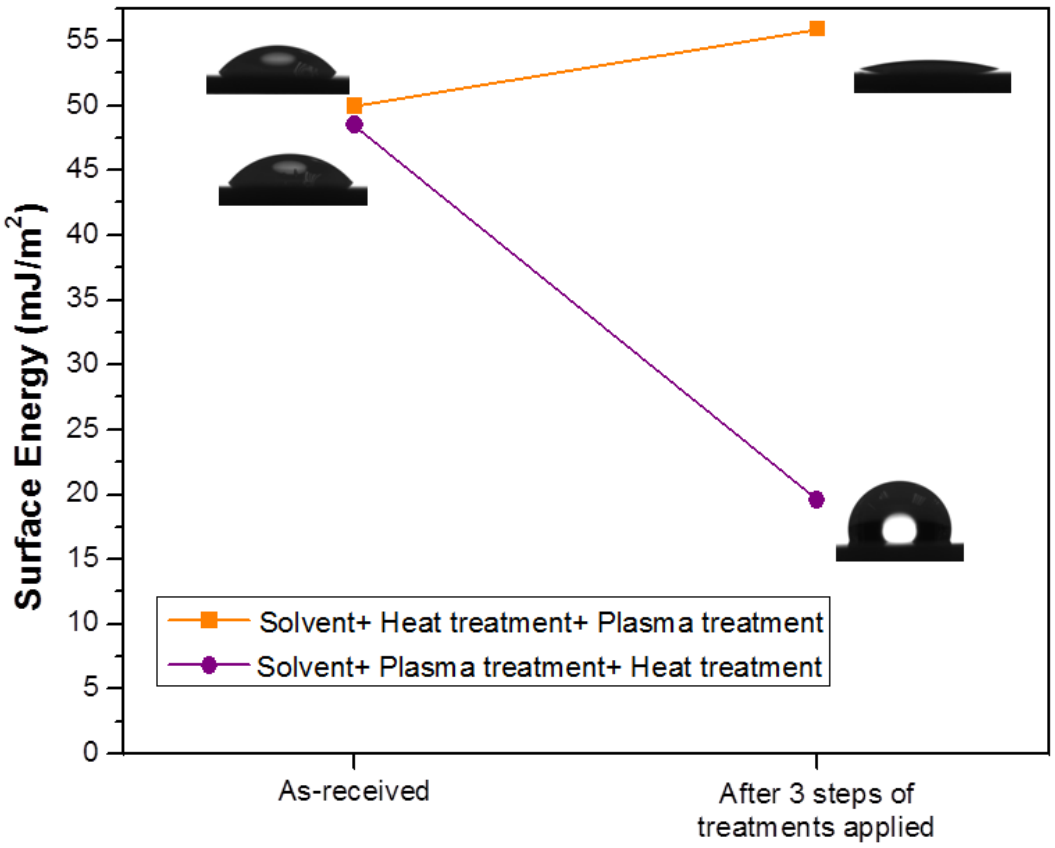


Figure 4-12: Surface energy change of the polycrystalline $Al_2O_3$ (*rms* 10-150 nm) before and after treatments applied.

to 55.8 mJ/m$^2$). When heat treatment is applied after the plasma treatment, the surface energy dropped significantly to 19.6 mJ/m$^2$. The corresponding adhesion strength has also dropped to a very low level at 5.3 MPa. The result suggests that when heating is the last step before Cu film deposition, it could very likely contaminate the surface by evaporating the residues inside the chamber back to the substrate surface. When heating is applied before plasma treatment, it might have played an adverse role by anchoring the surface contaminants, making it more difficult to be removed by the subsequent plasma treatment. We take note the

vacuum level ($5.0 \times 10^{-5}$ Torr) is not very high, therefore the residual oxygen inside the chamber might have helped "securing" the adhesion of contaminant molecules onto the substrate surface. The role played by oxygen residue is unclear so far, and more investigation is needed to understand its effect on surface condition and film adhesion. As heating and plasma treatment are often used for thin film deposition, our current work suggests that the two treatment procedures should not be applied in sequence before film deposition.

*4.3.1.5 Group 4*

As a further verification, the plasma cleaning substrates were placed under the ambient condition for 10 days before Cu film deposition (group 4 in Table 1). The obtained low strength at 7.7 MPa with a large standard deviation displays a good similarity with the as-received samples. The surface energy was reduced to 44.3 $mJ/m^2$, which is similar to the one before treatment. The decrease in adhesion strength (-77 %) and surface energy (-41%) were indicative of the return of impurities to substrate surface.

## 4.4 Chapter Summary

Surface pre-treatment is one of the imperative factors affecting the interfacial adhesion between materials. Different surface cleaning techniques and treatment sequences were studied for their effect on Cu film adhesion with

polycrystalline $Al_2O_3$ substrate. The treatments were categorized into 5 groups from group 0 (as-received sample) to group 4 (re-contaminated sample) using polycrystalline $Al_2O_3$ substrates with *rms* in the range of 10 – 150nm. The findings of this chapter are:

(1.) Embedded impurities or residues through the surface pores has weakened the Cu film adhesion to the $Al_2O_3$ substrate

(2.) There are changes on surface wettability and adhesion strength for different surface pre-treatments

(3.) Organic solvent cleaning with the aid of ultrasonication has very limited impact on improving the adhesion strength

(4.) Heat treatment and piranha acid soaking are not sufficient to remove surface contaminants

(5.) Humidity or residual solvent is not the key factor for adhesion enhancement

(6.) There is at least a 6-fold of adhesion strength increment by in-situ argon plasma cleaning

(7.) Plasma treatment is an effective way to provide a cleaner surface for better bonding

(8.) Development of dangling bonds after plasma treatment is the reason of excellent adhesion strength

(9.) There is an increase of amount of contaminant with the density of substrate surface pores

(10.) The re-contamination step is induced when heat treatment is applied either

before or after the plasma treatment

(11.) Multi-treatment steps are not recommended for Cu-$Al_2O_3$ bonding

(12.) Substrate has lost its plasma induced properties after exposed to the normal air atmosphere

# CHAPTER 5: COPPER-ALUMINA BONDING MECHANISMS

## 5.1 Introduction

Ceramic metallization has been a subject of interest in electronic devices for the past few decades. Ceramic substrate metalized with a layer of conductive film has been extensively studied mechanically, chemically and electrically [62, 74, 109, 114, 142, 143]. The unique material properties and excellent stability of ceramic substrate make it a good option in microelectronic packaging for critical applications [54, 69, 70, 72, 73]. Due to the high demands from market, a well-built and robust structure is needed to improve the system's reliability especially under harsh environment. According to Zhang et al. [20], mechanical failure mode is the major failure path in microelectronic devices, and interfacial debonding between heterogeneous materials is a great concern for reliability.

For adhesion enhancement, different factors include surface pre-treatment, surface cleanliness, joining techniques, bonding parameters etc., have to be considered. For Cu-$Al_2O_3$ bonding, various bonding methods such as eutectic joining [75], transient liquid bonding [104], cold gas spraying [78] and casting bonding [62] have been studied to achieve optimized bonding. However, these methods typically require a high processing temperature, and the process is not compatible with the existing packaging industry practice. For low temperature metallization, an adhesion layer (typically Ti/W) is often needed due to the poor

adhesion at the interface. Direct coating without the adhesion layer has a clear advantage, but the bonding mechanism between directly coated metal thin films and ceramic substrate is yet to be clarified, especially in terms of the quantitative contributions by different contributing mechanisms.

In this project, direct Cu-$Al_2O_3$ bonding was carried out by DC magnetron sputtering method without inserting any adhesion layer. Effort has been made to improve the adherence of Cu thin film on polycrystalline $Al_2O_3$ with different surface roughness as listed in Table 5.1. According to the ASTM standard D907-70 [144], adhesion is a state of affairs when there is a valence force or mechanical interaction or both of the actions take place to hold the surfaces together. In other definitions, adhesion can be classified into four main categories include interfacial bonding, inter-diffusion bonding, physical anchoring and intermediate layer adhesion [145]. Joint created between Cu thin films and $Al_2O_3$ substrate might be attributed by not only surface adsorption, but also the summation effect from other bonding mechanisms. Factors such as surface roughness, porosity density, surface morphology and topography will affect the interfacial joining and causing difficulties during the interface characterization. In order to have better understanding for a bonding system, it is crucial to justify the bonding mechanisms and quantify their contributions for adhesion improvement.

## 5.2 Experimental Setup

### 5.2.1 Sample preparation

Preparation step for polycrystalline $Al_2O_3$ substrate and Cu thin film deposition process have been described in section 3.2.1 and section 4.2.1 respectively.

After film deposition, in-situ annealing was performed directly inside the sputtering chamber without breaking the vacuum. The specimens were heated to 100 °C and 300 °C for 30 min respectively. The heating rate was set at 10 °C/min. The argon gas remained during the annealing. The specimens were taken out after the chamber has been cooled to room temperature slowly.

Monocrystalline $Al_2O_3$ substrates were purchased from Latech Scientific Supply Pte Ltd for comparison study. The substrates in the orientation of $(11\bar{2}0)$ have similar surface energy with polycrystalline $Al_2O_3$ and the surface roughness (root mean square, *rms*) is smaller than 0.5 nm. The cleaning step and the deposition parameters remained the same for both monocrystalline and polycrytsalline $Al_2O_3$ substrate.

### 5.2.2 Materials characterization and adhesion measurement

For the surface analysis, atomic force microscopy (DI-3100, Bruker Corporation) was used to measure the surface topography of the substrate with a

scan area of 20 × 20 μm. The number of sampling points was set at 512 along each line. Tapping mode was used with a frequency of 1.0 Hz, and the probe tip's radius was 15.0 - 20.0 nm. The effective area of a substrate was calculated using a MATLAB program based on the data extracted from the AFM scanned measurement. Scanning electron microscopy JEOL JSM 6360 with back scattering imaging was used to analyze the separated surfaces after the tensile test from both the Cu and $Al_2O_3$ sides. The results were used to interpret the failure site in the adhesion test.

Investigation on the chemical state was carried out by Kratos Axis Ultra X-ray photoelectron spectroscopy system (XPS) integrated with depth profiling analysis under the vacuum condition of $10^{-8}$ to $10^{-9}$. Calibration on the binding energies were completed by locating the C (1s) peak at 284.8 eV as internal reference. Spectra analysis and curve fitting for each element were performed using CasaXPS processing software. The XPS data provide fine details of the surface chemical state which SEM/EDX may not be able to.

Please refer to section 3.2.2 for the residual stress and adhesion strength measurements. Description of apparent surface energy measurement was included in section 4.2.2.

## 5.3 Results and Discussions

### 5.3.1 Adhesion strength of substrates with different roughness

As shown in Table 5.1, polycrystalline $Al_2O_3$ substrates with different surface roughness (root mean square, *rms*) are grouped in S1 (10 – 150 nm), S2 (200 – 350 nm) and S3 (350 – 500 nm). Substrates from group S1 have been polished through a CMP process. Substrates from S2 and S3 are the unpolished samples. Top views of the substrates were shown in the SEM micrographs. For polycrystalline $Al_2O_3$, pores are clearly revealed on the substrate surface and the density of surface porosity increases from S1 to S3. Results are compared with monocrystalline $Al_2O_3$ substrate that has very smooth surface morphology (*rms* < 0.5 nm) and very low surface porosity.

Table 5.1: Surface analysis for $Al_2O_3$ substrates with different roughness and and interface adhesion of Cu films on these substrates

| **Properties** | **Monocrystalline $Al_2O_3$** | **Polycrystalline $Al_2O_3$** | | |
|---|---|---|---|---|
| | | **S1** | **S2** | **S3** |
| *rms* (nm) | < 0.5nm | 10 - 150 | 200 - 350 | 350 - 500 |
| SEM image | 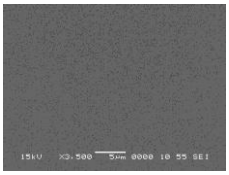 | 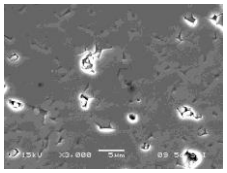 | 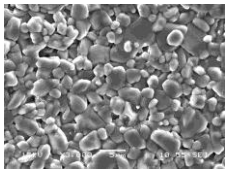 | 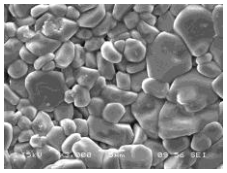 |
| Adhesion strength (MPa) | 5.9 ± 1.5 | 6.1 ± 1.7 | 7.7 ± 4.6 | 8.5 ± 3.2 |

| | | | | |
|---|---|---|---|---|
| Surface energy ($mJ/m^2$) | 46.6 | 51.7 | 63.3 | 66.1 |
| True contact area ($\mu m^2$, scan area: 20 $\mu m \times 20$ $\mu m$) | 400 | 407.5 | 446.8 | 486.6 |
| Effective adhesion strength (MPa) | 5.9 ± 1.5 | 6.0 ± 1.6 | 6.9 ± 4.1 | 7.0 ± 2.6 |
| Bonding mechanism | Adsorption | Adsorption + Mechanical locking | Adsorption + Mechanical locking | Adsorption + Mechanical locking |
| Diffusion bonding | No | No | No | No |
| % enhancement by mechanical interlocking | 0 | 1.7 | 16.9 | 18.6 |

From the adhesion strength measurement in Table 5.1, it shows an adhesion improvement of 44 % by increasing the substrate surface roughness. In addition, the increase of surface energy from 46.6 $mJ/m^2$ to 66.1 $mJ/m^2$ has also indicated a better wetting performance of the rough substrate. According to Wenzel's law (eq. 5.1), the wetting behavior of a material will be amplified by the surface roughness of that material, in which the hydrophobicity or the hydrohilicity of a material will be enhanced by increasing the surface roughness [146].

$$\cos \theta_m = r \cos \theta_Y, \qquad \text{(eq. 5.1)}$$

where r is the ratio of roughness for actual and projected area of the solid surface, $\theta_m$ and $\theta_Y$ are the measured contact angle and Young's contact angle respectively.

### 5.3.2 Correlation between surface roughness and effective area

The effective area of the substrates was calculated by a MALTAB program using the height information in discretized locations measured by AFM. Fig. 5-1 (a) shows the planar profile of a polycrystalline alumina substrate. From the 3D image generated in Fig. 5-1 (b), the surface topography of the substrate was clearly revealed in the direction of z-axis. Hence, it is crucial to work out the true contact area of a sample. Accordingly, effective adhesion strength was calculated, as shown in Table 5.1, based on true contact area.

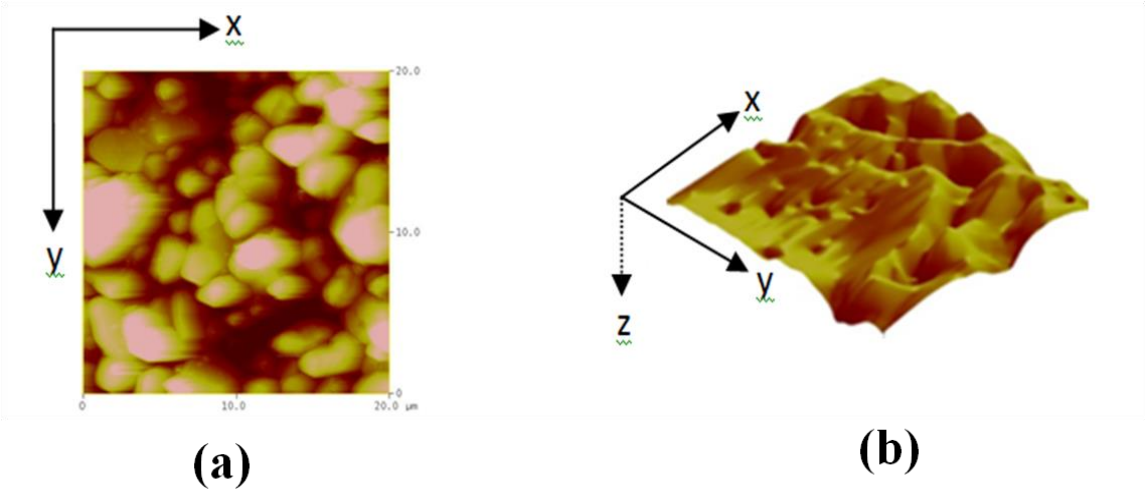


Figure 5-1: AFM surface profile of a polycrystalline $Al_2O_3$ substrate (a) 2D image (b) 3D image

The relationship of surface roughness to the effective area of a substrate, as indicated in Table 5.1, shows the increased effective area as the roughness increases. This means that the interface contact area is enlarged by the uneven surface structure of the polycrystalline $Al_2O_3$ substrates. In addition to the rough surface, the surface porosity has an impact on the Cu-$Al_2O_3$ adhesion too. Besides adsorption bonding on top surface, the sputtered atoms can be pinned down to the porous sites and locked tightly inside the concaved regions. The monocrystalline $Al_2O_3$ substrate has very flat surface, it shows no pores, voids and valley formation on the surface. During the deposition process, it is impossible for mechanical anchoring to take place. We believe that surface adsorption is the only contributing bonding mechanism in the Cu-monocrystalline $Al_2O_3$ bonded system.

To observe the film / substrate interface, SEM images are given in Figs. 5-2 and 5-3 for the cross-sectional views of the coated specimens. From Fig. 5-2, intimate contact between Cu film and $Al_2O_3$ substrate was observed. The same has occurred for other polycrystalline substrates with different surface roughness. Entire coverage of Cu sputtered atoms onto the polycrystalline $Al_2O_3$ with irregular surface structure was shown in Fig. 5-3. Throughout the deposition process, ions and/or atoms inside the sputtering chamber are moving ballistically from target to substrate by momentum transfer. The energetic Cu atoms will be moving randomly on the substrate surface or bombarded into the concave regions before final settlement. This leads to much improved Cu film adhesion with rough polycrystalline $Al_2O_3$ which has a higher effective bonding area.

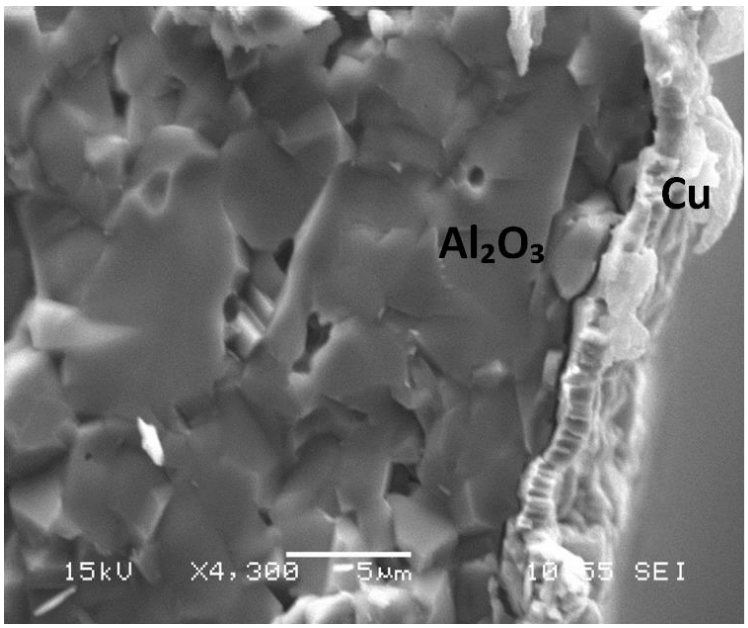


Figure 5-2: SEM side view image of Cu-$Al_2O_3$ bonding system with polycrystalline substrate from group S2.

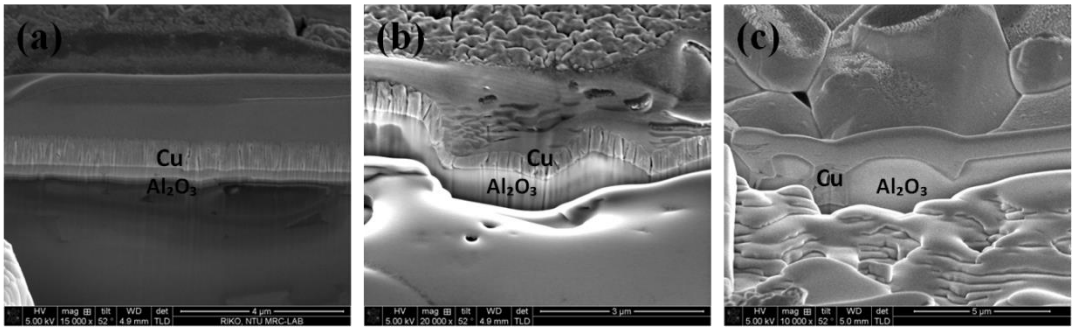


Figure 5-3: FIB-SEM cross sectional images of Cu-$Al_2O_3$ bonding using polycrystalline substrates from group (a) S1 (b) S2 and (c) S3.

The reported effective adhesion strength in Table 5.1 provides an approximation of the contribution to the adhesion enhancement by the mechanical interlocking mechanism. If we use the effective adhesion strength of monocrystalline sample as the baseline, assuming the only contributing mechanism is surface adsorption (to be elaborated later), contribution from mechanical

interlocking will then be differentiated. Detailed discussion will be made in the next two sections.

*5.3.2.1 Total effective area coded using MATLAB computing system*

The effective area of the substrates was calculated using a MALTAB program using the data extracted from AFM analysis. The scan area was set at 20 μm × 20 μm with sampling points of 512. An algorithm was proposed to calculate the effective area using Heron's formula (eq. 5.2). Basically, the effective area of a sample was calculated by summing up the area of the individual small cubic as illustrated in Fig. 5-4 (a) with sampling interval of 39 nm in both x- and y-directions. The 3D image extracted from the small cubic was illustrated in Fig. 5-4 (b). The irregular surface structure shows different vertical distances along the z-axis on every point of the substrate. This will absolutely complicate the final calculation on the effective area for polycrystalline $Al_2O_3$ substrate. Therefore, a method was proposed to find out the surface distances along x- and y-axis by elongating the structure in Fig. 5-4 (c) into a rectangular shaped of structure as illustrated in Fig. 5-4 (d). The effective area of an individual rectangular will then calculated using Heron's formula (eq. 5.2) based on MATLAB coding. The total area of a small cubic was taken based on the average value from four different directions (two diagonals from each axis) for error minimization. From the algorithm suggested, the effective area of a sample with the scale size of 20 μm was calculated from 262144 small cubic (Fig. 5-5), which able to provide better accuracy in the effective area analysis.

$S = (a + b + c) / 2,$ (eq. 5.2)

$A = \sqrt{S\,(S-a)(S-b)(S-c)},$

where S is the semiperimeter of a triangle, while A is the area of a triangle with side lengths of a, b, and c.

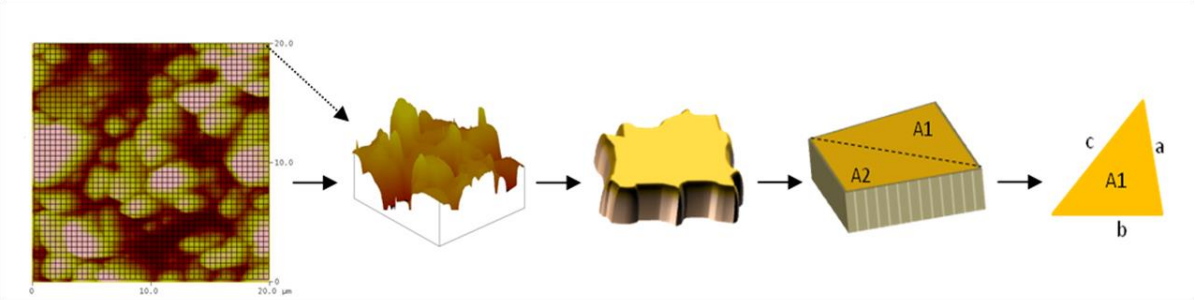


Figure 5-4: Illustration of area estimation using Heron's formula.

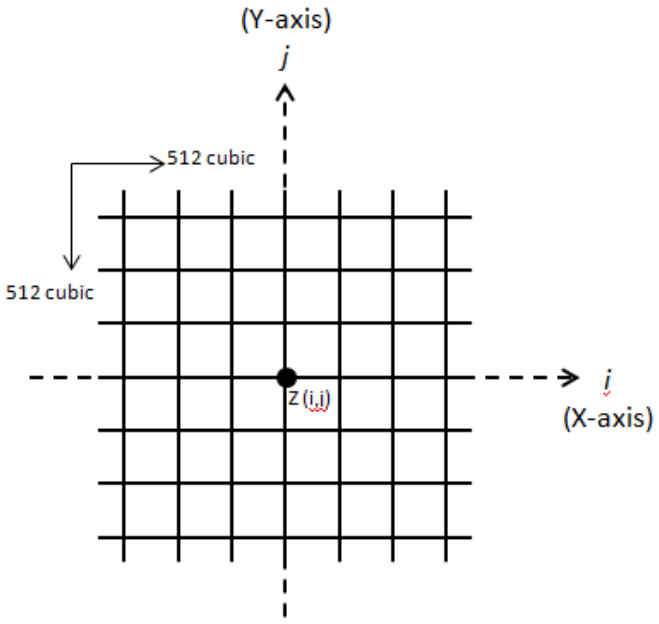


Figure 5-5: Effective area calculation of a polycrystalline $Al_2O_3$ substrate using 262144 of data points.

*5.3.2.2 Comparison of total effective area using 2D, 3D and MATLAB calculation*

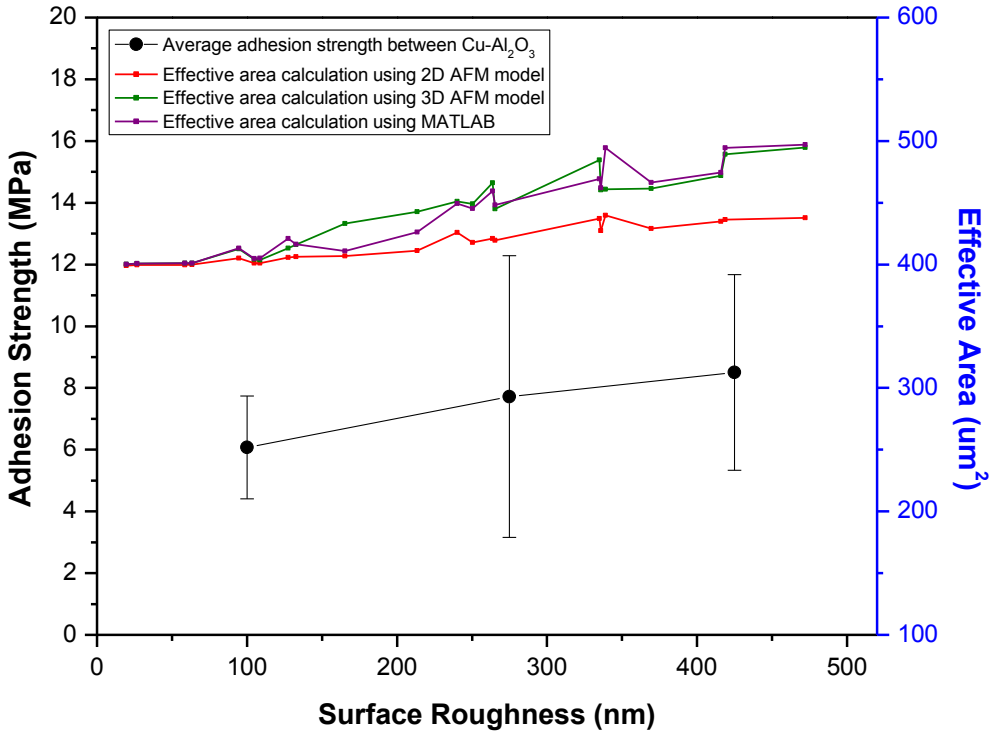


Figure 5-6: Methods comparison for total effective area calculation

The 2D and 3D AFM total effective area was calculated manually using Microsoft Office application. The simple 2D calculation was drafted using trapezoid area (Appendix A2) whereby the height of trapezium was kept at a constant value of 0.5882 µm. The 3D AFM area calculation was proposed by including the Z-matrix (Appendix A3). Among the methods used (Fig. 5-6), results are considered comparable for substrate with smaller surface roughness. However, there is a huge deviation on the effective area from AFM 2D methods when the substrate surface roughness increases. It implies the importance of surface porosity or the concave surface structure of the substrates to the true interface contact area

between Cu thin film and $Al_2O_3$ substrate. The joining profile between materials has to be figured out through the total contact area computation.

### 5.3.3 Surface adsorption

As mentioned above, monocrystalline $Al_2O_3$ substrate with very flat surface was used to quantify the contribution of various bonding mechanisms. From the SEM inspection in Fig. 5-7, a clean separation between Cu thin film and monocrystalline $Al_2O_3$ was observed. The very flat surface of the substrate shows no possibility for the physical locking bonding to take place. There was indeed no Cu residue on the substrate side after separation. From Fig. 5-7(b), the grain structure of the Cu thin film was clearly revealed. The smooth surface structure shows no failure such as cracking, buckling in the Cu film itself after the adhesion test.

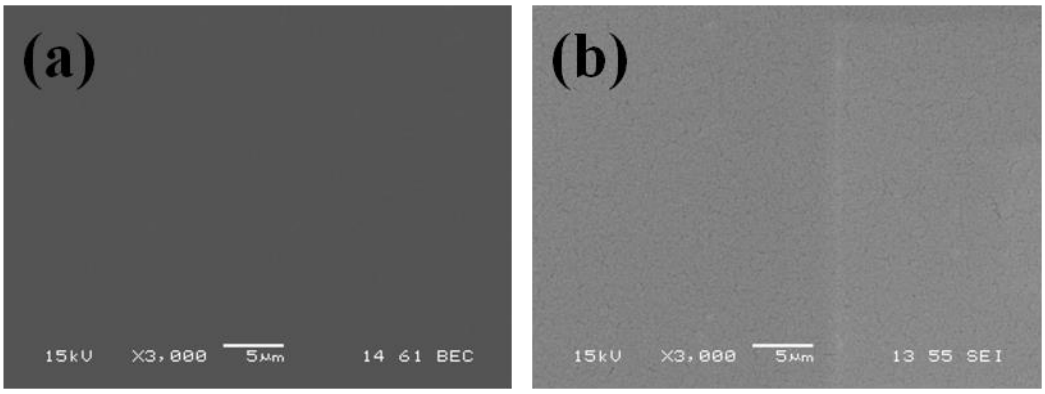


Figure 5-7: SEM images of separated Cu-monocrystalline $Al_2O_3$ bonding (a) monocrystalline $Al_2O_3$ substrate side and (b) copper side.

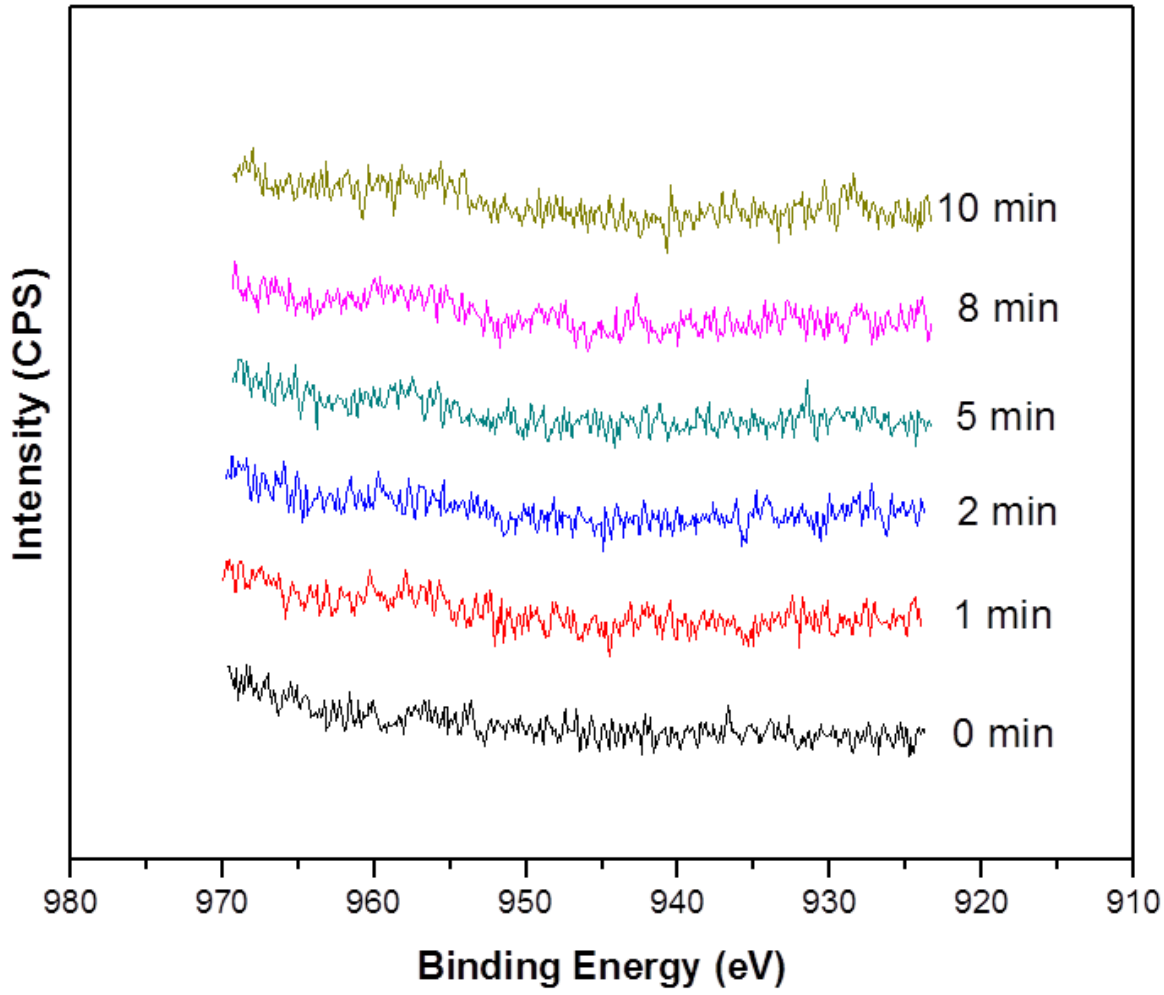


Figure 5-8: XPS spectra with depth profiling analysis on monocrystalline $Al_2O_3$ substrate after tensile test. The Ar plasma bombardment time is indicated in the graph.

To further verify the above claim, the surface after tensile test was also inspected using XPS integrated with depth profiling technique by argon plasma etching for 0, 1, 2, 5, 8 and 10 min. The purpose was to exam possible interaction between Cu film and $Al_2O_3$ substrate. From the XPS spectra analysis with binding energy in the range of 923 to 970 eV in Fig. 5-8, the Cu 2p peak with estimated binding energy range from 925 to 960 eV was not detected in the XPS spectra,

indicating there is no residual Cu left on this extremely flat substrate surface. This observation supports our early SEM observation that Cu thin film has been completely detached from monocrystalline $Al_2O_3$ substrate after the adhesion test. In addition, it also confirms that there is no chemical reaction between Cu and $Al_2O_3$. Therefore, physical surface adsorption is suggested to be the only bonding mechanism for Cu-monocrystalline $Al_2O_3$ bonding which is responsible for the observed low adhesion strength.

### 5.3.4 Mechanical interlocking

As discussed above, besides surface adsorption, mechanical interlocking and diffusion bonding mechanisms might exist for rough and polycrystalline substrates. For Cu-polycrystalline $Al_2O_3$ bonding in group S1, the substrates have surface roughness (*rms*) in the range of 10 – 150 nm. Fig. 5-9 shows the SEM images of separated surfaces of Cu thin film and polycrystalline $Al_2O_3$. There were some Cu residues on the substrate side after separation (Fig. 5-9 (a)). It is suspected the Cu atoms have locked mechanically and trapped inside the pores during deposition. On the Cu side as shown in Fig. 5-9 (b), the cracking lines and broken sites are suggestive of a higher separation force to pull the Cu film away from polycrystalline $Al_2O_3$ as compared with monocrystalline substrate. This is primarily due to the mechanical locking effect.

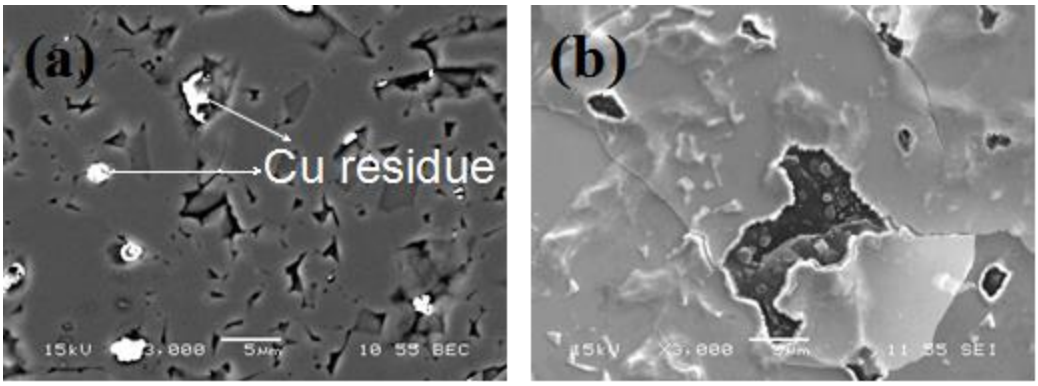


Figure 5-9: SEM images of separated Cu-polycrystalline $Al_2O_3$ bonding (a) polycrystalline $Al_2O_3$ substrate side and (b) copper side.

For Cu-polycrystalline $Al_2O_3$ bonding, a Cu 2p peak was observed on the substrate surface right after 1 min of Ar bombardment as presented in Fig. 5-10. However, Cu element was not detected in longer plasma etching times beyond 1 min. On the topmost layer of substrate (0 min), Cu film has been completely pulled away from the substrate surface. The results seem to indicate that there was only a small amount of Cu at sub- but very close to the top surface. With the Cu 2p XPS narrow spectrum analysis in Fig. 5-11, the obtained binding energies were caused by the splitting of spin orbital for Cu 2p 3/2 (931.0 eV) and Cu 2p 1/2 (951.1 eV) core level transition respectively. The Cu 2p spectrum was well fit by single component which attributed to the $Cu^0$ element [140], and there was no indication of chemical bonding between Cu and $Al_2O_3$. In addition, oxidized Cu is not detected.

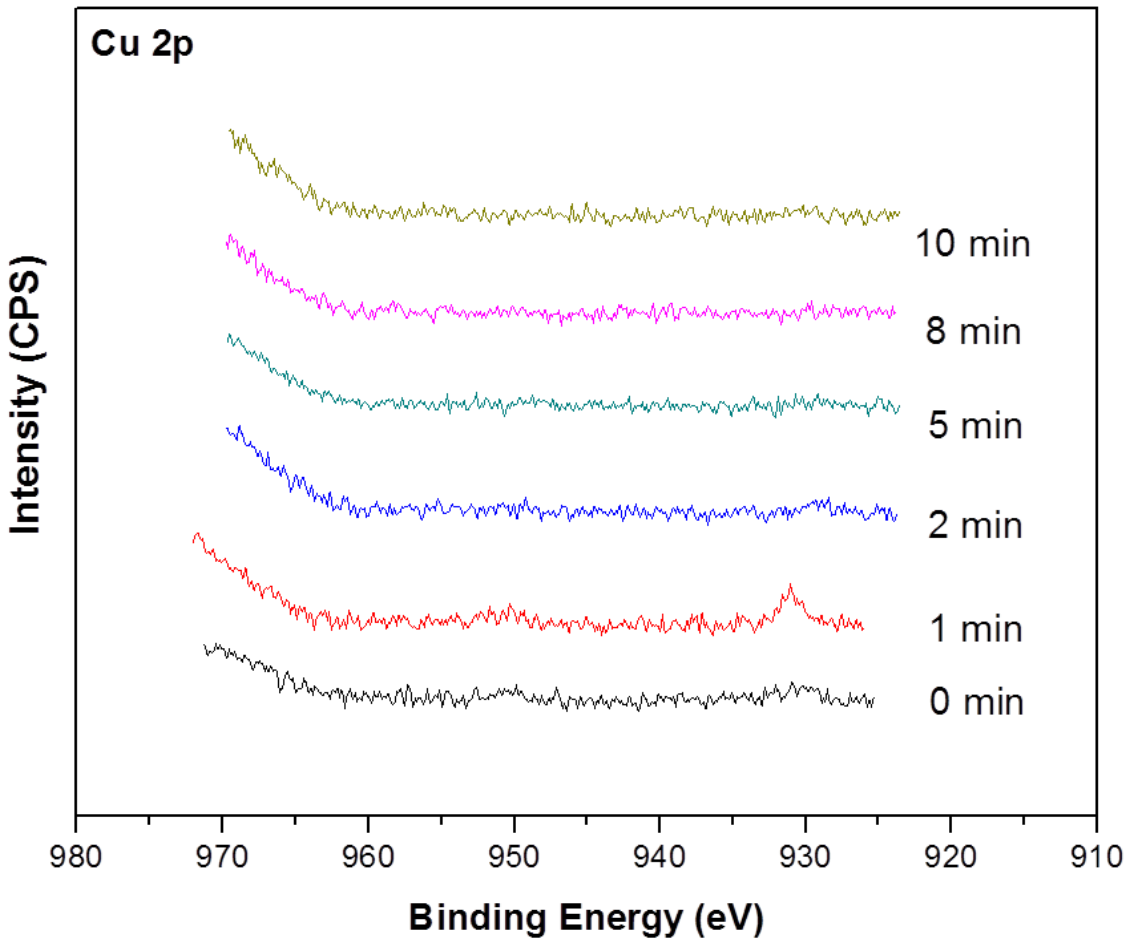


Figure 5-10: Cu 2p XPS spectra with depth profiling analysis on polycrystalline $Al_2O_3$ substrate after tensile test

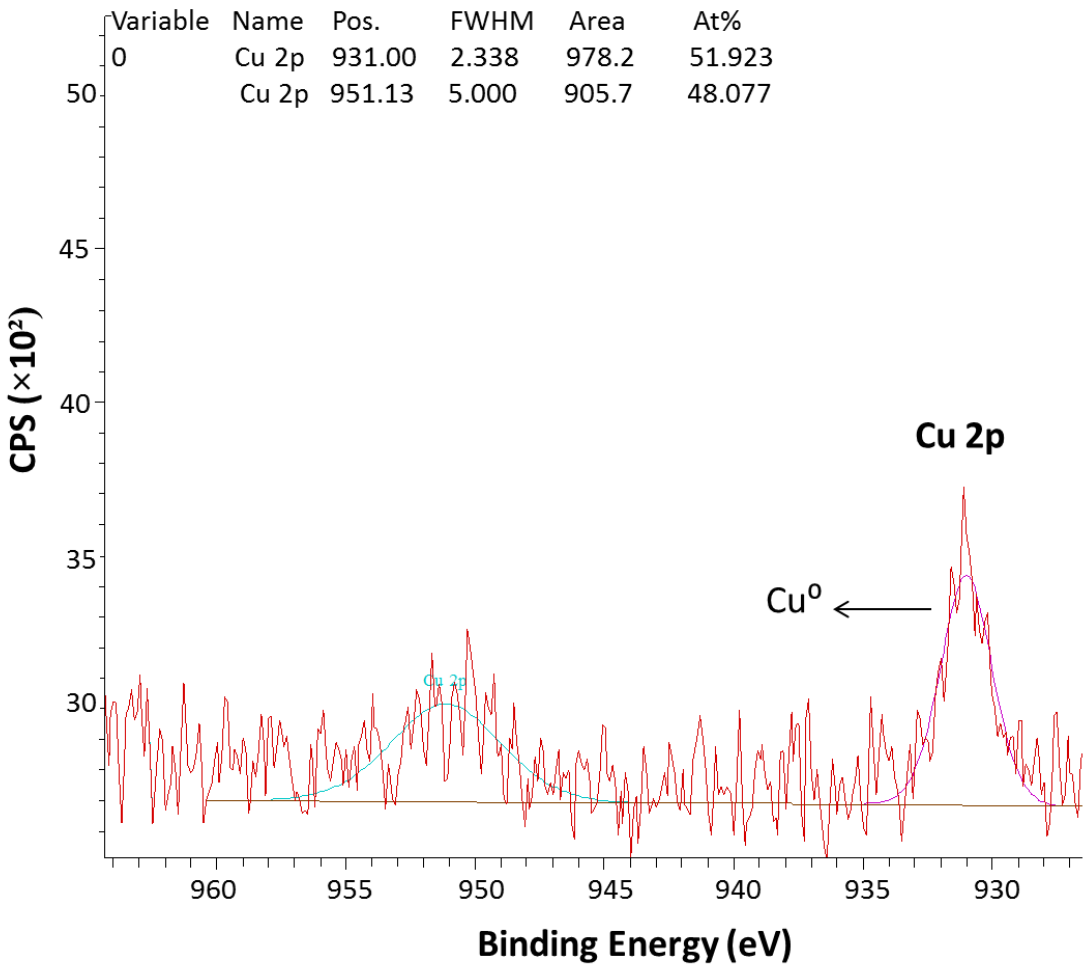


Figure 5-11: Cu 2p XPS narrow spectrum on polycrystalline $Al_2O_3$ substrate after 1 min of depth profiling.

Therefore in Cu-polycrystalline $Al_2O_3$ bonding, we believe the interfacial adhesion is contributed by physical adsorption and mechanical interlocking. Obviously mechanical locking is strongly affected by the surface roughness [16, 17] and the porosity density of the substrate. The uneven surface structure of $Al_2O_3$ has contributed to the increase of adhesion strength for Cu-$Al_2O_3$ bonding. It

is physically straight forward to understand that rough surface is easier to attract particles than substrate with smooth surface as illustrated in Fig. 5-12. The large contact area provided by the curved surface or the porous region increases the chance of permanent atoms settling by mechanical interlocking bonding.

The separated surfaces viewed from Cu and polycrystalline $Al_2O_3$ sides are presented in Fig. 5-13 and Fig. 5-14. The amount of Cu residues has increased with the substrate surface roughness from S1 (10 – 150 nm) to S3 (350 – 500 nm), and these residues preferably stayed around the porous regions (Fig. 5-13). From the SEM images in Fig. 5-14, similar surface features on the detached Cu films are observed. This proves that the Cu film is deposited by closely following the surface profile of the substrate. The observed broken sites on the Cu thin film suggest strong mechanical locking effect between Cu thin film and polycrystalline $Al_2O_3$ substrate. The observation indicates that besides atoms adsorption on the surface, sputtered Cu atoms with high mobility have sufficient energy to travel into the deeper region in substrate sub-surface via pores and voids. With more pore spaces on the substrate surface, more spaces will be created for Cu atoms to be deposited inside.


Figure 5-12: Schematic illustration of area in contact of an atom on a (a) smooth surface and (b) rough surface

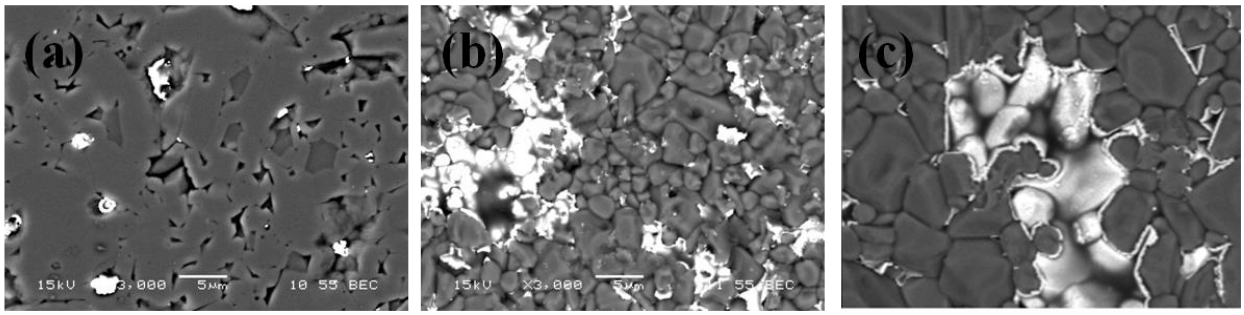


Figure 5-13: SEM micrographs of substrate surface after the tensile test by using polycrystalline $Al_2O_3$ with different surface roughness (a) group S1 (b) group S2 and (c) group S3.

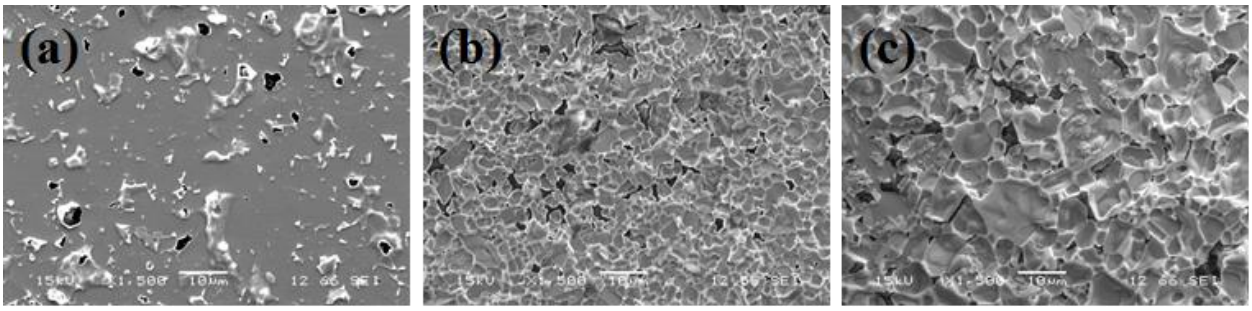


Figure 5-14: SEM micrographs of Cu film after the tensile test by using polycrystalline $Al_2O_3$ with different surface roughness (a) group S1 (b) group S2 and (c) group S3.

The preceding investigation is based upon the assumption that the true contact area of monocrystalline $Al_2O_3$ substrate is 400 $\mu m^2$ due to its extremely low surface roughness (< 0.5 nm). With the baseline study from Cu-monocrystalline $Al_2O_3$ bonding (indicated in red dotted line in Fig. 5-15), besides surface adsorption, the adhesion strength for $Al_2O_3$ substrates with higher surface roughness is improved by other bonding mechanisms. From the SEM images in Fig. 5-13, the adhesion enhancement is claimed to be contributed by mechanical interlocking bonding. The quantitative observation of mechanical interlocking

bonding (%MI) is determined by eq. 5.4. From Table 5.1, it shows an enhance contribution of mechanical interlocking from 1.7 % (group S1) to 18.6 % (group S3) with the increase of substrate surface roughness.

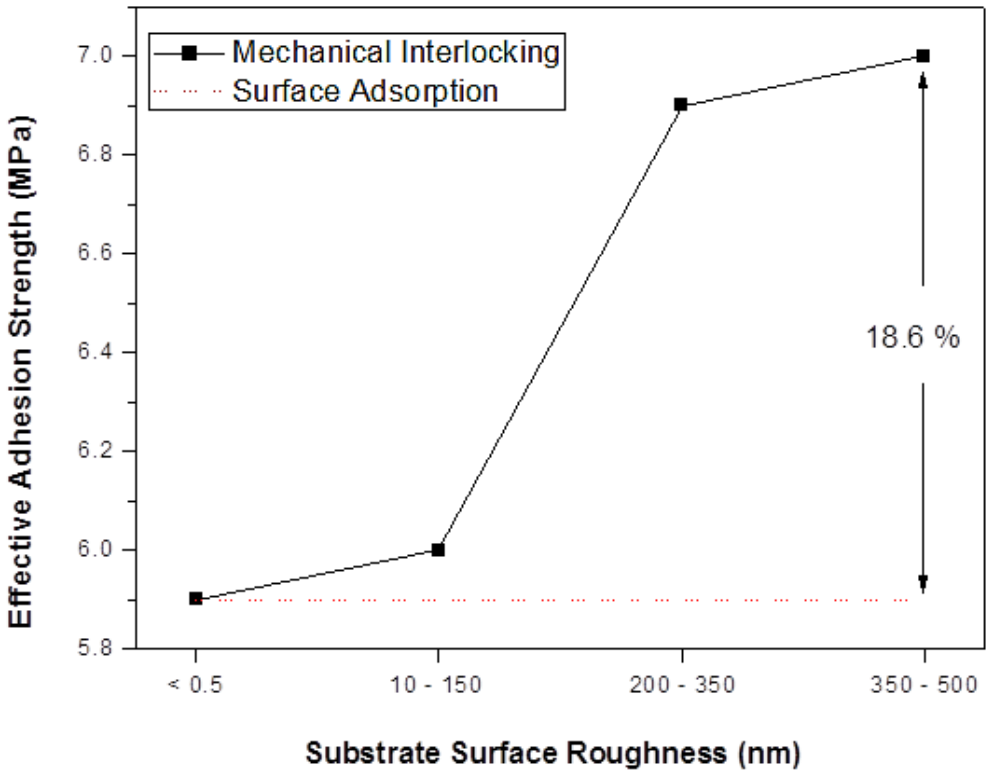


Figure 5-15: Impact of substrate surface roughness on the effective adhesion and the bonding mechanisms between Cu thin film and $Al_2O_3$ substrates

The effective adhesion strength is calculated with the equation below:

$$\sigma_E = \frac{\sigma}{A_T} \times A, \qquad \text{(eq. 5.3)}$$

where $\sigma$ is the measured adhesion strength, A and $A_T$ are the sample scan area and true contact area respectively.

The quantitative observation of mechanical interlocking bonding (%MI) is determined with the equation below:

$$\%MI = \frac{\sigma_{E\_PolyAl2O3} - \sigma_{E\_MonoAl2O3}}{\sigma_{E\_MonoAl2O3}} \times 100\ \%, \qquad \text{(eq. 5.4)}$$

where $\sigma_{E\_PolyAl2O3}$ is the effective adhesion strength of polycrystalline $Al_2O_3$ substrate with different surface roughness and $\sigma_{E\_PolyAl2O3}$ effective adhesion strength of monocrystalline $Al_2O_3$ substrate.

### 5.3.5 Diffusion bonding

At the as-deposited state, diffusion of Cu atoms into lattice or grain boundary of the substrate is quite unlikely due to the low deposition temperature and short duration. Following the previous discussion, we believe surface adsorption and mechanical interlocking are the only contributing factors to the observed adhesion. In this section, possibility of diffusion bonding is analyzed by applying in-situ post deposition annealing at 100 °C and 300 °C respectively for 30 min under inert gas atmosphere. Monocrystalline and polycrystalline S1 substrates were used for comparison study.

Post annealing is commonly used to alleviate the internal stress induced during the deposition to prevent interface delamination [147]. However, from Fig. 5-16, post annealing has weakened the interfacial bonding between Cu and monocrystalline $Al_2O_3$ substrate. The adhesion strength dropped from 5.9 ± 1.5

MPa (room temperature) to 3.2 ± 1.3 MPa after the 300 °C annealing. The Cu film stress was in the compressive state, it has increased from -111.8 MPa (as deposited) to -147.6 MPa after 300 °C annealing for 30 min. On the other hand, the Cu film stress for the polycrystalline substrate was in tension and it decreased from 116.7 MPa to 53.3 MPa after annealing. The exact reason for the opposite trend of influence requires further investigation, and it is suspected the presence (or absence) of grain boundaries and surface pores might be the reason for the difference. The lack of such surface features in monocrystalline $Al_2O_3$ substrate might have prevented the migration of Cu atoms into the porous structures, preventing the stress relief.

The adhesion strength with polycrystalline $Al_2O_3$ bonding (group S1) improved by 18% after post annealing at 300 °C for 30 min. There are two potential factors behind the improvement. The first one could be the reduction of the film stress which has reduced the stored elastic energy in the film. Such a reduction helps the enhancement of film adhesion. The second factor could be Cu diffusion deeper into the pores and voids, which will be analysed further later.

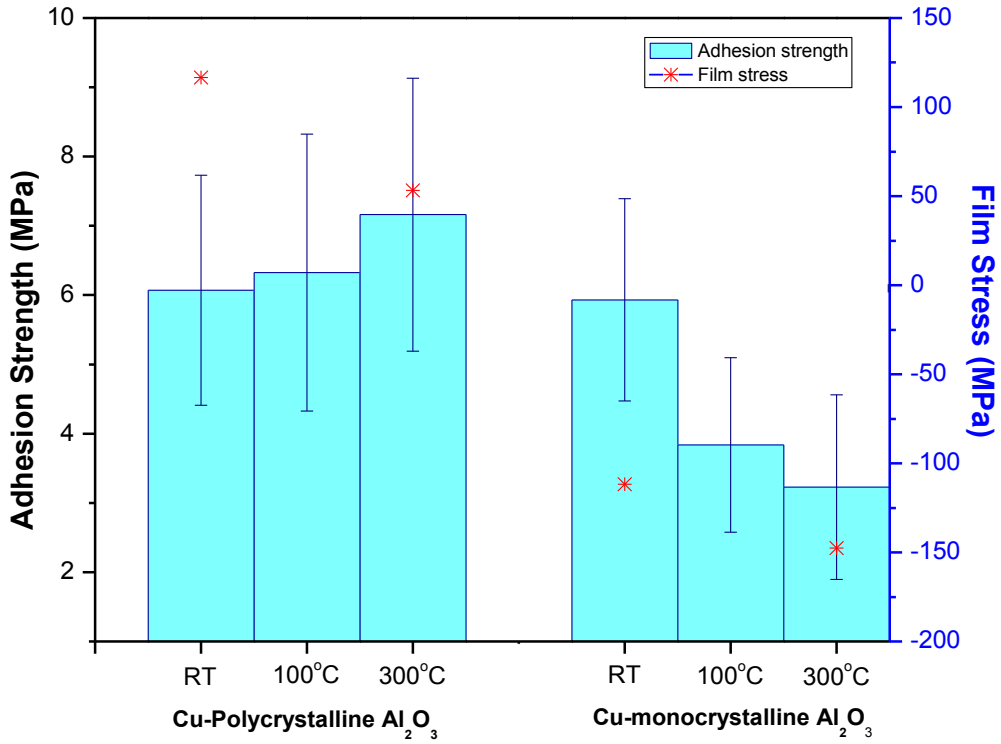


Figure 5-16: Effect of in-situ post annealing to the Cu-$Al_2O_3$ adhesion strength and film stress.

SEM inspection was carried out on the separated surfaces as shown in Fig. 5-17 for Cu-monocrystalline $Al_2O_3$ bonding. From Fig. 5-17(a), cracking lines were evidently exposed on the monocrystalline $Al_2O_3$ substrate. Cu film cracking was observed in Fig. 5-17 (b). The substrate surface cracking might be caused by the tensile stress imposed by the Cu film although the exact magnitude of such stress is difficult to estimate using a simple model.

For Cu-polycrystalline $Al_2O_3$ bonding, the separated surfaces of annealed sample show similar surface features (Fig. 5-18) as the ones without post-annealing. High percentage of the substrate surface has been occupied by Cu

residues under high temperature heating as indicated in Fig. 5-18 (a). This is in agreement with the observed adhesion improvement.

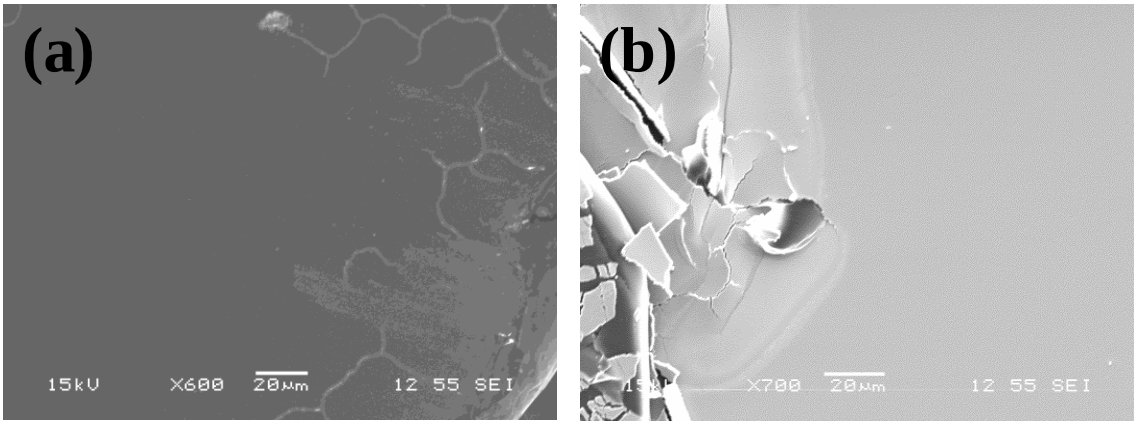


Figure 5-17: SEM images of separated Cu-monocrystalline $Al_2O_3$ bonding after post annealing at 300 °C for 30 min (a) monocrystalline $Al_2O_3$ substrate side and (b) copper side.

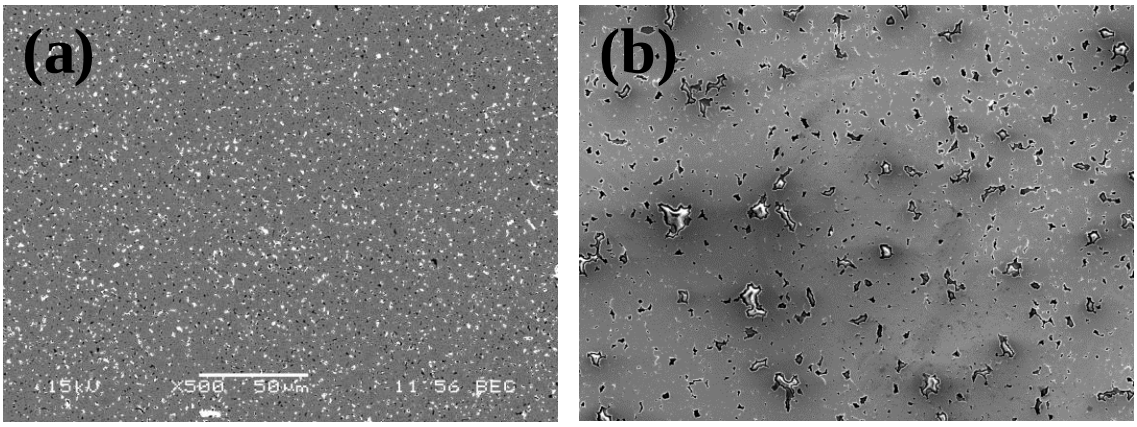


Figure 5-18: SEM images of separated Cu-polycrystalline $Al_2O_3$ bonding after post annealing at 300 °C for 30 min (a) polycrystalline $Al_2O_3$ substrate side and (b) copper side. Same scale bar is applied for the images.

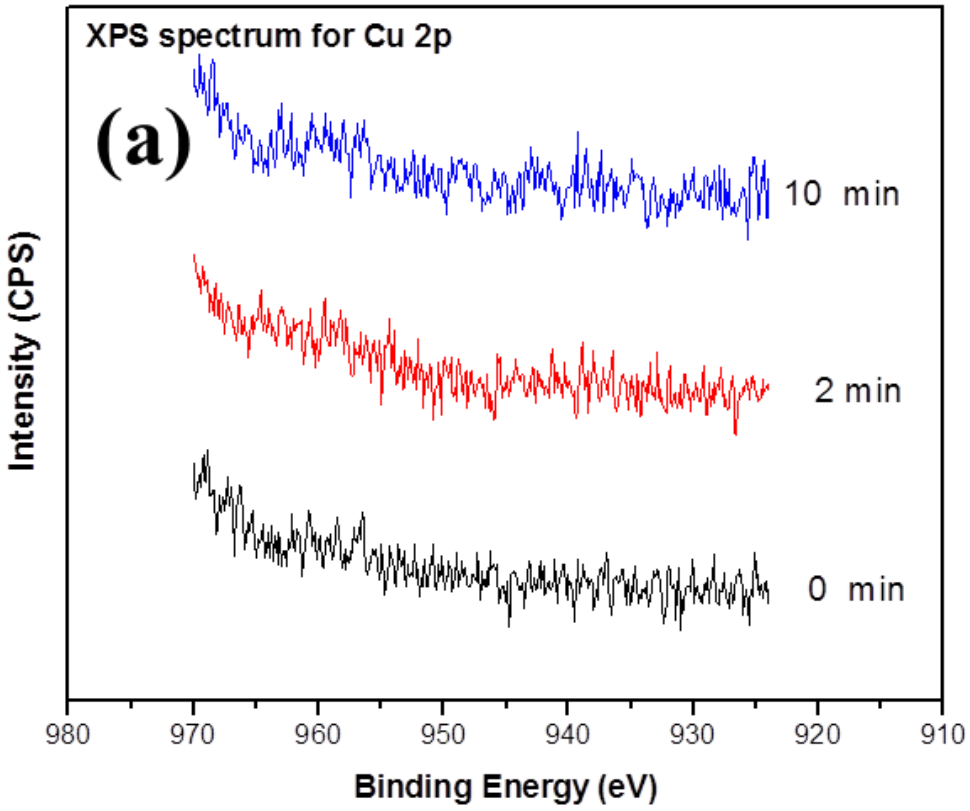
XPS spectrum for Cu 2p
(a)
10 min
2 min
0 min
Intensity (CPS)
980
970
960
950
940
930
920
910
Binding Energy (eV)

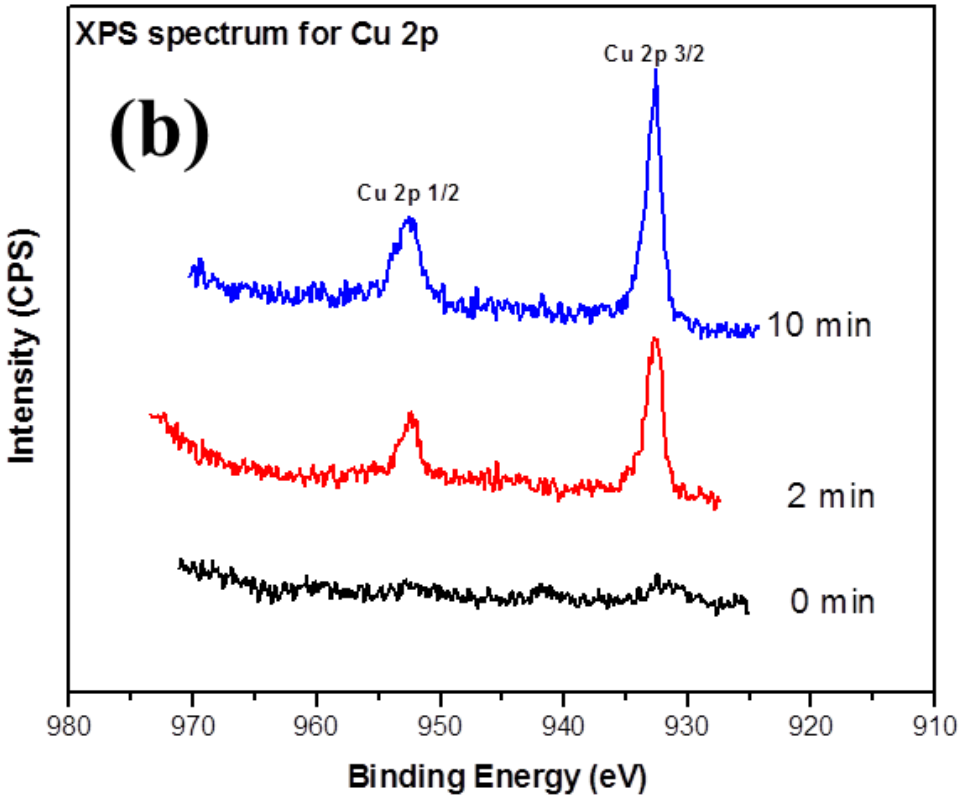
XPS spectrum for Cu 2p
(b)
Cu 2p 3/2
Cu 2p 1/2
10 min
2 min
0 min
Intensity (CPS)
980
970
960
950
940
930
920
910
Binding Energy (eV)

Figure 5-19: XPS spectra with depth profiling analysis on post-annealed (a) monocrystalline $Al_2O_3$ and (b) polycrystalline $Al_2O_3$ substrate after tensile test.

To further investigate the distribution of Cu in the substrate, XPS analysis integrated with depth profiling was conducted on the substrate after film separation. Plasma etching for up to 10 min was carried out on the substrates annealed at 300 °C for 30 min (Fig. 5-19). On the monocrystalline $Al_2O_3$ surface, no indication of Cu element was observed within the binding energy range of 923 eV to 970 eV (Fig. 5-19 (a)). The clean separation at the interface shows the absence of physical locking or diffusion bonding mechanisms in the monocrystalline substrate. However, Cu 2p peaks were detected on the polycrystalline $Al_2O_3$ substrate after 2 and 10 min etching. Based on reported Cu ($Cu^0$, $Cu^+$ and $Cu^{2+}$) binding energies [148], the Cu 2p 3/2 orbital in Fig. 5-18 was only well fitted by $Cu^0$ with binding energy of 932.45 eV. Formation of cupric oxide (CuO) and cuprous oxide ($Cu_2O$) were not detected. According to the reactivity series of metal, Al has higher reactivity and more exothermic (-1675.69 kJ/mol) compared to Cu (-156.06 kJ/mol) [150]. Al has faster reaction during heating to form $Al_2O_3$. However, it also implies the difficulty for reverse reaction in which Al is not easy to be extracted from $Al_2O_3$. Therefore, formation of Cu oxide is not easy to take place under this circumstance.

This is also confirmed by the O 1s XPS narrow spectrum in Fig. 5-21 that no chemical reaction has taken place between Cu and oxygen. The Cu 2p peaks were not visible for surface scan due to the very low signal-to-noise ratio. The presence of Cu atoms deeper inside the substrate is evident compared with the XPS

depth profile of untreated sample. We attribute the increase of the adhesion strength of the polycrystalline sample to the diffusion of Cu into deeper subsurface of the substrate, as well as the relief of film stress. The increase of adhesion strength is about 18 % after annealing; however we are able to distinguish the exact contribution from diffusion mechanism and stress relief. Future investigation is needed to further clarify this point.

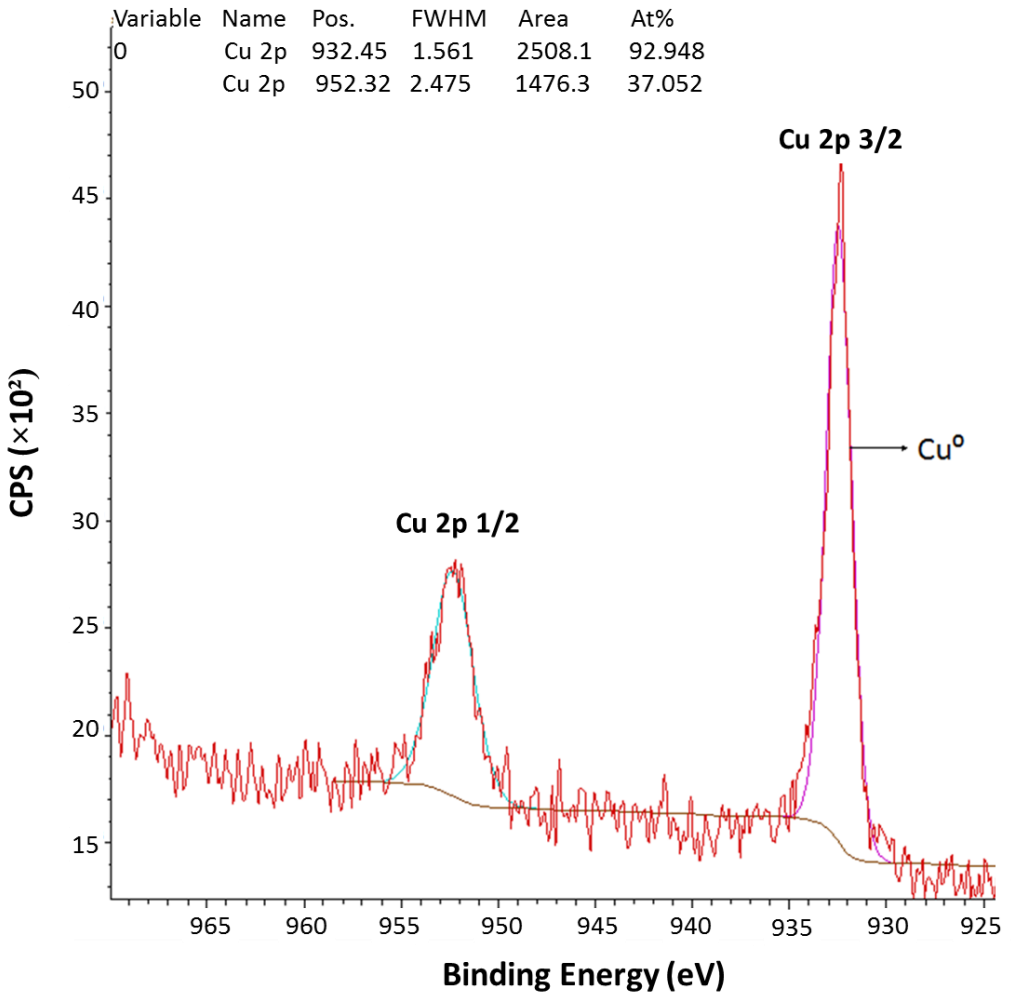


Figure 5-20: Cu 2p XPS narrow spectrum on post-annealed polycrystalline $Al_2O_3$ substrate after 10 min of depth profiling.

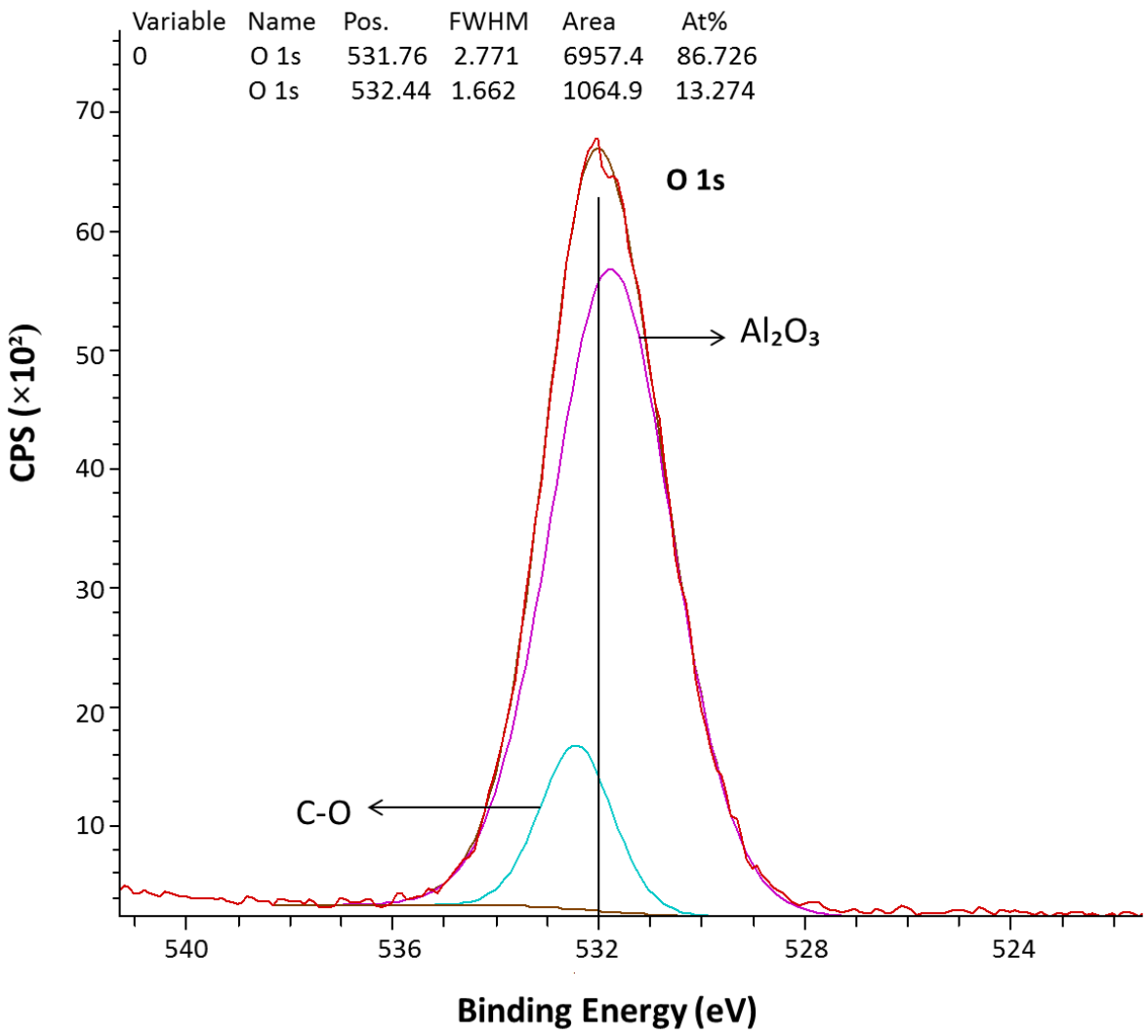


Figure 5-21: O 1s XPS narrow spectrum on post-annealed polycrystalline $Al_2O_3$ substrate after 10 min of depth profiling.

## 5.4 Chapter Summary

Surface roughness is an imperative factor for all types of adhesion. It is equally important to have knowledge on the interfacial bonding mechanism. Besides bonding mechanism justification, the contribution of individual mechanism was also quantified for Cu-polycrystalline $Al_2O_3$ bonding.

(1.) There are changes on the surface energy, interface contact area and the bonding mechanism between monocrystalline and polycrystalline $Al_2O_3$ substrates

(2.) There is an increase of adhesion strength with substrate surface roughness

(3.) Adhesion improvement of more than 40% has achieved using $Al_2O_3$ substrate from S3 group (*rms:* 350 – 500nm)

(4.) Higher effective area is observed for substrate with higher density of substrate surface pores.

(5.) Surface adsorption provides majority of contribution to the interface bonding especially for Cu-monocrystalline $Al_2O_3$ bonding

(6.) Surface porosity is another contributing factor for adhesion enhancement by anchoring reaction between thin films and subtrate

(7.) Mechanical interlocking has contributed up to 18.6 % on the film adhesion

(8.) Diffusion bonding is only activated after post deposition heat treatment

(9.) No chemical interaction between Cu thin film and $Al_2O_3$ substrate before and after annealing under vacuum condition

# CHAPTER 6 CONCLUSION AND FUTURE WORKS

## 6.1 Conclusion

Experiments in this study have revealed key factors, as well as the bonding mechanisms that contribute to the Cu-polycrystalline $Al_2O_3$ bonding enhancement. Improvement on interfacial bonding can be achieved through deposition technology, as well as the surface composition, cleanliness of the bonded surfaces and the substrate microstructure. Plasma treatment is the most effective surface cleaning technique, leading to film adhesion at greater than 34 MPa, well above the set target of 10 MPa of the project. The key findings and their contributions on Cu-$Al_2O_3$ bonding will be elaborated below.

### 6.1.1 Effect of processing conditions to Cu-polycrystalline $Al_2O_3$ bonding

The mechanical integrity of the interfacial joining for Cu-$Al_2O_3$ bonding prepared by DC magnetron sputtering, with different bonding parameters such as sputtering time, deposition pressure and in-situ post annealing have been investigated. Evolutions of structural, morphological and mechanical properties of the Cu thin films as functions of bonding conditions were analyzed. By changing the deposition time, the Cu thin films exhibited a transformation of film microstructure and the change of crystal orientation with the film thickness. However, the adhesion strength of Cu-$Al_2O_3$ bonding is not sensitive to the film

thickness. Increasing the deposition pressure to an optimized level (10 mTorr in this study) accompanied improved residual film stress of 45.3 MPa has yielded the highest adhesion strength of 8.6 ± 0.3 MPa compared to other deposition pressures. The distributions of residual stresses are strongly affected by the kinetic movement and the mobility of Cu adatoms during film growth. The internal stress during the annealing process allows to be lowered for a bonding system. In-situ post annealing for the bonding system was conducted at two different temperatures. It was also found that post annealing at 300 °C for 30 min has contributed up to 18 % on film adhesion by reducing the film stress from 116.7 MPa to 53.3 MPa. It is believed the surface porosity helps to improve the bonding by acting as a stress releasing agent upon heating.

### 6.1.2 Importance of surface treatments for bonding

In this study, Cu-$Al_2O_3$ bonding with different surface pre-treatments was prepared for the investigation of interface chemistry and adhesion strength. Besides surface cleaning techniques, the effect of treatment sequences was also studied to check on the adhesion tendency of Cu thin films on the $Al_2O_3$ substrate. The treatments step is applied to remove the surface contaminants prior to bonding. However, tt was found that organic solvent cleaning, heat-treatment, and piranha acid soaking have very limited impact in improving the adhesion strength.

Argon plasma treatment is the most effective pre-treatment, and it can increase the bond strength by more than six times. The adhesion strength of 34

MPa has been achieved with the plasma cleaning time of 10 min. By contact angle analysis, a drastic drop in contact angle from > $90^o$ to less than $10^o$ is caused by large number of dangling bonds of the substrate surface. The substrate surface has been activated and increase in the surface wettability for better interfacial bonding. From the XPS bonding configuration analysis, the O-H bond formation after plasma treatment is suggestive of bond stabilization on the substrate surface due to the dangling bonds created after strong Ar bombardment. The microscopic flatness of the substrate was not deteriorated by the plasma activation process it is therefore recommended that film deposition to be carried out immediately after the cleaning step inside the sputter deposition chamber without breaking the vacuum.

Caution should be exercised that heating the substrate either before or after the plasma treatment is not recommended as it serves as re-contamination rather than helping the surface cleaning.

### 6.1.3 Bonding mechanisms for Cu-polycrystalline $Al_2O_3$ bonding

Different types of bonding mechanisms have been studied for their contribution to adhesion between magnetron sputtered Cu film and $Al_2O_3$ substrate. Surface adsorption provides majority of contribution to the observed adhesion strength. Comparison between substrates with very low roughness and the ones with higher roughness and surface porosity has revealed that mechanical interlocking is another contributing factor behind the observed adhesion strength increase in the latter. Quantitatively, the mechanical interlocking bonding

mechanism has contributed up to 18.6 % to the Cu film adhesion with $Al_2O_3$ polycrystalline substrate with surface roughness of 350 - 500 nm. Diffusion bonding mechanism may be operative only with post deposition annealing treatment. However at this stage, we are not able to quantify its contribution as annealing has also reduced film stress change when increased strength was found in the polycrystalline sample. XPS analysis confirms that Cu atoms have diffused deeper into the substrate, and there is no chemical reaction between Cu and $Al_2O_3$ during the annealing treatment.

## 6.2 Overall Contribution

In this study, the highest adhesion strength greater than 34 MPa was achieved for direct bonding of Cu thin film to polycrystalline $Al_2O_3$ through DC magnetron sputtering process. This is an abrupt increase compare to 6.1 MPa without plasma cleaning. According to the MIL-STD-883 E (method 2027.2), the achieved value has far exceeded the military standard of 10 MPa. By understanding the key factors on adhesion improvement for Cu-polycrystalline $Al_2O_3$ bonding, the processing steps are uncomplicated and can be easily done at room temperature condition. In addition, no adhesion layer such as titanium, chromium, or tantanum etc. is needed to improve the wetting behavior of Cu to the $Al_2O_3$ substrate.

Several key factors have been studied and guidelines have also been proposed for enhanced Cu-$Al_2O_3$ interface adhesion:

- Substrates with higher surface energy promote stronger adhesion with Cu thin film. Increase of surface energy can be done through surface pre-treatment. Plasma treatment is the most effective among commonly applied surface treatment techniques.
- Minimization of Cu film stress during deposition process to prevent interface failure. Change of deposition pressure or adding a post annealing step helps to reduce the film stress for Cu-polycrystalline $Al_2O_3$ bonding.
- Adhesion strength for Cu-$Al_2O_3$ bonding can be improved by using substrates with higher surface roughness. Rougher surface is able to tightly lock the deposited Cu atoms with greater contact area.
- Substrates with higher degree of surface porosity can further enhance the Cu film adhesion on the $Al_2O_3$ substrate. Besides adhesion improvement, it acts as stress releasing agent upon heating.

In addition, analysis on bonding mechanism between Cu thin film and $Al_2O_3$ substrates has been carried out. Besides bonding mechanisms justification, the contribution of individual mechanism has been quantified in order to have better understanding and more in depth study for Cu-polycrystalline $Al_2O_3$ bonding. Physical adsorption and mechanical interlocking bonding were investigated. Contribution of mechanical interlocking increased with surface roughness and has contributed up to 18.6 % for the bonding system. Diffusion bonding was activated after post deposition annealing, and applied to the substrates with high surface porosity. For Cu-monocrystalline $Al_2O_3$ bonding, physical adsorption is the single bonding mechanism due to its very flat surface structure.

## 6.3 Recommended Future Works

Several recommendations for future works will be proposed in order to have deeper understanding and further improvement for the Cu-$Al_2O_3$ bonding.

**Bonding optimization and reliability testing:**

Besides post deposition annealing, deposition time and working pressure, others processing conditions are suggested for further bonding optimization:

- Vary the deposition power from 100 W to 300 W
- Increase of substrate temperature during the deposition process
- Change of working distance for the substrate-to-target by placing a beaker with different sizes onto the target holder (Fig. 6-1)

With proper deposition conditions, reliability testing such as thermal cycling and high pressure testing are suggested for further bonding enhancement for Cu-$Al_2O_3$.

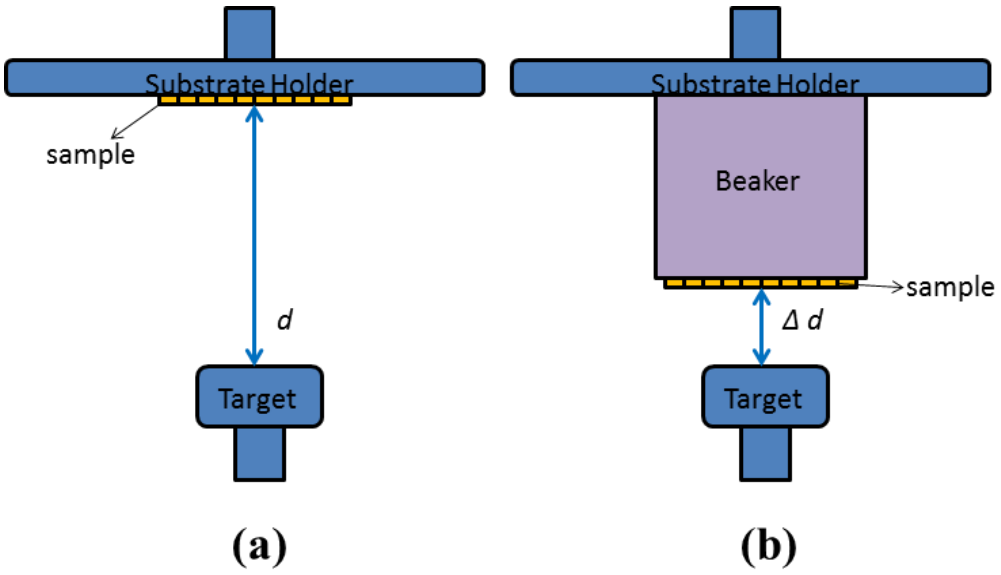


Figure 6-1: Change of substrate-to-target distance during sputtering process (a) long distance (b) short distance.

**Adhesion analysis using the optimized pressure for different types of surface pre-treatments**

The optimized pressure of 10 mTorr has been achieved for Cu-$Al_2O_3$ bonding in this study. Future work is recommended to deposit the Cu thin films on the $Al_2O_3$ substrate using 10 mTorr of deposition pressure for the suggested surface treatments in Chapter 4. It is believed a better performance could be achieved by incorporating the optimized conditions during the sputtering process for Cu-$Al_2O_3$ bonding system.

**Study of bonding mechanism for sample with plasma treatment**

Bonding mechanism analysis has been carried out for Cu-polycrystalline $Al_2O_3$ and Cu-monocrystalline $Al_2O_3$ bonding in Chap 5. The tested samples were solvent cleaned with the aid of ultrasonication prior to bonding. Besides surface adsorption and mechanical interlocking, no chemical interaction was detected between Cu thin films and $Al_2O_3$ substrate.

For $Al_2O_3$ substrates with plasma treatment, surface activation is suspected after strong Ar bombardment. We believe the excellent adhesion strength is achieved through surface activation between Cu and $Al_2O_3$. It is important to study the bonding mechanism for Cu-polycrystalline $Al_2O_3$ bonding after plasma treatment. However, Cu thin film is difficult to be removed due to the strong adhesion at the interface. Work has to be done to remove the Cu film before further analysis.

**Comparison study using monocrystalline $Al_2O_3$ with different orientations**

The comparison study has been completed using monocrystalline $Al_2O_3$ with the crystal orientation of $(11\bar{2}0)$. This plane was selected due to the similar surface energy with polycrystalline $Al_2O_3$ substrates. For further analysis, monocrystalline $Al_2O_3$ with other orientations: (0001), $(10\,\bar{1}0)$ and $(\bar{1}012)$ are suggested to check their effect to the interface bonding between Cu thin films and $Al_2O_3$ substrate. Complexity hexagonal crystal structure (Fig. 6-2) of $Al_2O_3$ has

been a topic of interest in many applications. The arrangement of the anions and cations within the lattice structure will strongly affect the surface chemistry for a bonding.

The correlation between surface energy and the interfacial adhesion strength for Cu-$Al_2O_3$ bonding was carried out using monocrystalline $Al_2O_3$ with different orientations (Fig. 6-3). The surface chemistry analysis is proposed to check their impact to the interaction between Cu thin films and $Al_2O_3$ substrate. We believe the arrangement of $Al^{3+}$, $O^{2-}$ and the empty sites from dissimilar planes is leading to different bonding mechanism through interstitial, vacancy or other points of defects. Simulation using Accelrys Materials Studio 4.4 is proposed to evaluate the interface energy between Cu thin films and $Al_2O_3$ substrate and compare with the experimental results.

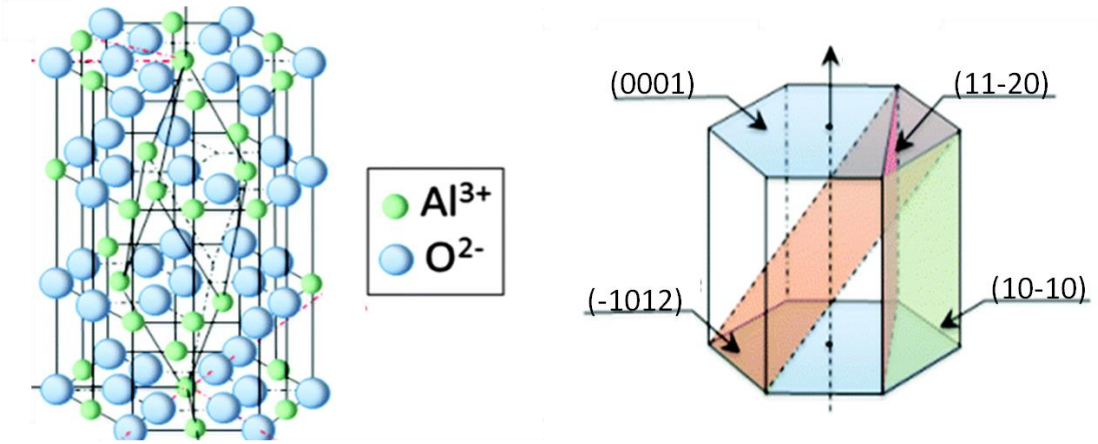


Figure 6-2: Crystal structure of corundum $Al_2O_3$ [149].

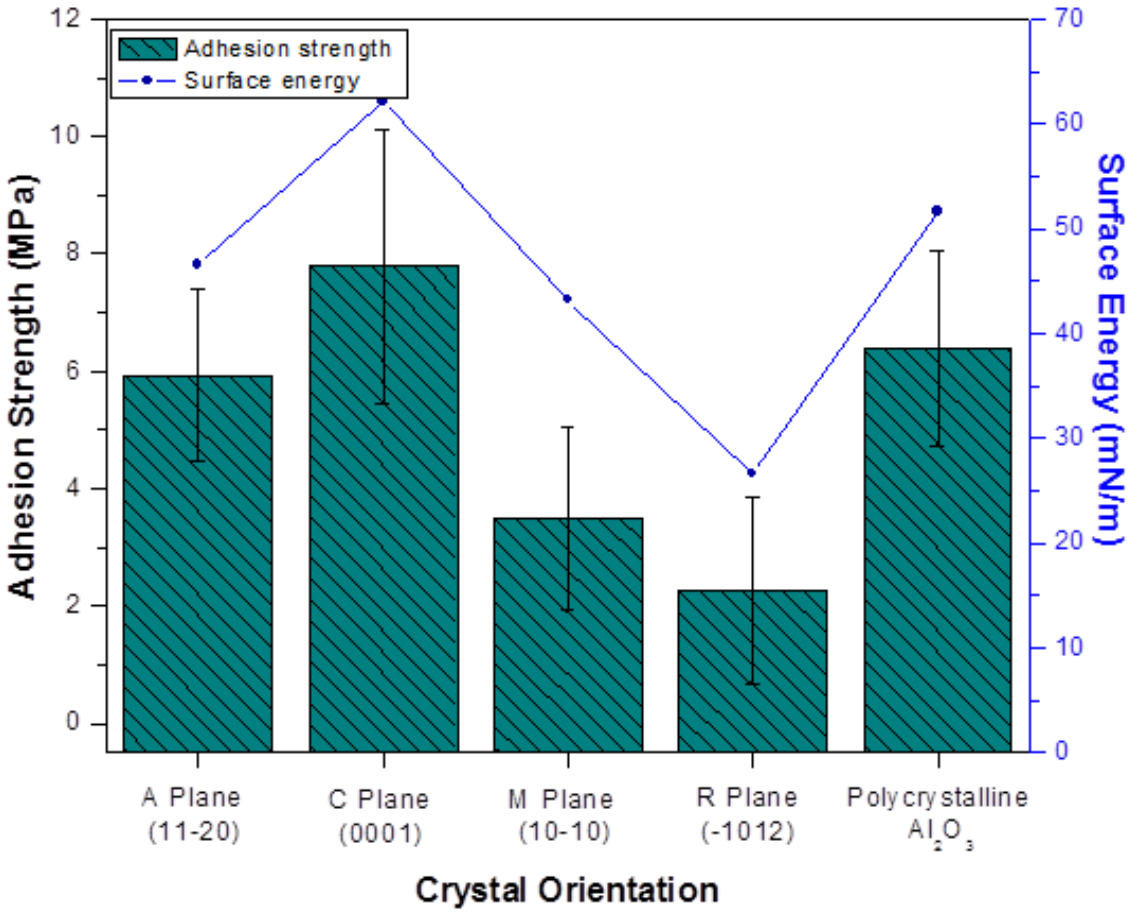


Figure 6-3: Correlation between crystal orientations to the surface energy and adhesion strength for Cu-$Al_2O_3$ bonding.

**Correlation between adhesion strength and work of adhesion:**

Work of adhesion, $W_{ad}$ is denoted as the energy needed to create two free surfaces from the interface between bonded materials with the equation as shown in eq. 6.1 [10].

$$W_{ad} = \Upsilon_f + \Upsilon_s - \Upsilon_{f,s}, \quad (6.1)$$

where $\Upsilon_f$ and $\Upsilon_s$ are the surface energy of the film and substrate respectively, $\Upsilon_{f,s}$ is the energy from the film-substrate interface.

In this study, we found that surface energy of a material is one of the factors affecting the interface adhesion of a bonding. The candidate believes the relationship between adhesion strength and the surface energy is an interesting topic to be studied and it will have a significant effect on the adhesion of a bonding system. For polycrystalline and monocrystalline $Al_2O_3$, the surface energies of the substrates are different with their specific crystal orientations. It is believed the contact angle of molten Cu droplet on $Al_2O_3$ substrate will subsequently affect the value of $\Upsilon_{Cu/Al2O3}$.

According to the eq. 6.1, the work of adhesion could be calculated from the surface energy measurement. The correlation study between work of adhesion ad adhesion strength is suggested in the future work to compare the results theoretically and experimentally.

The relationship between work of adhesion, $W_{ad}$ and adhesion strength has not been published experimentally. Surface energy of a particular material can be checked with contact angle measurement using three different solvents with known surface energy. However, the surface energy analysis of a bonding system is difficult. For Cu-$Al_2O_3$ bonding, molten Cu droplet onto the $Al_2O_3$ has been tried using compact arc melter from Edmund Bühler GmbH (Fig. 6-4) and checked on the contact angle as indicated Fig. 6-5. The surface energy of Cu-$Al_2O_3$ ($\Upsilon_{Cu/\ Al2O3}$) bonding can be then calculated using eq 6.2. The preparation must be well

controlled and completed in less than 5 seconds. The substrate might be broken into pieces due to the extreme high pressure from the electrode. The consistency of this experiment is difficult to sustain.

$$\Upsilon_{Cu/\ Al2O3} = \Upsilon_{Al2O3} - \Upsilon_{Cu} \cos \theta_c, \qquad (6.2)$$

where $\Upsilon_{Al2O3}$ and $\Upsilon_{Cu}$ are the surface energy of $Al_2O_3$ substrate and Cu thin film respectively, $\theta_c$ is the contact angle.

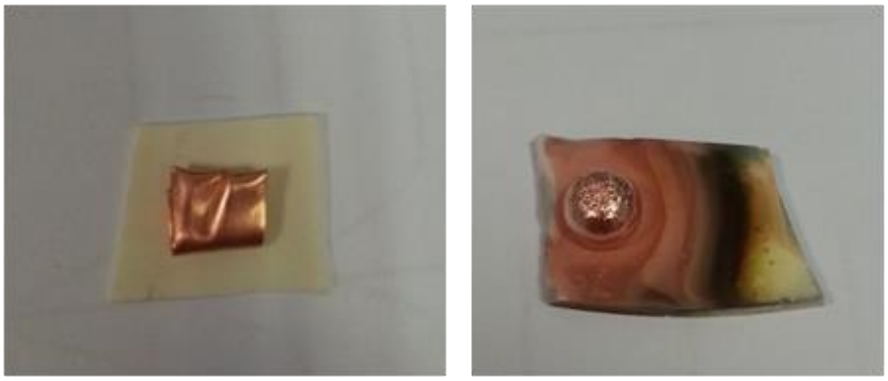

Figure 6-4: Molten Cu droplet on polycrystalline $Al_2O_3$ by compact arc melter.

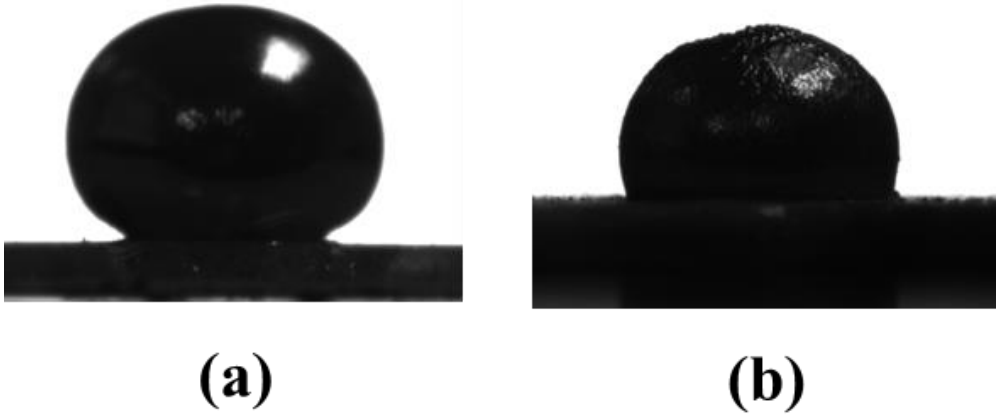


Figure 6-5: Cross sectional view of molten Cu droplet on (a) monocrystalline and (b) polycrystalline $Al_2O_3$ substrate.

# REFERENCES

**The copyrighted materials are used with permission in this thesis.**


1. Tan, C.W. and J. Miao, Optimization of sputtered Cr/Au thin film for diaphragm-based MEMS applications. Thin Solid Films, 2009. 517(17): p. 4921-4925.
2. Ranade, M.B., Adhesion and removal of fine particles on surfaces. Aerosol Science and Technology, 1987. 7(2): p. 161-176.
3. Waters, P. and A.A. Volinsky, Stress and moisture effects on thin film buckling delamination. Experimental Mechanics, 2007. 47(1): p. 163-170.
4. C. Andersson, B.V., C. Noritake, P. Sun, P.E. Tegehall, D.R. Andersson, G. Wetter, J. Liu, Thermal cycling of lead-free Sn-3.8Ag-0.7Cu 388PBGA packages. Soldering & Surface Mount Technology, 2009. 21(2): p. 28-38.
5. Shang, P.J., Z.Q. Liu, D.X. Li, J.K. Shang, Bi-induced voids at the Cu3Sn/Cu interface in eutectic SnBi/Cu solder joints. Scripta Materialia, 2008. 58(5): p. 409-412.
6. Gan, C.L. and U. Hashim, Reliability assessment and activation energy study of Au and Pd-Coated Cu Wires post high temperature aging in nanoscale semiconductor packaging. Journal of Electronic Packaging, 2013. 135(2): p. 021010-021010.
7. Frisk, L., Study of structure and failure mechanisms in ACA interconnections using SEM, scanning electron microscopy, Dr. Viacheslav Kazmiruk (Ed.). 2012.
8. Lim, J.D., R.J.R. Phua, I.M. Riko, A. Sharif, Dy, J,Z, Lim, F.L. Lau et al. Study of thin film metallization adhesion in ceramic multichip module. Proceedings of Electronic Packaging Technology Conference, Singapore, pp. 67-71, 2012.

9. Doane, D.A. and P.D. Franzon, Multichip module technologies and alternatives : the basics. New York : Van Nostrand Reinhold, c1993., 1993. ISBN: 0442012365.
10. Khanna, V.K., Adhesion–delamination phenomena at the surfaces and interfaces in microelectronics and MEMS structures and packaged devices. Journal of Physics D: Applied Physics, 2011. 44(3): p. 034004.
11. Defense, D.o., Test method standard microcircuits, MIL-STD-883E, in Substrate attach strength, Method 2027.21996.
12. Cheng, W., P. Dunn, and R. Brach, Surface roughness effects onmicroparticle adhesion. The Journal of Adhesion, 2002. 78(11): p. 929-965.
13. Sharma, M.M., H. Chamoun, D.S.H. Sita Rama Sarma, R.S. Schecter, Factors controlling the hydrodynamic detachment of particles from surfaces. Journal of Colloid and Interface Science, 1992. 149(1): p. 121-134.
14. Johnson, K., Mechanics of adhesion. Tribology International, 1998. 31(8): p. 413-418.
15. Kim, S.H., S.W. Na, N.-h. Lee, Y.W. Nam, Y.-h. Kim, Effect of surface roughness on the adhesion properties of Cu/Cr films on polyimide substrate treated by inductively coupled oxygen plasma. Surface and Coatings Technology, 2005. 200(7): p. 2072-2079.
16. Lin, Y.S. and H.M. Liu, Enhanced adhesion of plasma-sputtered copper films on polyimide substrates by oxygen glow discharge for microelectronics. Thin Solid Films, 2008. 516(8): p. 1773-1780.
17. Yang, C.-h., S.-c. Lee, J.-m. Wu, T.-c. Lin,, The properties of copper films deposited on polyimide by nitrogen and oxygen plasma pre-treatment. Applied Surface Science, 2005. 252(5): p. 1818-1825.
18. iswanadham, P. and P. Singh, Failure modes and mechanisms in electronic packages [electronic resource]. Boston, MA: Springer US: Imprint: Springer, 1998., 1998. ISBN: 9781461560296.
19. Tummala, R.R., Fundamentals of microsystems packaging . New York: McGraw-Hill, 2001,. 2001. ISBN: 0071371699

20. Zhang, G.Q., W.D. Driel, and X.J. Fan, Mechanics of microelectronics [electronic resource]. Dordrecht: Springer, 2066., 2006. (Solid Mechanics and Its Applications: 141). ISBN: 9781402049354
21. Hsueh, C.H. and A.G. Evans, Residual stresses and cracking in metal/ceramic systems for microelectronics packaging. Journal of the American Ceramic Society, 1985. 68(3): p. 120-127.
22. Wuchen, W., M. Held, P. Jacob, P. Scacco, A. Birolini, Thermal stress related packaging failure in power IGBT modules. in Power Semiconductor Devices and ICs, 1995. ISPSD '95., Proceedings of the 7th International Symposium on. 1995.
23. Yoshino, Y., H. Ohtsu, and T. Shibata, Thermally induced failure of copper-bonded alumina substrates for electronic packaging. Journal of the American Ceramic Society, 1992. 75(12): p. 3353-3357.
24. Cardenas-Garcia, J.F. and M.C. Chyu, Thermally induced failure of microelectronic structures. Journal of Electronic Packaging, 1990. 112(1): p. 80-82.
25. DeMilo, C., C. Bergad, R. Forni, T. Brukilacchio, Thermally induced stresses resulting from coefficient of thermal expansion differentials between an LED sub-mount material and various mounting substrates. SPIE Proceedings Vol. 6486, 2007.
26. Qu, J. Mechanics of polymer/metal interfaces in microelectronic packaging. in Adhesive Joining and Coating Technology in Electronics Manufacturing, 2000. Proceedings. 4th International Conference on. 2000.
27. Teh, L.K., M. Teo, E. Anto, C.C. Wong, S.G. Mhaisalkar, P.S. Teo, E.H. Wong, Moisture-induced failures of adhesive flip chip interconnects. Components and Packaging Technologies, IEEE Transactions on, 2005. 28(3): p. 506-516.
28. Xiaosong, M., K.M.B. Jansen, L.J. Ernst, W.D. van Driel, O. van der Sluis, G.Q. Zhang et al., Moisture diffusion model verification of packaging materials. in Electronic Packaging Technology & High Density Packaging, 2008. ICEPT-HDP 2008. International Conference on. 2008.

29. Van Gils, M., P. Habets, G.Q. Zhang, W.D. van Driel, P. Schreurs, Characterization and modelling of moisture driven interface failures. Microelectronics and reliability, 2004. 44(9-11): p. 1317-1322.
30. Tay, A.A.O. and T.Y. Lin, Influence of temperature, humidity, and defect location on delamination in plastic IC packages. Components and Packaging Technologies, IEEE Transactions on, 1999. 22(4): p. 512-518.
31. Tay, A.A.O. and T.Y. Lin, Moisture diffusion and heat transfer in plastic IC packages. Components, Packaging, and Manufacturing Technology, Part A, IEEE Transactions on, 1996. 19(2): p. 186-193.
32. Xuejun, F., G.Q. Zhang, W.D. van Driel, L.J. Ernst, Interfacial delamination mechanisms during soldering reflow with moisture preconditioning. Components and Packaging Technologies, IEEE Transactions on, 2008. 31(2): p. 252-259.
33. Zhang, G.Q., W.D. Driel, X.J. Fan. Characterization and modelling of moisture behaviour, in mechanics of microelectronics, 2006, Springer Netherlands. p. 281-375.
34. Chan, Y. and D. Luk, Effects of bonding parameters on the reliability performance of anisotropic conductive adhesive interconnects for flip-chip-on-flex packages assembly II. Different bonding pressure. Microelectronics Reliability, 2002. 42(8): p. 1195-1204.
35. Yin, C., H. Lu, C. Bailey, Y-C. Chan, The effect of reflow process on the contact resistance and reliability of anisotropic conductive film interconnection for flip chip on flex applications. Microelectronics Reliability, 2003. 43(4): p. 625-633.
36. Zonghe, L. and L. Johan, Anisotropically conductive adhesive flip-chip bonding on rigid and flexible printed circuit substrates. Components, Packaging, and Manufacturing Technology, Part B: Advanced Packaging, IEEE Transactions on, 1996. 19(3): p. 644-660..
37. Frisk, L. and A. Cumini, Reliability of ACA bonded flip chip joints on LCP and PI substrates. Soldering & Surface Mount Technology, 2006. 18(4): p. 12-20..

38. Frisk,L., Study of Structure and failure mechanisms in ACA interconnections using SEM. Scanning Electron Microscopy, Dr. Viacheslav Kazmiruk (Ed.), ISBN: 978-953-51-0092-8, InTech, DOI: 10.5772/36965, 2012.
39. Yufeng Jin, Z.W., Jing Chen, Introduction to microsystem packaging technology (electronic resource). Boca Raton, FL: CRC Press/ Taylor & Francis, c2011., 2011. ISBN: 9781439865972: p. 232
40. Black, J.R., Electromigration failure modes in aluminum metallization for semiconductor devices. Proceedings of the IEEE, 1969. 57(9): p. 1587-1594
41. Jen, M.H.R., L.-c. Liu, and Y.-s. Lai, Electromigration test on void formation and failure mechanism of FCBGA lead-free solder joints. Components and Packaging Technologies, IEEE Transactions on, 2009. 32(1): p. 79-88.
42. Ye, H., M. Lin, and C. Basaran, Failure modes and FEM analysis of power electronic packaging. Finite Elements in Analysis and Design, 2002. 38(7): p. 601-612.
43. Huang, Z.H., R.E. Jones, and A. Jain, Experimental investigation of electromigration failure in Cu-Sn-Cu micropads in 3D integrated circuits.Microelectronic Engineering, 2014 (122): p 46-51.
44. Zhao, X., M. Saka, M. Muraoka, M. Yamashita, H. Hokazono, Electromigration behaviors and effects of addition elements on the formation of a Bi-rich layer in Sn58Bi-based solders. Journal of Electronic Materials, 2014(11): p. 4179.
45. Lee, T.Y., K.N. Tu, S.M. Kuo, D.R. Frear, Electromigration of eutectic SnPb solder interconnects for flip chip technology. Journal of Applied Physics, 2001. 89(6): p. 3189.
46. Kelly, M., T. Diep, S. Twerefour, G. Servais, D. Lin, G. Shah, A comparison of electrostatic discharge models and failure signatures for CMOS integrated circuit devices. Electrical Overstress/Electrostatic Discharge Symposium Proceedings, 1995

47. Sangameswaran, S., D.C. Jeroen, G. Groeseneken, J.D.W. Ingrid, Reliability test methodology for MEMS and MOEMS under electrical overstress and electrostatic discharge stress. Journal of Micro/Nanolithography, MEMS, and MOEMS, 2012. 11(2): p. 021204-1-021204-8.
48. Ruan, J., N. Nolhier, M. Bafleur, L. Bary, F. Coccetti, T. Lisec, R. Plana, Electrostatic discharge failure analysis of capacitive RF MEMS switches, 2007, Elsevier B.V. p. 1818.
49. Ruan, J., G.J. Papaioannou, N. Mauran, N. Nolhier, M. Bafleur, F. Coccetti, R. Plana, ESD failure signature in capacitive RF MEMS switches. Microelectronics Reliability, 2008. 48(8–9): p. 1237-1240.
50. Greason, W.D. and G.S.P. Castle, The effects of electrostatic discharge on microelectronic devices a review. industry applications, IEEE Transactions on, 1984. IA-20(2): p. 247-252.
51. Vinson, J.E. and J.J. Liou, Electrostatic discharge in semiconductor devices: protection techniques. Proceedings of the IEEE, 2000. 88(12): p. 1878-1902..
52. Ueng, H.Y. and C.Y. Liu, The aluminum bond-pad corrosion in small outline packaged devices. Materials Chemistry and Physics, 1997. 48(1): p. 27-35.
53. Uno, T., Bond reliability under humid environment for coated copper wire and bare copper wire. Microelectronics Reliability, 2011. 51(1): p. 148-156.
54. Tan, C.W., A.R. Daud, and M.A. Yarmo, Corrosion study at Cu–Al interface in microelectronics packaging. Applied Surface Science, 2002. 191(1–4): p. 67-73.
55. Hillman, C., B. Castillo, and M. Pecht, Diffusion and absorption of corrosive gases in electronic encapsulants. Microelectronics Reliability, 2003. 43(4): p. 635-643.
56. Song, J.-m., C.-h. Tsai, and Y.-p. Fu, Electrochemical corrosion behaviour of Bi–11Ag alloy for electronic packaging applications. Corrosion Science, 2010. 52(7): p. 2519-2524.

57. Tong, X.C., Advanced materials for thermal management of electronic packaging. [electronic resource]. New York, NY: Springer 2011. ISBN: 9781441977595

58. Zribi, A., R.R. Chromik, R. Presthus, J. Clum, K. Teed, L. Zavalij, J. DeVita, J. Tova, E.J. Cotts, Solder metallization interdiffusion in microelectronic interconnects. Components and Packaging Technologies, IEEE Transactions on, 2000. 23(2): p. 383-387.

59. Gan, C.L., H. Uda, Wearout reliability and intermetallic compound diffusion kinetics of Au and PdCu wires used in nanoscale device packaging. Journal of Nanomaterials, 2013. 2013: p. 9.

60. Dupont, L., S. Lefebvre, Z. Khatir, S. Bontemps, Evaluation of substrate technologies under high temperature cycling. in Integrated Power Systems (CIPS), 2006 4th International Conference on. 2006..

61. Dupont, L., Z. Khatir, S. Lefebvre, S. Bontemps, Effects of metallization thickness of ceramic substrates on the reliability of power assemblies under high temperature cycling. Microelectronics Reliability, 2006. 46(9–11): p. 1766-1771..

62. Ning, X.-S., Y. Lin, R. Peng, H. Zhou, K. Chen, Development of a directly bonded aluminum/alumina power electronic substrate. Materials Science and Engineering: B, 2003. 99(1–3): p. 479-482.

63. Shen, Y.G., Effect of deposition conditions on mechanical stresses and microstructure of sputter-deposited molybdenum and reactively sputter-deposited molybdenum nitride films. Materials Science and Engineering: A, 2003. 359(1–2): p. 158-167.

64. Chen, C.-j. and K.-l. Lin, Internal stress and adhesion of amorphous Ni–Cu–P alloy on aluminum. Thin Solid Films, 2000. 370(1–2): p. 106-113.

65. Chen, L., N. Magtoto, B. Ekstrom, J. Kelber, Effect of surface impurities on the Cu/Ta interface. Thin Solid Films, 2000. 376(1–2): p. 115-123.

66. Zantye, P.B., A. Kumar, and A.K. Sikder, Chemical mechanical planarization for microelectronics applications. Materials Science and Engineering: R: Reports, 2004. 45(3–6): p. 89-220..

67. Benz, M., K.J. Rosenberg, E.J. Kramer, J.N. Israelachvili, The deformation and adhesion of randomly rough and patterned surfaces. The Journal of Physical Chemistry B, 2006. 110(24): p. 11884-11893.
68. García, S.J., H.R. Fischer, and S. van der Zwaag, A critical appraisal of the potential of self healing polymeric coatings. Progress in Organic Coatings, 2011. 72(3): p. 211-221
69. Zhang, J., J. Gu, L. Li, B. Wei, Bonding of alumina and metal using bulk metallic glass forming alloy. International Journal of Modern Physics B, 2009. 23(06n07): p. 1306-1312.
70. Ramos, F. and M.T. Vieira, Adhesion improvement of RF-sputtered alumina coatings as determined by the scratch test. Journal of Adhesion Science and Technology, 1993. 7(8): p. 801-811.
71. Essa, A.A. and A.S. Bahrani, The friction joining of ceramics to metals. Journal of Materials Processing Technology, 1991. 26(2): p. 133-140.
72. R. Kužel, J.S., M. Matejka, New trends in power microelectronics DCB packages. Microelectronics International, 1992. 9(2): p. 6-8.
73. Schulz-Harder, J., Advantages and new development of direct bonded copper substrates. Microelectronics Reliability, 2003. 43(3): p. 359-365.
74. Entezarian, M. and R.A.L. Drew, Direct bonding of copper to aluminum nitride. Materials Science and Engineering: A, 1996. 212(2): p. 206-212.
75. Yoshino, Y., Role of oxygen in bonding copper to alumina. Journal of the American Ceramic Society, 1989. 72(8): p. 1322-1327.
76. Beraud, C., M. Courbiere, C. Esnouf, D. Juve, D. Treheux, Study of copper-alumina bonding. Journal of Materials Science, 1989. 24(12): p. 4545-4554.
77. Chida, N., H. Fujinuma, M. Matsuura, S. Tsukahara, Copper or molybdenum metallization of ceramics by ion beam dynamic mixing. Nippon seramikkusu kyokai gakujutsu ronbunshi, 1992. 100(4): p. 417-421.
78. Wielage, B., T. Grund, C. Rupprecht, S. Kuemmei, New method for producing power electronic circuit boards by cold-gas spraying and

investigation of adhesion mechanisms. Surface and Coatings Technology, 2010. 205(4): p. 1115-1118.

79. Morgan, R., P. Fox, J. Pattison, W. O'Nell, Analysis of cold gas dynamically sprayed aluminium deposits. Materials Letters, 2004. 58(7–8): p. 1317-1320..

80. Halitim, F., N. Ikhlef, S. Abdeslam, G. Fantozzi, The effect of chromium and titanium implantation on the mechanical properties of polycrystalline alumina: The role of residual stress. Ceramics International, 1997. 23(6): p. 509-512.

81. Zhang, J.X., R.S. Chandel, and H.P. Seow, Effects of chromium on the interface and bond strength of metal–ceramic joints. Materials Chemistry and Physics, 2002. 75(1–3): p. 256-259.

82. Lloyd, J.R., J. Clemens, and R. Snede, Copper metallization reliability. Microelectronics Reliability, 1999. 39(11): p. 1595-1602.

83. Lin, C.H. and W.K. Leau, Copper-silver alloy for advanced barrierless metallization. Journal of Electronic Materials, 2009. 38(11): p. 2212-2221.

84. Pecht, M., R. Agarwal, F.P. McCluskey, J.S. Terrance, S. Javadpour, R. Mahajan, Electronic packaging materials and their properties. Boca Raton: CRC Press, c1999., 1999. (The Electronic Packaging Series). ISBN: 0849396255

85. Manepalli, R. and F. Stepniak, Silver metallization for advanced interconnects. IEEE Transactions on Advanced Packaging, 1999. **22**(1): p. 4.

86. Manepalli, R. and F. Stepniak, Silver metallization for advanced interconnects. IEEE Transactions on Advanced Packaging, 1999. 22(1): p. 4.

87. Haisma, J., G.A.C.M Spierings, T.M. Michielsen, C.L. Adema, Surface preparation and phenomenological aspects of direct bonding. Philips Journal of Research, 1995. 49(1): p. 23-46..

88. Grebinski, T.J., Surface treatment to remove impurities in microrecesses, Purusar Corp, 1987. WO1989000895 A1..

89. Ohmi, T., T. Imaoka, T. Kezuka, J. Takano, M. Koruge, Segregation and removal of metallic impurity at interface of silicon and fluorine etchant. Journal of the Electrochemical Society, 1993. 140(3): p. 811-818.
90. Yacobi, B.G., S. Martin, K. Davis, A. Hudson, M. Hubert, Adhesive bonding in microelectronics and photonics. Journal of Applied Physics, 2002. 91(10): p. 6227
91. Chen, J.-k., C.Y. Hsieh, C.F. Huang, P.M. Li, S.W. Kuo, F.C. Chang, Using solvent immersion to fabricate variably patterned Poly(methyl methacrylate) brushes on silicon surfaces. Macromolecules, 2008. 41(22): p. 8729-8736..
92. Lacombe, R., Adhesion measurement methods: theory and practice, 2005. CRC Press, p. 7-73.
93. Kinbara, A. and I. Kondo, Adhesion measurement of thin metal films by scratch, peel, and pull methods. Journal of Adhesion Science and Technology, 1993. 7(8): p. 767-782.
94. Hull, T.R., J.S. Colligon, and A.E. Hill, Measurement of thin film adhesion. Vacuum, 1987. 37(3–4): p. 327-330
95. Buchwalter, L.P., Relative adhesion measurement for thin film microelectronics structures. The Journal of Adhesion, 2000. 72(3-4): p. 269-291.
96. Kim, J., K.S. Kim, and Y.H. Kim, Mechanical effects in peel adhesion test. Journal of Adhesion Science and Technology, 1989. 3(1): p. 175-187.
97. K.L.Mittal, Electrocomponent science and technology. adhesion measurement of thin films, 1976. 3, 21-42.
98. Meneve. J., H. Ronkainene, P. Andersson, K. Vercammen. D. Camino, et al., Scratch adhesion testing of coated surfaces-Challenges and new directions. Adhesion Measurement of Films & Coatings: Volume 2, 2001. 2: p. 79..
99. P. Benjamin, C.W., Measurement of adhesion of thin films. Proceedings of the Royal Society of London A: Mathematical, Physical and Engineering Sciences, 1960. 254(1277).

100. Butler, D.W., C.T.H. Stoddart, and P.R. Stuart, The stylus or scratch method for thin film adhesion measurement: some observations and comments. Journal of Physics: D Applied Physics, 1970. 3(6): p. 1..

101. Charalambides, P.G., J. Lund, A.G. Evans, R.M. McMeeking, A test specimen for determining the fracture resistance of bimaterial interfaces. Journal of Applied Mechanics-transactions of The Asme, 1989. 56(1).

102. Shaviv, R., S. Roham, and P. Woytowitz, Optimizing the precision of the four-point bend test for the measurement of thin film adhesion. Microelectronic Engineering, 2005. 82(2): p. 99-112.

103. Severin, J.W., Hokke, R., Wel, H. van der & With, G. de, The influence of thermal treatments on the adhesion of electrolessly deposited Ni(P) layers on alumina ceramic. Journal of the Electrochemical Society, 1994. 141(3): p. 816-824.

104. Z Zhang, G., J. Zhang, P. Yi, D. Chai, Joining of $Al_2O_3p$/Al composites by transient liquid phase (TLP) bonding and a novel process of active-transient liquid phase (A-TLP) bonding. Materials Science & Engineering A, 2008. 488: p. 146-156.

105. Rowcroft, P., Ceramic to metal seals metallized by sputtering. Journal of Physics E: Scientific Instruments, 1970. 3(3): p. 211.

106. Rong, C., J. Zhang, C. Liu, S. Yang, Surface metallization of alumina ceramics by pulsed high energy density plasma process. Applied Surface Science, 2002. 200(1–4): p. 104-110.

107. Kuramoto, N., H. Taniguchi, and I. Aso, Translucent A1N ceramic substrate. Components, Hybrids, and Manufacturing Technology, IEEE Transactions on, 1986. 9(4): p. 386-390.

108. Shimada, Y., K. Utsumi, M. Suzuki, H. Takamizawa, M.Nitta, T. Watari, Low firing temperature multilayerg glass-ceramic substrate. IEEE Transactions on Components, Hybrids & Manufacturing Technology, 1983. **6**(4): p. 382.

109. Burgess, J.F., C.A. Neugebauer, G. Flanagan, R.E. Moore, The direct bonding of metals to ceramics and application in electronics. Active and Passive Electronic Components, 1976(4): p. 233.
110. He, H., R. Fu, D. Wang, X. Song, M. Jing, A new method for preparation of direct bonding copper substrate on $Al_2O_3$. Materials Letters, 2007. 61(19–20): p. 4131-4133.
111. Pietranico, S., S. Pommier, S. Lefebvre, S. Pattofatto, Thermal fatigue and failure of electronic power device substrates. International Journal of Fatigue, 2009. 31(11–12): p. 1911-1920.
112. Pietrzak, K., W. Olesinska, D. Kalinski, A. Strojny-Nedza, The relationship between microstructure and mechanical properties of directly bonded copper-alumina ceramics joints. Bulletin of the Polish Academy of Sciences: Technical Sciences, 2014. 62(1): p. 23.
113. Burgess, J.F., C.A. Neugebauer, The direct bonding of metals to ceramics and application in electronics. ElectroComponent Science and Technology, 1976. 2(4).
114. Paik, K.W. and C.A. Neugebauer, Direct bonding of copper to aluminum nitride substrates, Harris Corporation, 1995. US5418002A
115. Lei, T.G., J.N. Calata, K.D.T Ngo, G.-Q. Lu, Effects of large-temperature cycling range on direct bond aluminum substrate. Device and Materials Reliability, IEEE Transactions on, 2009. 9(4): p. 563-568.
116. Weirauch, D.A., Jr., A reappraisal of wetting in the system A1-$A1_2O_3$from 750–1000°C, in ceramic microstructures ’86, J. Pask and A. Evans, Editors. 1987, Springer US. p. 329-339
117. Li, C.-j., G.-j. Yang, and A. Ohmori, Relationship between particle erosion and lamellar microstructure for plasma-sprayed alumina coatings. Wear, 2006. 260(11–12): p. 1166-1172.
118. Tucker, R.C., Thermal spray coatings: broad and growing applications. International journal of powder metallurgy, 2002. 38(7): p. 45-53.
119. Zavareh, M.A., A.A.D.M. Sarhan, B.B.A. Razak, W.J. Basirun, Plasma thermal spray of ceramic oxide coating on carbon steel with enhanced wear

and corrosion resistance for oil and gas applications. Ceramics International, 2014(9): p. 14267.

120. Marx, S., A. Paul, A. Köhler, G. Hütti, Cold spraying: Innovative layers for new applications. Journal of Thermal Spray Technology, 2006. 15(2): p. 177-183.

121. Hodder, K.J., J.A. Nychka, and A.G. McDonald, Comparison of 10 μm and 20 nm Al-$Al_2O_3$ metal matrix composite coatings fabricated by low-pressure cold gas dynamic spraying. Journal of Thermal Spray Technology, 2014(5): p. 839.

122. Meydanoglu, O., B. Jodoin, and E.S. Kayali, Microstructure, mechanical properties and corrosion performance of 7075 Al matrix ceramic particle reinforced composite coatings produced by the cold gas dynamic spraying process. Surface & Coatings Technology, 2013: p. 108.

123. McPherson, R., On the formation of thermally sprayed alumina coatings. Journal of Materials Science, 1980. 15(12): p. 3141-3149.

124. Cook, G., III and C. Sorensen, Overview of transient liquid phase and partial transient liquid phase bonding. Journal of Materials Science, 2011. 46(16): p. 5305-5323

125. Glaeser, A.M., Transiemt liquid phase ceramic bonding, The Regents of the University of California, 1994. US5234152A

126. MacDonald, W. and T. Eagar, Transient liquid phase bonding. Annual review of materials science, 1992. 22(1): p. 23-46.

127. Yan, J., Z. Xu, G. Wu, S. Yang, Interface structure and mechanical performance of TLP bonded joints of $Al_2O_3$p/6061Al composites using Cu/Ni composite interlayers. Scripta Materialia, 2004. 51(2): p. 147-150.

128. Desideri, D., T. Cavallin, A. Maschio, M. Natali, Characterisation of copper thin films deposited on machinable glass-ceramic and glass by DC magnetron sputtering. Science, Measurement & Technology, IET, 2014. 8(1): p. 1-8..

129. Bunshah, R.F., Handbook of deposition technologies for films and coatings. [electronic resource] : science, technology, and applications. Park Ridge,

N.J. : Noyes Publications, ©1994. (Materials science and process technology series. Electronic materials and process technology). ISBN: 159124045X

130. Abadias, G., Y.Y. Tse, Ph. Guérin, V. Pelosin, Interdependence between stress, preferred orientation, and surface morphology of nanocrystalline TiN thin films deposited by dual ion beam sputtering. Journal of Applied Physics, 2006. 99(11): p. 113519.
131. Petrov, I., P.B. Barna, L. Hultman, J.E. Greene, Microstructural evolution during film growth. Journal of Vacuum Science & Technology A, 2003. 21(5): p. S117-S128.
132. Liang, X., B. Wang, and Y. Liu, Thickness effect of a thin film on the stress field due to the eigenstrain of an ellipsoidal inclusion. International Journal of Solids and Structures, 2009. 46(2): p. 322-330.
133. Rui, H., W. Robl, H. Ceric, T. Detzel, G. Dehm., Stress, sheet resistance, and microstructure evolution of electroplated cu films during self-annealing. Device and Materials Reliability, IEEE Transactions on, 2010. 10(1): p. 47-54.
134. Steiner, H., C. Eisenmenger-Sittner, and B. Schwarz. Temperature induced recrystallization of copper coatings deposited on adhesion promoting molybdenum interlayers. in Journal of Physics: Conference Series. 2008. IOP Publishing.
135. Dukryel, K., P. Hyunah, and L. Chongmu. Recrystallization by annealing on the copper films deposited by pulsed electroplating on the ECR plasma cleaned copper seed layer. in Plasma Science, 2003. ICOPS 2003. IEEE Conference Record - Abstracts. The 30th International Conference on. 2003.
136. Jankowski, K., A. Wymyslowski, and D. Chicot, Combined loading and failure analysis of lead-free solder joints due to creep and fatigue phenomena. Soldering & Surface Mount Technology, 2014. 26(1): p. 22-26.
137. Yu, C.-f., C.-m Chan, L.-c. Chan, K.-c. H, Cu wire bond microstructure analysis and failure mechanism. Microelectronics Reliability, 2011. 51(1): p. 119-124

138. Sparavigna, A.C., Role of plasma surface treatments on wetting and adhesion. Engineering, 2010. 2(6): p. 397-402.
139. Ben Amor, S., G. Baud, M, Jacquet, G. Nansé, P. Fioux, M. Nardin, XPS characterisation of plasma-treated and alumina-coated PMMA. Applied Surface Science, 2000. 153(2–3): p. 172-183.
140. Alexander V. Naumkin, A.K.-v., Stephen W. Gaarenstroom, and Cedric J. Powell, NIST X-ray photoelectron spectroscopy database , NIST Standard Reference Database 20, Version 4.1 2012, U.S. Secretary of Commerce on behalf of the United States of America.
141. Redhead, P.A., Hydrogen in vacuum systems: an Overview. AIP Conference Proceedings, 2003. 671: p. 243-254.
142. D.M, Aluminum-nitride copper bonding improves MCMs. Electronic Design, 1994. 42(4): p. 27.
143. Djokic, S., R. Lepard, and R. Roy, Electroless/electrolytic methods for the preparation of metallized ceramic substrates, 1995. US5849170A.
144. ASTM D907-70, in Definition of terms relating to adhesion.: American Society for Testing and Materials.
145. Chapman, B.N., Thin film adhesion. Journal of Vacuum Science and Technology, 1974. 11(47).
146. Wenzel, R.N., Resistance of solid surfaces to wetting by water. Industrial & Engineering Chemistry, 1936. 28(8): p. 988-994.
147. Puchert, M.K., P.Y. Timbrell, and R.N. Lamb, Postdeposition annealing of radio frequency magnetron sputtered ZnO films. Journal of Vacuum Science & Technology A, 1996. 14(4): p. 2220-2230.
148. Goh, S.W., A.N. Buckley, R.N. Lamb, R.A. Rosenberg, D. Moran, The oxidation states of copper and iron in mineral sulfides, and the oxides formed on initial exposure of chalcopyrite and bornite to air. Geochimica et Cosmochimica Acta, 2006. 70(9): p. 2210-2228.
149. Pezzotti, G. and W. Zhu, Resolving stress tensor components in space from polarized Raman spectra: polycrystalline alumina. Physical Chemistry Chemical Physics, 2015. 17(4): p. 2608-2627.

150. Chase, M. W., Jr. (1998). NIST-JANAF Themochemical Tables, Fourth Edition, J. Phys. Chem. Ref. Data, Monograph 9, .

## LIST OF PUBLICATIONS

Journal articles:

[1.] Lim, J. D, S. S. Y. Susan, M. W. R. Daniel, K.C. Leong, C.C. Wong "Surface roughness effect on copper–alumina adhesion", Microelectronics Reliability, 2013, Vol. 53(9–11), pp. 1548-1552

[2.] Lim, J. D., P. M. Lee, M. W. R. Daniel, K.C. Leong, Z. Chen. "Effect of surface treatment on adhesion strength between magnetron sputtered copper thin films and alumina substrate." Applied Surface Science, 2015. Vol. 355, pp. 509-515

[3.] Lim, J. D., P. M. Lee, M. W. R. Daniel, K. C. Leong, Z. Chen. "Bonding mechanisms between magnetron sputtered copper thin films and alumina substrate." – To be submitted

Conference Presentations:

[1.] Lim. J.D., J. R. P. Eric, et al. "Study of thin film metallization adhesion in ceramic multichip module", 14th Electronics Packaging Technology Conference, EPTC 2012, Singapore, December-*Oral*

[2.] Lim. J. D., M.W.R. Daniel, C.C. Wong "Adhesion characteristics between thin film copper and $Al_2O_3$ substrate", 7th International Conference on Materials for Advanced Technologies, ICMAT 2013, Singapore, June-*Poster*

[3.] Lim. J. D., S.S.Y. Susan, M.W. R. Daniel, K.C. Leong, C.C. Wong "Surface roughness effect on copper–alumina adhesion", 24th European Symposium on Reliability of Electron Devices, Failure Physics and Analysis, ESREF 2013, France, October-*Oral*

[4.] Lim. J. D., Lim, P. M. Lee, M.W. R. Daniel, K.C. Leong, Z. Chen " Improving copper-ceramic bonding through interface engineering", 47th Symposium on Mircoelectronics, International Microelectronics Assembly and Packaging Society, IMAPS 2014, United States of America, October- *Oral*

## APPENDIX A1: 2D AFM Total Effective Area Calculation for a Rough Surface (Manually)

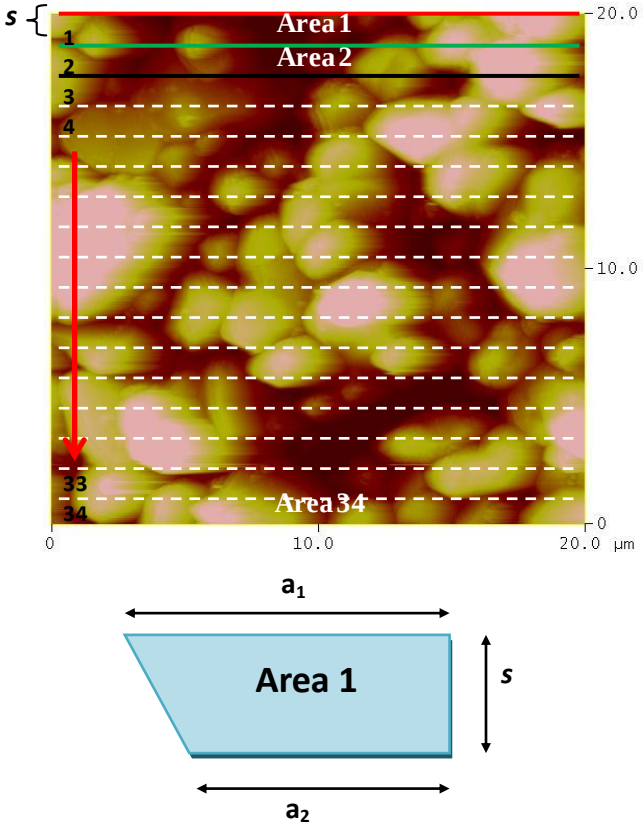


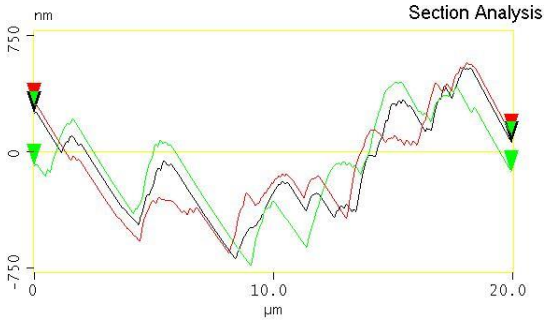


| | | |
|---|---|---|
| Surface distance | 20.882 µm | $a_1$ |
| Horiz distance(L) | 19.961 µm | |
| Vert distance | 197.01 nm | |
| Angle | 0.565 ° | |
| Surface distance | 20.986 µm | $a_2$ |
| Horiz distance | 19.961 µm | |
| Vert distance | 47.142 nm | |
| Angle | 0.135 ° | |
| Surface distance | 20.880 µm | $a_3$ |
| Horiz distance | 19.961 µm | |
| Vert distance | 190.25 nm | |
| Angle | 0.546 ° | |
| Spectral period | DC | |
| Spectral freq | 0 /µm | |
| Spectral RMS amp | 112.90 nm | |

The surface distances of red, green and dark colour lines were stated clearly as $a_1$, $a_2$ and $a_3$ respectively in the AFM section analysis above. The lines were drawn manually using Nanoscope III 5.12r2 imaging software (Digital Instruments) with line spacing, *s* maintained at 0.5882 µm. The 2D total effective area of a rough surface was calculated based on the area of a trapezoid as illustrated. The colour

lines with different roughness are imagined to be stretched in a straight line and formed a trapezium. With the surface distance analyzed from the AFM imaging software, the area of a trapezoid can be calculated using the area formula stated below. Hence, the 2D total effective area of a sample can be estimated by summing up all the trapezoids from area 1 to area 34.

Area of a trapezoid = $0.5 \times s \times (a_1 + a_2)$

Estimated total effective area of a rough surface

= Area 1 + Area 2 + ... + Area 34

$= 0.5 \times s \times [(a_1 + a_2) + (a_2 + a_3) + \ldots + (a_{34} + a_{35})]$

$= 0.5 \times s \times [\sum_{n=1}^{34} (a_n + a_{n+1})]$

## APPENDIX A2: 3D AFM Total Effective Area Calculation for a Rough Surface (Manually)

**2D Total Area Calculation** **3D Total Area**

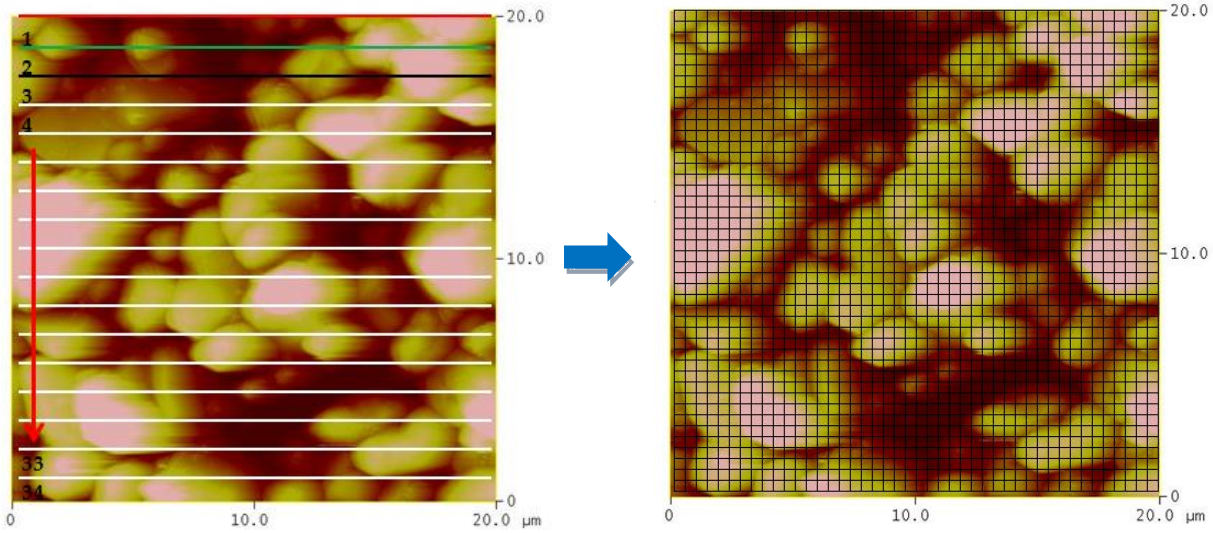


In AFM 3D total effective area calculation, total 841 of data points were analyzed. The precision of this area calculation is higher compared to the 2D area calculation which only has 34 data points in Appendix A2. Besides, the Z-matrix of individual data point will also be taken for the area calculation. Therefore, the height of the trapezoid will be different for every area calculation. Similar to the 2D calculation theory, the total contact area of a sample will be calculated by adding up all the data points. The method used to calculate the individual data points was shown in the next page.

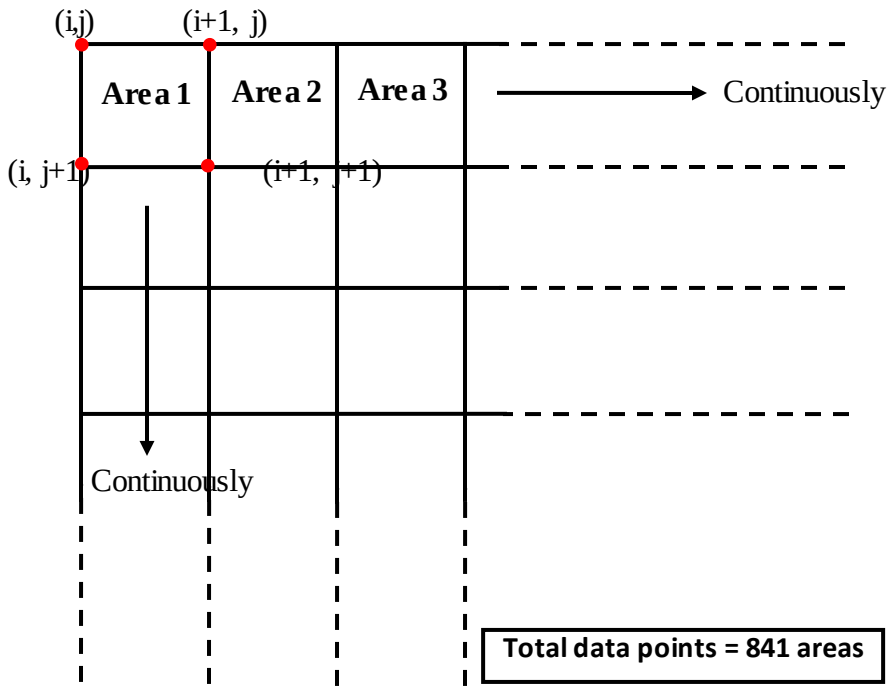


Effective area calculation for individual data point:

Area 1= 0.5 x [(i+1, j) – (i,j)] + [(i+1, j+1) – (i, j+1)] x [(i+1, j+1) – (i+1,j)]

Area 2= 0.5 x [(i+2, j) – (i+1, j)] + [(i+2, j+1) – (i+1, j+1)] x [(i+2, j+1) – (i+1, j)]

Area 3= 0.5 x [(i+3, j) – (i+2, j)] + [(i+3, j+1) – (i+2, j+1)] x [(i+3, j+1) – (i+2, j)]

And continue with the following data points.

## APPENDIX A3: Algorithm Code of Total Effective Area for a Rough Surface

The MATLAB algorithm code was used to calculate the total effective area for the polycrystalline substrate with different surface roughness. Calculation of the area was based on the average value taken along the X- and Y-axis with two diagonals for each axis as shown below:

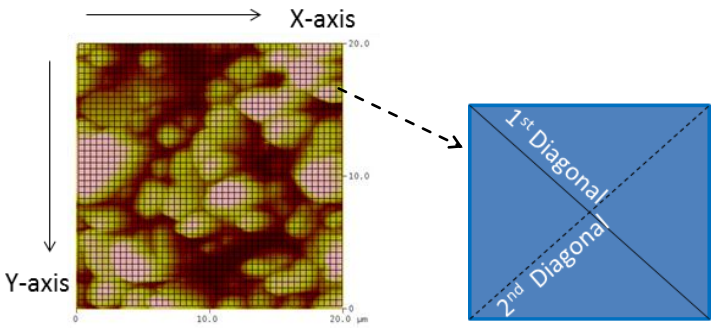


Average Effective Area of a small cubic= $(A_x\_D1 + A_x\_D2 + A_y\_D1 + A_y\_D2)/4$

Along the X-axis:

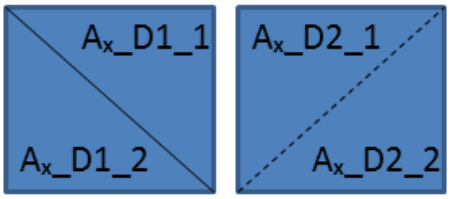


$A_x\_D1 = A_x\_D1\_1 + A_x\_D1\_2$

$A_x\_D2 = A_x\_D2\_1 + A_x\_D2\_2$

Along the Y-axis:

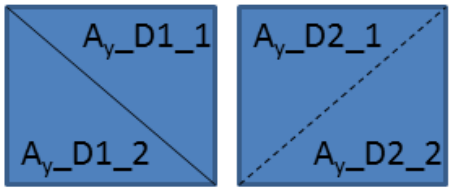


$A_y\_D1 = A_y\_D1\_1 + A_y\_D1\_2$

$A_y\_D2 = A_y\_D2\_1 + A_y\_D2\_2$

```
% This is script to calculate effective area of rough polycrystalline Al2O3

% with different Rms

% It takes input of space or tab delimited Z matrix

% Calculates effective area from a small rectangular

% Summing up the two triangles within a rectangular to get the area
% Calculation based on the x-axis and y-axis to get the average value


scan_size = 20; % scan size in the unit of micrometer

A_scan = scan_size^2 % in micron square

Z_temp = textread('Batch 2_Polish_sample 1_length scale.txt', '','delimiter',' ','emptyvalue',NaN);

[x,y]=size(Z_temp); % lattice size of area scan,512 sample line

lattice_size = x;

lattice_spacing = scan_size/(lattice_size-1); % in the unit of nanometer;

d = lattice_spacing;

Z = Z_temp*1e6; %AFM output come in meter, change it to micrometer


%Calculation using Heron's formula

%Calculation along positive-x direction

A_eff_1_1 = 0; % first half of the lattice area
```

```
for j=1:1:(lattice_size-1)
    for i=1:1:(lattice_size-1)
        a = ( d^2  + (Z(i+1,j)-Z(i,j))^2  )^0.5;
        b = ( d^2  + (Z(i,j+1)-Z(i,j))^2  )^0.5;
        c = ( 2*d^2  + (Z(i,j+1)-Z(i+1,j))^2  )^0.5;
        S = 0.5*(a+b+c);
        A_eff_1_1 = A_eff_1_1 + (S*(S-a)*(S-b)*(S-c))^0.5;
    end
end

A_eff_1_2 = 0; % second half of the lattice  area
for j=1:1:(lattice_size-1)
    for i=1:1:(lattice_size-1)
        a = ( d^2  + (Z(i+1,j+1)-Z(i,j+1))^2  )^0.5;
        b = ( d^2  + (Z(i+1,j+1)-Z(i+1,j))^2  )^0.5;
        c = ( 2*d^2  + (Z(i,j+1)-Z(i+1,j))^2  )^0.5;
        S = 0.5*(a+b+c);
        A_eff_1_2 = A_eff_1_2 + (S*(S-a)*(S-b)*(S-c))^0.5;
    end
end
```

```
A_eff_1 = A_eff_1_1 + A_eff_1_2


%Calculation on postitive-y direction
A_eff_2_1 = 0; % first half of the lattice area
for i=1:1:(lattice_size-1)
    for j=1:1:(lattice_size-1)
        a = ( d^2 + (Z(i+1,j)-Z(i,j))^2 )^0.5;
        b = ( d^2 + (Z(i,j+1)-Z(i,j))^2 )^0.5;
        c = ( 2*d^2 + (Z(i,j+1)-Z(i+1,j))^2 )^0.5;
        S = 0.5*(a+b+c);
        A_eff_2_1 = A_eff_2_1 + (S*(S-a)*(S-b)*(S-c))^0.5;
    end
end


A_eff_2_2 = 0; % second half of the lattice area
for i=1:1:(lattice_size-1)
    for j=1:1:(lattice_size-1)
        a = ( d^2 + (Z(i+1,j+1)-Z(i,j+1))^2 )^0.5;
        b = ( d^2 + (Z(i+1,j+1)-Z(i+1,j))^2 )^0.5;
        c = ( 2*d^2 + (Z(i,j+1)-Z(i+1,j))^2 )^0.5;
```

```
        S = 0.5*(a+b+c);
        A_eff_2_2 = A_eff_2_2 + (S*(S-a)*(S-b)*(S-c))^0.5;
    end
end

A_eff_2 = A_eff_2_1 + A_eff_2_2

% second diagonal will be included to get the average effective area

%Calculation along positive-x direction,2nd diagonal
A_eff_1_1_d2 = 0; % first half of the lattice area
for j=1:1:(lattice_size-1)
    for i=1:1:(lattice_size-1)
        a = ( d^2 + (Z(i+1,j)-Z(i,j))^2 )^0.5;
        b = ( d^2 + (Z(i+1,j+1)-Z(i+1,j))^2 )^0.5;
        c = ( 2*d^2 + (Z(i+1,j+1)-Z(i,j))^2 )^0.5;
        S = 0.5*(a+b+c);
        A_eff_1_1_d2 = A_eff_1_1_d2 + (S*(S-a)*(S-b)*(S-c))^0.5;
    end
end
```

```
A_eff_1_2_d2 = 0; % second half of the lattice area
for j=1:1:(lattice_size-1)
    for i=1:1:(lattice_size-1)
        a = ( d^2 + (Z(i+1,j+1)-Z(i,j+1))^2 )^0.5;
        b = ( d^2 + (Z(i,j+1)-Z(i,j))^2 )^0.5;
        c = ( 2*d^2 + (Z(i+1,j+1)-Z(i,j))^2 )^0.5;
        S = 0.5*(a+b+c);
        A_eff_1_2_d2 = A_eff_1_2_d2 + (S*(S-a)*(S-b)*(S-c))^0.5;
    end
end

A_eff_1_d2 = A_eff_1_1_d2 + A_eff_1_2_d2

%Calculation along positive-j direction, 2nd diagonal
A_eff_2_1_d2 = 0; % first half of the lattice area
for i=1:1:(lattice_size-1)
    for j=1:1:(lattice_size-1)
        a = ( d^2 + (Z(i+1,j)-Z(i,j))^2 )^0.5;
        b = ( d^2 + (Z(i+1,j+1)-Z(i+1,j))^2 )^0.5;
```

```
        c = ( 2*d^2  + (Z(i+1,j+1)-Z(i,j))^2  )^0.5;
        S = 0.5*(a+b+c);
        A_eff_2_1_d2 = A_eff_2_1_d2 + (S*(S-a)*(S-b)*(S-c))^0.5;
    end
end

A_eff_2_2_d2 = 0; % second half of the lattice area
for i=1:1:(lattice_size-1)
    for j=1:1:(lattice_size-1)
        a = ( d^2  + (Z(i+1,j+1)-Z(i,j+1))^2  )^0.5;
        b = ( d^2  + (Z(i,j+1)-Z(i,j))^2  )^0.5;
        c = ( 2*d^2  + (Z(i+1,j+1)-Z(i,j))^2  )^0.5;
        S = 0.5*(a+b+c);
        A_eff_2_2_d2 = A_eff_2_2_d2 + (S*(S-a)*(S-b)*(S-c))^0.5;
    end
end

A_eff_2_d2 = A_eff_2_1_d2 + A_eff_2_2_d2
% Total effective area based on the 4 directions
A_eff_total = (A_eff_1 + A_eff_2 + A_eff_1_d2 + A_eff_2_d2)/4
```